

**TWO LINEAR SLOT NOZZLE VIRTUAL IMPACTORS
FOR CONCENTRATION OF BIOAEROSOLS**

A Dissertation

by

JOHN STEVEN HAGLUND

Submitted to the Office of Graduate Studies of
Texas A&M University
in partial fulfillment of the requirements for the degree of
DOCTOR OF PHILOSOPHY

August 2003

Major Subject: Mechanical Engineering

**TWO LINEAR SLOT NOZZLE VIRTUAL IMPACTORS
FOR CONCENTRATION OF BIOAEROSOLS**

A Dissertation

by

JOHN STEVEN HAGLUND

Submitted to Texas A&M University
in partial fulfillment of the requirements
for the degree of

DOCTOR OF PHILOSOPHY

Approved as to style and content by:

Andrew R. McFarland
(Chair of Committee)

Dennis L. O'Neal
(Member)

Yassin A. Hassan
(Member)

William H. Marlow
(Member)

Dennis L. O'Neal
(Head of Department)

August 2003

Major Subject: Mechanical Engineering

ABSTRACT

Two Linear Slot Nozzle Virtual Impactors for Concentration
of Bioaerosols. (August 2003)

John Steven Haglund, B.S., Montana State University; M.S., Texas A&M University

Chair of Advisory Committee: Dr. Andrew R. McFarland

Two experimental configurations of linear slot nozzle virtual impactors were constructed and experimentally investigated for use as bioaerosol concentrators. In one configuration, the Linear Slot Virtual Impactor (LSVI), the nozzle was a straight slot having a length of 89 mm (3.5"). In the second configuration, the Circumferential Slot Virtual Impactor (CSVI), the nozzle was curvilinear following a circular path having a diameter of 152.4 mm (6.0") and the resulting total slot length was 479 mm (18.8"). Multiple prototypes of the two configurations were constructed having nozzle widths that varied from 0.508 mm (0.015") to 0.203 mm (0.008"). Optical and physical measurements were made of the nozzle dimensions in the critical region of the virtual impactor units. For the LSVI units the misalignment between the acceleration nozzle and the receiver nozzle was measured between 6 μm (0.00025") and 29 μm (0.00114"). This represented a range of 2% to 10% misalignment relative to the acceleration nozzle width. The CSVI Unit 1 and 2 misalignments were measured to be 15 μm (0.00061") and 9 μm (0.00036"), or 10% and 1.8% relative misalignment, respectively. The virtual impactors were tested with liquid and solid monodisperse aerosol particles. For operation at flow rate conditions predicted from the literature to produce a cutpoint of

0.8 $\mu\text{m AD}$, an acoustic resonance was observed, corresponding to significant nozzle wall losses of particles and an absence of normal particle separation in the virtual impactor. The onset of the resonance phenomenon was observed to begin at a nozzle Reynolds number of approximately 500 for the LSVI configuration, and 300 for the CSVI configuration. For flow rates just below the onset of resonance, normal virtual impactor behavior was observed. The value of Stk_{50} was 0.58 for both devices, corresponding to a particle cutpoint size of 1.1 $\mu\text{m AD}$ for the LSVI configuration and 2.2 $\mu\text{m AD}$ for the CSVI. The collection efficiency was greater than 72% for all particle sizes larger than twice the cutpoint up to the largest particle size tested ($\approx 10 \mu\text{m AD}$). The peak collection efficiency for both concentrators was greater than 95%.

ACKNOWLEDGEMENTS

Funding for this project was provided by the U.S. Army, Soldier Biological Chemical Command (SBCCOM), Edgewood Chemical Biological Center (ECBC), under supervision of Dr. Edward Steubing and Dr. Jerry Bottiger (Texas Engineering Experiment Station, Contract Numbers 32525-63020 and 32525-69420); Los Alamos National Lab (LANL), under supervision of Dr. Tom Wehner (Texas Engineering Experiment Station Contract Number 32525-68240).

The successful conclusion of this project was the result of significant contributions, both technical and non-technical, from many individuals. I gratefully acknowledge the assistance of the following people, as well as any I may have overlooked:

- My advisor and committee chair, Dr. Andrew McFarland, for his continued support and guidance of my studies.
- My committee members, Dr. Dennis O'Neal, Dr. Yassin Hassan, and Dr. William Marlow for their technical insights and general support of my academic efforts.
- Mr. Bill McMillan, for his design insights and his ability to achieve the near-impossible machining tolerances without which this study would not have been possible.
- Mr. James Dworaczyk and Mr. Dave Weber of Machine Works (Bryan, TX) for their invaluable suggestions and skill in making detailed measurements on the CSVI units.

- Mr. Sridhar Hari, for suggestions on blade profile improvements, and for his perseverance in completing the companion numerical studies through a myriad of geometrical and parametric changes.
- Finally, I wish to thank my friends and colleagues in the Aerosol Technology Laboratory at Texas A&M University who have all helped me in my studies at one time or another, Dr. Sumit Chandra, Dr. Denis Phares, Mr. Matt Richardson, Mr. Vishnu Vijayaraghavan, Mr. Brandon Moncla, Mr. Youngin Seo, Mr. Nagaraj Ramakrishna, Mr. Amit Gupta, Mr. Rishiraj Das, Mr. Travis Owens, Mr. Michael Wiley, Mr. John Vaughan, Ms. Tina Famighetti, and Ms. Ginny Whisnant.

TABLE OF CONTENTS

	Page
ABSTRACT	iii
ACKNOWLEDGEMENTS	v
TABLE OF CONTENTS	vii
LIST OF TABLES	ix
LIST OF FIGURES.....	x
INTRODUCTION.....	1
Background	1
Virtual Impaction for Bioaerosol Concentration.....	3
THEORY.....	6
LITERATURE REVIEW.....	12
PROTOTYPE DESCRIPTIONS.....	16
Conceptual Bioaerosol Concentrators.....	16
LSVI Units	17
CSV Units	19
Pressure Drop	20
MEASUREMENT OF CRITICAL GEOMETRY.....	21
LSVI Units	21
CSV Units	22
Nominal and As-Measured Nozzle Geometry	24

	Page
EXPERIMENTAL METHODOLOGY	26
Preliminary Monodisperse Liquid Fluorescent Aerosol Tests	26
Polystyrene Latex Particles with Aerodynamic Particle Sizer	27
Acoustic Measurements	29
Monodisperse Liquid and Polystyrene Latex Fluorescent Aerosol Tests	30
Quality Assurance	33
Uncertainty Analysis	35
RESULTS AND DISCUSSION	42
Preliminary Monodisperse Liquid Fluorescent Aerosol Tests	42
Polystyrene Latex Particles with Aerodynamic Particle Sizer	44
Acoustic Measurements	44
Liquid and Polystyrene Latex Fluorescent Monodisperse Aerosol Tests	48
Modeling	50
Treatment of Polydisperse Test Aerosols	52
SUMMARY	54
REFERENCES	55
APPENDIX A TABLES AND FIGURES	60
APPENDIX B SOUND MEDIA FILES	121
VITA	123

LIST OF TABLES

TABLE		Page
1	Comparison of cutpoint Stokes numbers of virtual impactor studies at minor/total flow ratio of 10%.....	61
2	Nozzle width and misalignment of LSVI units.....	78
3	Nozzle width, variance and misalignment of CSVI units.....	80
4	Optical filters and tracer dye used in fluorometric analysis of test aerosols.....	89
5	Preliminary results of testing LSVI units with liquid monodisperse aerosols ...	90
6	Final results of testing slot-nozzle virtual impactor units with monodisperse test aerosols	110
7	Comparison of cutpoint Stokes numbers for virtual impactors at 10% minor/total flow ratio of present and previous studies.....	120

LIST OF FIGURES

FIGURE	Page
1 The concept of virtual impaction	62
2 Theoretical power required for a slot nozzle virtual impactor/concentrator operating at 500 L/min with 0.8 μm AD cutpoint (minor loss coefficient, $K = 1$)	63
3 Conceptual design of a bioaerosol concentrator based on multiple stages of linear slot nozzle virtual impactors	64
4 Conceptual design of a bioaerosol concentrator based on multiple stages of circumferential slot nozzle virtual impactors	65
5 Photograph of prototype LSVI unit.....	66
6 Photograph of prototype CSVI unit (split into half-assemblies).....	67
7 Four-block assembly of LSVI units (left acceleration blade detached)	68
8 Nozzle cross-section of LSVI Unit 0	69
9 Nozzle cross-section of LSVI Units 1-4	70
10 Nozzle cross-section of LSVI Units 5 and 6	71
11 Nozzle cross-section of LSVI Units 7 and 8	72
12 Nozzle cross-section of CSVI Unit 1	73
13 Nozzle cross-section of CSVI Unit 2	74
14 Pressure drop in major flow for LSVI Unit 8 at 10% minor/total flow ratio	75
15 Pressure drop in major flow for CSVI Unit 2 at 10% minor/total flow ratio	76
16 Image pair for LSVI nozzle width and alignment measurement (upper half acceleration nozzle, lower half receiver nozzle)	77

FIGURE	Page
17	Locations of points measured by coordinate measurement machine for survey of CSVI nozzle geometry (receiver blade in gold, acceleration blade in gray)..... 79
18	Nozzle width and alignment on circumference of CSVI Unit 1 81
19	Radial position of nozzle tip on circumference of CSVI Unit 1 82
20	Nozzle width and alignment on circumference of CSVI Unit 2 83
21	Radial position of nozzle tip on circumference of CSVI Unit 2 84
22	Test apparatus for liquid and solid PSL monodisperse aerosols for LSVI units 85
23	Test apparatus for liquid and solid PSL monodisperse aerosols for CSVI units 86
24	Test apparatus for LSVI units tested with PSL particles and aerodynamic particle sizer (APS) 87
25	Configuration of Collison nebulizer and pressure control for constant generation of PSL particles for fixed duration 88
26	Comparison of particle deposition on LSVI Unit 3 on the acceleration nozzle (a) and the receiver nozzle (b) for 2.5 μm AD monodisperse liquid aerosol particles tagged with sodium fluorescein tracer 91
27	Comparison of particle deposition on LSVI Unit 6 receiver nozzle WITHOUT secondary expansion (a) and LSVI Unit 7 receiver nozzle WITH secondary expansion (b) for monodisperse liquid aerosol particles tagged with fluorescent tracer 92
28	Deposition of 6.8 μm AD monodisperse liquid aerosol particles on the receiver nozzle in LSVI Unit 7 (b) due to the presence of a burr on the opposed segment of the acceleration nozzle (a)..... 93
29	Deposition of 6.6 μm AD monodisperse liquid aerosol particles on the receiver nozzle throat in CSVI Unit 1 94

FIGURE	Page
30	Collection efficiency of LSVI Unit 8 for solid monodisperse PSL particles sampled by APS for nozzle Reynolds numbers below 400 at 20% minor/total flow ratio 95
31	Collection efficiency of LSVI Unit 8 for solid monodisperse PSL particles sampled by APS for nozzle Reynolds numbers above 400 at 20% minor/total flow ratio 96
32	Sound power spectrum of LSVI Unit 8 at a total flow rate of 42.5 L/min 97
33	Variance of sound power spectrum of LSVI Unit 8 at a total flow rate of 42.5 L/min 98
34	Sound power spectrum of LSVI Unit 8 at a total flow rate of 47.2 L/min 99
35	Variance of sound power spectrum of LSVI Unit 8 at a total flow rate of 47.2 L/min 100
36	Frequency of maximum acoustic intensity for LSVI Unit 8 101
37	Amplitude of peak acoustic tone for LSVI Unit 8 102
38	Sound power spectrum of CSVI Unit 2 at a total flow rate of 130 L/min 103
39	Variance of sound power spectrum of CSVI Unit 2 at a total flow rate of 130 L/min 104
40	Sound power spectrum of CSVI Unit 2 at a total flow rate of 140 L/min 105
41	Variance of sound power spectrum of CSVI Unit 2 at a total flow rate of 140 L/min 106
42	Frequency of maximum acoustic intensity for CSVI Unit 2 at a 10% minor/total flow ratio 107
43	Amplitude of peak acoustic tone for CSVI Unit 2 at a 10% minor/total flow ratio 108

FIGURE	Page
44	Collection efficiency in the minor flow of LSVI Unit 8 at a nozzle Reynolds number of 445 at 10% minor/total flow ratio..... 109
45	Collection efficiency in the major flow of LSVI Unit 8 at a nozzle Reynolds number of 445 at 10% minor/total flow ratio..... 111
46	Collection efficiency in the left and right major flow of LSVI Unit 8 at a nozzle Reynolds number of 445 at 10% minor/total flow ratio 112
47	Wall losses in the accelerator and receiver nozzle throat of LSVI Unit 8 at a nozzle Reynolds number of 445 at 10% minor/total flow ratio 113
48	Collection efficiency in the minor flow of CSVI Unit 2 at a nozzle Reynolds number of 270 at 10% minor/total flow ratio..... 114
49	Wall losses in the accelerator and receiver nozzle throat of CSVI Unit 2 at a nozzle Reynolds number of 270 at 10% minor/total flow ratio 115
50	Collection efficiency in the minor flow of LSVI Unit 8 and CSVI Unit 2 at 10% minor/total flow ratio 116
51	Wall-loss corrected collection efficiency in the minor flow of LSVI Unit 8 and CSVI Unit 2 at 10% minor/total flow ratio 117
52	Model fit to wall-loss corrected collection efficiency data of LSVI Unit 8 and CSVI Unit 2 at 10% minor/total flow ratio 118
53	Comparison of collection efficiency curves of LSVI and CSVI units with variance in test aerosol particle size 119

INTRODUCTION

Background

Systems for the detection of dangerous airborne particulate matter in real-time at a specific location- point detection systems- include devices for the detection of nuclear, biological and chemical (NBC) aerosols. There are both military and civilian applications for such devices. In the nuclear industry, radioactive particulate continuous air monitors (CAMs) provide protection to personnel in laboratories and industrial facilities with radioactive materials. The U.S. military has field-deployable chemical and biological (CB) agent detection systems to protect military personnel in the event of a CB attack. In addition to the military application, the anthrax attacks experience by the U.S. Postal Service in 2001 and the sarin nerve-agent attack in the Tokyo subway system in 1995 have suggested a civilian need for CB detectors in sensitive locations. Although chemical agent and radioactive particulate detectors have matured through several design generations, practical biological point detection systems are relatively new, and significant advancements will be required before biological agent detects achieve performance capabilities on par with chemical agent and radioactive particulate matter monitors.

The U.S. Army deployed the first biological agent point detector in 1995, the Integrated Biological Detection System (BIDS). The U.S. Navy also deployed a similar system, the Interim Biological Agent Detector (IBAD), aboard the USS LaSalle in 1994

This dissertation follows the style and format of *Aerosol Science and Technology*.

(Wolf and Hohe, 2000). The BIDS and IBADs devices were stop-gap systems assembled from available technologies and were intended for subsequent replacement by the next generation of “ground-up” designed biological point detectors. In 1996, the four service branches of the U.S. military enacted a joint program, the Joint Biological Point Detection System (JBPDS), to develop a biological point detector to replace the BIDS and IBAD systems (Moshier and Buonaugurio, 2000). As the JBPDS was intended as joint service equipment, it must operate over a wide range of environmental conditions. In the current configuration, the JBPDS system is capable of sampling ambient air at a flow rate of 780 L/min for the presence of ten biological agents. It has a minimum detection threshold less than 25 agent containing particles per liter of air (ACPLA). The size and weight of the JBPDS are significantly greater than chemical or radioactive particulate monitors.

Research and development is currently underway on the second generation device, Block II JBPDS. Furthermore, a variant objective of the joint biological point detection program, the Joint Biological Tactical Detection System (JBTDS) calls for a system specialized for portability and rapid forward deployment. A special emphasis of the research and development on the JBPDS Block II and JBTDS is placed on minimizing the size and weight of devices. In January 1998, the Aerosol Technology Laboratory at Texas A&M University was contracted by the U.S. Army Soldier Biological Chemical Command (SBCCOM), Edgewood Chemical Biological Center (ECBC) for studies supporting the JBPDS program. The studies discussed below were conducted in support of the contract.

Virtual Impaction for Bioaerosol Concentration

One of the major obstacles that must be overcome by a biological point detector is the relatively low concentration of biological agent particles that can constitute a serious threat. In general, a release of bioagent particles may be a few tens of ACPLA, potentially orders of magnitude below ambient background aerosol concentrations (Farthing, 1998). The point detector must collect and identify any biological agents present in the vast background of ambient particulate. There are several detection technologies among which are: nucleic acid-based, antibody/antigen reaction-based, and ligand-based. These detection methods require that the biological particles be collected in an aqueous suspension (hydrosol). The detection threshold for most approaches is on the order of at least 10^3 particles (Rosen, 1999). In order that biological point detector detect the presence of a few tens of ACPLA within a response time sufficient to protect personnel, the aerosol sampled by the detector must be concentrated many orders of magnitude. Typically, concentration factors on the order of 10^6 are required (Rosen, 1999). One of the critical tasks in the development of small, portable, biological agent detection systems suitable for field applications is efficient concentration of airborne particles. Such concentration devices and their associated power supplies must be small and lightweight.

Virtual impaction is a technique widely used for aerosol concentration. The two common configurations of virtual impactor geometry are the axi-symmetric (circular or round nozzle) and the planar-symmetric (rectangular or slot nozzle) virtual impactor. In the case of the axi-symmetric virtual impactor, a pair of opposed round nozzles form the

impactor, in the case of the planar-symmetric virtual impactor, the nozzles are in the form of linear slots. For both geometries, aerosol is drawn into one nozzle, the acceleration nozzle, and impinged on an opposed nozzle, the receiver nozzle, having an aperture usually 50% larger than the acceleration nozzle (Figure 1). The momentum of the fluid leaving the acceleration nozzle carries the particle-laden airstream into the receiver nozzle where it doubles back out of the receiver nozzle in a hairpin turn. Most of the flow then is then drawn off in the gap between the nozzles and is carried away from the nozzle centerline. The remaining flow (typically 10%) is drawn under vacuum from the receiver nozzle. Particles above the cutpoint size- defined here as the size at which 50% of the particles divert from the major flow and enter the minor flow stream- have sufficient momentum to carry them beyond the hairpin turn and enter the receiver nozzle flow, thus forming an aerosol of greater concentration than that entering the device.

For bioaerosol concentration, the virtual impactor should have a cutpoint below the particle size range of interest. Although a specific virtual impactor will have a fixed flow rate for a desired cutpoint, arbitrary throughputs can be achieved by operating several virtual impactors in parallel and greater concentration factors can be achieved through multiple stages of virtual impaction operated in series.

When designing a virtual impactor/concentrator, consideration should be given to the relationship of the virtual impactor/concentrator within the overall bioaerosol detection system. The concentrated aerosol which is the product of the virtual impactor is passed to a detector, either directly as an aerosol in the case of dry-based optical

detection or after conversion to concentrated hydrosol in the case of wet-based PCR or antibody/antigen detection. In either case, there will be a minimum number of bioaerosol particles or organisms that can be recognized by the detector. The need to meet the detection threshold establishes the minimum volume sampled by the virtual impactor for a given concentration of the ambient bioaerosol. Looking at the problem on a rate basis, there is a minimum flow rate required to achieve detection of a given concentration of biological agent within a given response time. Thus, the basis of evaluation of virtual impactor designs for use as bioaerosol concentrators should be for identical flow rate and cutpoint.

THEORY

The particle and gas phase flow behavior in the virtual impactor is governed by two dimensionless parameters, the Stokes number (Stk) and the Reynolds number (Re):

$$Stk_{L_c} = \frac{\rho_p \cdot D_p^2 \cdot C_c \cdot U_o}{18 \cdot \mu_f \cdot L_c}$$

$$Re_{L_c} = \frac{\rho_f \cdot U_o \cdot L_c}{\mu_f}$$

where:

D_p = particle diameter

ρ_p = particle density

C_c = slip correction factor

U_o = mean velocity at acceleration nozzle exit

μ_f = fluid kinematic viscosity

L_c = critical dimension; for circular jets L_c is the nozzle radius ($D/2$) for Stk and nozzle diameter (D) for Re , for slot jets L_c is the nozzle half-width ($W/2$) for Stk and the full-width (W) for Re .

The Stokes number is the dominant parameter governing particle behavior in the virtual impactor. The cutpoint Stokes number (Stk_{50}) - the value of the Stokes number

corresponding to the particle cutpoint size- is weakly a function of Reynolds number owing to minor differences in the flow field inside the virtual impactor nozzle at different Reynolds numbers.

For bioaerosol concentration, it is also important to consider the pressure drop incurred in moving air through the virtual impactor. The pressure drop is a function of the acceleration nozzle throat velocity:

$$\Delta P = K \cdot \frac{\rho_f \cdot U_o^2}{2}$$

where:

$K =$ the minor loss coefficient.

The theoretical power required for operation of the virtual impactor, i.e. the minimum power required to move air through the virtual impactor without consideration of blower/pump inefficiencies or pressure losses within the flow handling system, is given by:

$$\dot{W}_{ideal} = Q\Delta P$$

where:

$\dot{W}_{ideal} =$ the ideal power required

$Q =$ total flow rate through the virtual impactor

From the standpoint of virtual impactor design for bioaerosol concentration, it is useful to group the fluid and particles properties appearing in the Stokes number into a single parameter, the particle relaxation time, τ .

$$Stk_{L_c} = \frac{\tau \cdot U_o}{L_c}$$

$$\tau = \frac{\rho_p \cdot C_c \cdot D_p^2}{18 \cdot \mu_f}$$

This form of the Stokes number is insightful from a design standpoint as the parameters U_o and L_c reside within the freedom of the designer while the biological agent and ambient air conditions determine the parameters in τ . For bioaerosol detection, the cutpoint of the virtual impactor should be low enough to concentrate the smallest particle size that can be expected in a biological agent release. A bacterial agent like anthrax may consist of single-spores having aerodynamic diameter of about 0.9 μm AD. In order to achieve a cutpoint low enough to concentrate particles of this size, the virtual impactor must have the proper nozzle dimension and mean nozzle velocity. For a given cutpoint, the choice available is between larger nozzle dimensions and larger mean nozzle velocity, or smaller nozzle dimension and smaller mean nozzle velocity.

Once the required cutpoint and flow rate for the detection system are fixed, the power required to operate a virtual impactor is only a function of nozzle width. For fixed flow rate and cutpoint operation, the power increases with the square of the nozzle width (for constant value of the minor loss coefficient). For example, we may fix the cutpoint at 0.8 μm AD and the flow rate at 500 L/min (17.7 CFM), and assuming the value of the minor loss coefficient is approximately unity, the ideal power increases with the square of the nozzle dimension (Figure 2).

Virtual impactors with smaller nozzle dimension require less power to operate for a given cutpoint and flow rate. The comparison can be made, to the first approximation, to virtual impactor designs having different cutpoints and flow rates. Since the cutpoint is largely controlled by Stokes number, and the Stokes number varies with the square of particle diameter, the nozzle velocity can be varied to adjust the cutpoint. Halving the cutpoint requires increasing the nozzle velocity (and hence total flow) by a factor of four. On this basis, the virtual impactor design using the smallest nozzle dimension will always use the least power per unit volume of aerosol concentrated for a given cutpoint. Nozzle minimization is a vital consideration for reducing the size, weight and cost of a bioaerosol sampler using virtual impaction as the means for concentrating the ambient aerosol.

As noted, virtual impactors can be of either the round or slot nozzle configuration. Practical bioaerosol detection systems require flow rates of many tens or hundreds of L/min to detect the concentration of biological agents that can be expected in a release. For small dimension round-nozzle virtual impactors, an array of many

nozzles (tens or hundreds) is usually required, and for slot nozzles, the total slot length must be sufficient to supply the required total flow, either as one continuous slot, or as an array of slots of intermediate length. From the standpoint of manufacturability, either approach has difficulties, especially as the nozzle critical dimension approaches the level of tolerance control for the manufacturing process. For an array of many round nozzles, the risk of producing defective nozzles, particularly considering that each nozzle requires small dimension chamfers and fillets, becomes high. For slot nozzles, nozzle edge straightness and parallelism become difficult to achieve as the nozzle dimension becomes small. Both designs require precise alignment mechanisms to align the centers of the receiver and acceleration nozzles.

Apart from manufacturing considerations, slot nozzles maintain one advantage over round nozzles: greater resistance to fouling from debris. Round nozzles are more easily bridged by airborne fibers. Once a fiber bridges the nozzle, additional particles attach to the fiber, eventually fouling the nozzle and preventing proper function of the virtual impactor. Although slot nozzles can also become bridged by fibers, their long dimension allows them to avoid fouling to a greater degree than round nozzles.

Two significant theoretical and practical considerations of bioaerosol concentrator design are:

- in order to minimize blower power (and hence sampler size and weight), the critical dimension of the virtual impactor nozzle should be made as small as practically possible.

- for small dimension virtual impactors, slot nozzles have a greater ability to resist fouling and are easier to construct for large volume flow rate applications than are arrays of many round nozzles.

The objective of this study was to design, characterize and optimize a prototype slot nozzle virtual impactor scalable for use in a bioaerosol concentration system. The present study focused on slot nozzles, as both straight nozzle elements and also as a curvilinear slot in which the slot ends were joined. To evaluate the potential of slot nozzle virtual impactors for use as bioaerosol concentrators, and to optimize their geometry for minimum wall losses, a parallel numerical and experimental study was undertaken. Results of the numerical study are to be reported in the work by Hari (2003).

LITERATURE REVIEW

Substantial research, both experimental and theoretical has been conducted on the subject of virtual impactors. The original concept proposed of the virtual impactor called for the replacement of the ‘real’ impaction surface in a normal inertial impactor with a ‘virtual’ surface formed at the inlet of a near-stagnant air cavity, thus eliminating problems associated with particle bounce and re-entrainment effecting normal impactors (Hounam and Sherwood, 1965; Conner, 1966). Several early virtual impactor studies proposed methods for separating the fine mode particles (aerodynamic particle size, $D_p < 2.5 \mu\text{m AD}$) from coarse mode particles ($D_p > 2.5 \mu\text{m AD}$) typically present in ambient background aerosols. Subsequent theoretical studies sought to predict performance and improve virtual impactor design (Ravenhall et al., 1978; Forney et al., 1978; Hassan et al., 1979). Early studies relied on the assumption of potential flow to determine the flow field inside the impactor. Later studies (Marple and Chien, 1980) included viscous effects by numerically solving the time-averaged flow field with the full Navier-Stokes equations and applying subsequent particle tracking to determine the particle behavior inside the virtual impactor. One of the issues addressed in the theoretical studies was the problem of particle wall losses observed in earlier experimental studies, particularly for particle sizes near the cutpoint.

Loo and Cork (1988) conducted an extensive experimental study to optimize nozzle geometry in axi-symmetric jet virtual impactors for minimum particle wall losses. Their recommendations define the benchmark in axi-symmetric virtual impactor design.

The results of Loo and Cork (1988) demonstrate the need to maintain accurate alignment between the acceleration and receiver nozzle to minimize nozzle wall losses. They observed a 1% increase in nozzle wall losses with each 0.05 mm (1.6% relative to the acceleration jet diameter) increase in nozzle misalignment.

Besides theoretical studies, Forney et al. (1982) experimentally investigated the sensitivity of the ratio of acceleration nozzle to receiver nozzle width with using a half-plane slot nozzle having infinitely variable acceleration nozzle and receiver nozzle width. Forney et al. (1982) also studied the flow field in their device by use of tracer dye in a water analog model. Their flow field studies indicated a discrete regime of stable flow field behavior for acceleration nozzle Reynolds numbers from 700 to 2000. For Reynolds numbers greater than 2000, periodic fluctuations or unstable behavior in the flow field was observed. Han and Moss (1997) conducted a similar water analog study of axi-symmetric virtual impactors and found the regime resulting in stable laminar flow to be for nozzle Reynolds numbers from 2000 to 7000. Outside of this regime, different portions of the flow field would exhibit period fluctuations, even for Reynolds numbers below 1000.

Studies have been conducted on axi-symmetric virtual impactors having a clean air core introduced at the acceleration nozzle inlet to eliminate the fine-particle contamination normally present in the minor flow stream (coarse particle stream) of a typical virtual impactor (Masuda et al., 1979; Chen and Yeh, 1987). Chein and Lundgren (1995) used the clean air core virtual impactor to generate near-monodisperse

test aerosols by processing polydisperse aerosol sources with the clean air core virtual impactor.

Multistage virtual impactor systems have been constructed for use as bioaerosol concentrators. In 1976, Peterson (2003) developed a slot-nozzle virtual impactor that was later incorporated as a component in a commercial multi-stage virtual impactor/concentrator system (SCP Dynamics Model 1001, Minneapolis, MN) for use in the BIDS bioaerosol point detection system. The SCP Dynamics system had four stages of virtual impaction, the second of which utilized a short rectangular nozzle ($L/W \approx 1$) for bioaerosol concentration. The device had a particle cutpoint of approximately $2.5 \mu\text{m AD}$, but was observed to have significant nozzle wall losses for particles larger than about $6 \mu\text{m AD}$ (Haglund et al. 2002).

More recently, studies have been conducted on submicrometer cutpoint and linear slot nozzle virtual impactors for concentration of fine mode ambient aerosols. Sioutas et al. (1994a) developed a multi-jet, axi-symmetric nozzle virtual impactor for concentration of ambient fine particles having a reported cutpoint between 0.1 and $0.2 \mu\text{m AD}$. Higher aerosol throughputs have been achieved by using long slot ($L/W \gg 1$) linear nozzle virtual impactors. Sioutas et al. (1994b) explored the influence of Reynolds number and flow ratio using two long slot ($L/W = 43, 65$) virtual impactors. The value reported for the cutpoint Stokes number was between 0.3 and 0.25 for nozzle Reynolds numbers of 2370 and 1100 , respectively, at a minor flow ratio of 0.1 . Sioutas et al. (1994c) studied a long slot ($L/W = 170$) virtual impactor concentrator having an acceleration nozzle width of 0.33 mm ($0.013''$) and a total flow rate of 225 L/min (7.9

ft³/min). They observed the value of the cutpoint Stokes number to be 0.20 at a Reynolds number of 4460 and at a minor-to-total flow ratio of 0.1. Ding and Koutrakis (2000) have made a similar study of short slot nozzle ($L/W = 2.5$) virtual impactors and observed higher values for the cutpoint Stokes number. They report values of the cutpoint Stokes number to be between 0.68 and 0.80 for most nozzle Reynolds numbers between 4400 and 15,000. A summary of cutpoint Stokes numbers for virtual impactors is found in Table 1.

PROTOTYPE DESCRIPTIONS

Conceptual Bioaerosol Concentrators

In order to concentrate the ambient aerosol at the volumetric flow rate required for practical bioaerosol detection systems- a provisional value of 500 L/min was assumed at the outset of the study- by means of a minimized slot nozzle virtual impactor, long total slot lengths were required ($L/W > 5000$). Two basic geometrical configurations were proposed: an array of approximately eight slot nozzle elements each having a total slot length of 127 mm (5.0") operated in parallel, and a circumferential slot nozzle having a diameter of 152.4 mm (6.0") having a total slot length of 479 mm (18.8").

In the case of the array of linear slot nozzles, the inlet flow was first to be divided among the elements of nozzle array and the minor flow from each element then combined to form the concentrated aerosol output. The major flow exhaust was to be recovered at either end of the array stack (Figure 3). The concentrated minor flow could then be processed by a geometrically similar second or even third stage impactor for further concentration (with appropriately reduced total slot length in each subsequent stage to reflect the reduction in volumetric flow).

In the case of the circumferential concentrator, the inlet aerosol was to enter on the circumference of the blade inlets, following a path radially inwards to the virtual impactor blades. The concentrated minor flow was to be collected at the central axis of the device, and the major flow was diverted to a vacuum plenum on the outer annulus of

the device. Subsequent stages of virtual impactors could then be nested within the outer stage impactor for additional concentration (Figure 4).

On the basis of virtual impactor theory relating to the particle separation characteristics of slot nozzle virtual impactors, either the linear array or the circumferential slot nozzle should perform identically as a bioaerosol concentration device, provided the total slot length and critical geometries are equivalent (note: the radius of curvature in the circumferential slot nozzle is approximately 150 times greater than the slot width). This equivalency is exclusive of any end-effects or differences in aerosol aspiration that the conceptual designs may have. One important advantage the circumferential design has over the linear array design is relative compactness for the same total slot length.

The complete conceptual designs were not constructed for this study; however the critical single-stage elements of each proposed system were fabricated and characterized in order to determine the expected performance of bioaerosol concentrators based upon the conceptual designs. In the case of the linear array, a series of linear slot nozzle virtual impactors (LSVI) were constructed and evaluated individually (Figure 5). For the circumferential device, two geometrically similar ‘outer’ stage circumferential slot nozzle virtual impactors (CSVI) were constructed and tested (Figure 6).

LSVI Units

The construction of the LSVI units, nine in total, occurred as a progression where subsequent units incorporated remedies to problems encountered in earlier units. Some

changes were in response to problems in manufacturing while others were reflective of geometric improvements suggested by aerosol experiments or the numerical predictions of the companion study (Hari, 2003).

Although each LSVI unit had differences in geometry or manufacturing approach, all LSVI units were built up from a basic four-block assembly (Figure 7). The blocks were stacked in such a way that the lower left and right blocks formed the receiver nozzle while the upper left and right blocks formed the acceleration nozzle. The major flow passages exited from the sides of the four-block assembly. The nozzle blocks were aligned with dowel pins and fastened with 10-32 machine screws. The overall length of the stack was 152 mm (6"), however since a portion of each end of the blocks formed a sealed interface, the slot length varied between 89 mm (3.5") and 127 mm (5.0") for the nine LSVI units. The slot width varied from 0.457 mm (0.018") to 0.305 mm (0.012"), so all units were effectively infinite-length linear nozzles ($L/W > 200$).

The aerosol entered and was recovered from the LSVI unit critical zone through four rectangular ports 25.4 mm (1") wide and having length equal to the slot length. In order to introduce aerosol into and recover aerosol from LSVI Units 0-6, four cover plates were placed over each port. The cover plates had a 15.9 mm (0.625") diameter hole and a 152 mm (6") length segment of smooth-bore tubing to deliver aerosol to a 47 mm (1.9") diameter filter for analysis. The cover plates were attached with machine screws and sealed with vacuum grease or o-rings. The final two LSVI units constructed in this study, LSVI Units 7 and 8 had an unreduced channel passage equal in cross-

section to the rectangular flow ports described above, connecting to flow streams (minor and major) to a 102 mm (4") diameter filter.

The nominal blade geometries of the LSVI units are given in Figures 8 to 11.

CSVl Units

Preliminary measurements revealed difficulty in maintaining tolerance and alignment within the desired precision for the LSVI units. These problems were attributed to the tolerance limits that could be achieved on the CNC milling machine used to manufacture the LSVI units. It was assumed that greater tolerance and precision could be achieved with the circumferential slot virtual impactor in which the critical dimensions are machined on a CNC lathe. In the CSVl units, the nozzle throats are formed on the circumference of four annular blades. The flow enters the acceleration nozzle flowing radially inward. The major flow was then diverted both up and down axially in the impactor, and then exhausted through a series of ten evenly-spaced 'spokes' to the vacuum annulus as described above and shown in Figure 4. The minor flow containing the concentrated aerosol continued on the radially inward trajectory and was collected at the central axis of the device. This concentrated aerosol was drawn through a 25.4 mm (1.0") tube for subsequent collection on a 102 mm (4.0") glass fiber filter.

Two single-stage CSVl prototype devices were constructed. The first, CSVl Unit 1, had a nominal acceleration slot width of 0.203 mm (0.008"). The second device, CSVl Unit 2, had a nominal acceleration slot width of 0.508 mm (0.020"). One significant difference in the manufacturing of the two devices was that, although both

were constructed from 7075 Al on a precision CNC lathe, the first unit was clamped during machining using a hydraulic chuck. For CSVI Unit 2, the blades were first threaded onto a custom mandrel and held with axial (rather than radial) pressure during manufacture. Aside from differences in nominal slot width and fixturing technique, the two CSVI units were otherwise identical (Figures 12 and 13).

Pressure Drop

As noted above, the pressure loss incurred in moving air through the virtual impactor is an important consideration for minimizing the size and weight of bioaerosol concentration systems. The pressure drop at various flow rates for the LSVI and CSVI units was measured (Figures 14 and 15). For the LSVI, the minor loss coefficient, K , averaged 1.9 for nozzle Reynolds numbers from 223 to 445. For the CSVI the minor loss coefficient averaged 1.5 for Reynolds numbers from 157 to 367. Different pressure drops were noted on the left and right major flow path of the LSVI unit when the flow system was adjusted for constant flow through each passage. The reason for the different ΔP values was due to slight mechanical skewness in the nozzle and is discussed below.

MEASUREMENT OF CRITICAL GEOMETRY

LSVI Units

Since proper nozzle geometry was identified as one of the critical parameters influencing virtual impactor performance, measurements of nozzle width and alignment were made on all the LSVI and CSVI units studied. It was discovered that standard measurement techniques requiring physical contact (micrometers, calipers, feeler gauges) caused deflection of, or damage to, the nozzle blades. In order to inspect the nozzle geometry, each LSVI unit was mounted on the stage of a compound microscope with the receiver slot facing the objective lens. The microscope was equipped with a digital camera and had total magnification of 40X. The camera was focused on the edge defining the inlet plane of the receiver nozzle and the image stored electronically. Since the receiver nozzle was nominally $\frac{1}{3}$ wider than the acceleration nozzle, the camera was refocused to bring into view the edges of the acceleration nozzle visible just inside of the receiver blade edges, and another image was then recorded. The LSVI unit was then rotated 180 degrees in the image plane and another pair of like images were taken. Comparison of the original and rotated image pairs eliminated any camera parallax. This process was repeated for each end and at the center of the LSVI unit, resulting in 12 total images.

Once the nozzles were photographed, the images were imported into image editing software. For each image, a line segment was fit by inspection to a substantial length of each nozzle edge visible. It was determined that the manual fit of the line segment was within one or two pixels of that determined by least squares regression of

points along the irregular nozzle edge. The pixel locations for the endpoints of the fitted line segment were then recorded. A third line segment connecting the midpoints of the two edge segments was computed. By comparison of the midpoints of the acceleration nozzle edges and the receiver nozzle edges, the nozzle misalignment could be determined (Figure 16). Also, by comparing the slopes of the fitted line segments, the parallelism of the nozzle edges could be determined. The pixel data was then converted to physical dimension by calibration of the microscope/camera with a stage micrometer.

Nozzle misalignment ranges from 29 μm (0.00114”) to 6 μm (0.00025”) in absolute measurement, or 10% to 2% relative to acceleration nozzle width (Table 2). The measured relative nozzle misalignment was greater than the value of 1.6% recommended by Loo and Cork (1988) for axi-symmetric virtual impactors required to keep nozzle wall losses to a minimum. The difficulty in achieving sufficiently low relative misalignment in the LSVI units was a prime motivation for development of the CSVI designs.

CSV I Units

Unlike the LSVI, it was not possible to use microscopy to inspect the nozzle throat on the CSVI. To measure the nozzle alignment of the CSVI, the device was separated into two half-assemblies, each half comprised of one receiver blade and one acceleration blade. The physical locations of six points on a ray from center to edge of each half-assembly were taken with a Coordinate Measurement Machine (Mitutoyo America Corporation, Model Bright 910, Aurora, IL) using a 300 micron probe tip. Three points were measured to determine the elevation of the half-assembly interface,

the acceleration throat, and the receiver throat. Three more points were measured to determine the radial position of the acceleration nozzle outlet, the receiver nozzle inlet, and the pilot taper (Figure 17). By comparison with the elevations on each half, the nozzle widths and centerline misalignment were computed. Data from the radial position predicted the eccentricity and deviation from circularity of the nozzle. The set of six measurement points were repeated at 48 positions evenly-spaced around the circumference of each half-assembly. This data, in combination with a timing reference mark on each half-assembly, provided a 360 degree assessment of the nozzle geometry.

The average nozzle width, nozzle width variance, and alignment are seen in Table 3. With respect to Table 3, the nozzle deviation was defined as the average of the deviation (either positive or negative) of the nozzle centerlines around the circumference of each CSVI unit. The nozzle misalignment was defined as the average of the absolute value of the nozzle centerline deviation. The misalignment of CSVI Unit 1 was much greater than the deviation, indicating nozzle misalignment resulting from a consistent defect around the circumference of the unit. The misalignment of CSVI Unit 2 was significantly less than for Unit 1, and was nearly equal to the deviation of CSVI Unit 2, indicating misalignment error due only to variance of nozzle profile around the circumference rather than a machining defect.

For CSVI Unit 1, the elevation data reveals a variation in throat width and nozzle alignment to be $13\ \mu\text{m}$ ($0.00056''$) and $15\ \mu\text{m}$ ($0.00061''$), respectively. The plot of the nozzle throat location relative to the unit parting line around the circumference of the device exhibits a sinusoidal wave pattern of periodicity three (Figure 18). In discussions

with the machinist, it was determined that this deviation was the result of deformation cause by the hydraulic chuck that held the components during manufacture. The radial variation of nozzle position shows a different pattern. Here the deviation was clearly a single sine wave (Figure 19). This pattern was the result of eccentricity between the half-assemblies. The radial misalignment as a result of eccentricity averaged $36 \mu\text{m}$ (0.0014”).

For CSVI Unit 2, the variation in nozzle width and radial position did not exhibit a clear sinusoidal variance, and overall variance was much reduced from CSVI Unit 1 (Figures 20 and 21). The improvements in nozzle tolerance of CSVI Unit 2 were attributed to the change in the fixturing process during manufacture.

Nominal and As-Measured Nozzle Geometry

The data from measurement of nozzle geometry was used to construct three nozzle profiles for the LSVI units for incorporation into the parallel numerical study. The first profile was the nominal geometry, i.e. the objective geometry of the manufacturing process. The second profile generated was the average as-measured nozzle dimensions. For dimensions that could not be measured, the nominal dimension was used in the second profile. The third profile was the ‘worst-case’ profile. The worst case was taken as the combination of measured quantities from the set of three measurements along the length of the slot that resulted in the greatest misalignment/skewness. It should be noted that at no point along the length of the slot were the ‘worst-case’ dimensions measured, but this geometry was assumed to represent

an outer boundary of dimensional inaccuracy within which the nozzle was assumed to lay at all points along the length.

EXPERIMENTAL METHODOLOGY

Preliminary Monodisperse Liquid Fluorescent Aerosol Tests

Tests were conducted with monodisperse liquid aerosols to characterize the collection efficiency in the major and minor flow of the virtual impactors. Liquid monodisperse test aerosols were generated with a Berglund-Lui (Berglund and Lui, 1973) vibrating orifice aerosol generator (TSI Model 3050, St. Paul, MN). The non-volatile liquid was oleic acid tagged with 10% sodium fluorescein salt (uranine) fluorescent tracer for subsequent determination of aerosol mass. The mean size of the aerosol droplets was determined by impacting them on a glass slide coated with an oil-phobic film. The droplets were then measured with an optical microscope. From knowledge of the degree of gravitational flattening of the oil droplets on the slide, the original spherical size of the droplets was calculated (Olan-Figueroa et al., 1982).

An Aerodynamic Particle Sizer (APS Model 3310, TSI, Inc., St. Paul, MN) was used to monitor the size distribution of the test aerosol throughout the tests. Because liquid droplets are known to distort when accelerated in the APS measurement section (Griffiths et al., 1986; Chen et al., 1990), the APS data was corrected from the optical measurement data. A scaling factor was applied to the APS particle size spectrum so that mode size of the APS spectrum matched the aerodynamic particle size determined by the optical measurement of the impacted droplets.

The generated test aerosol was drawn into one end of an aerosol delivery duct. At the opposite end, a sample was extracted and collected on a glass fiber filter after passing the aerosol through the virtual impactor. For tests with the LSVI units, separate

filters were collected for the left and right major flow path, and the minor flow. Next, a reference aerosol sample was extracted and collected on a filter where the point of extraction and flow rate were the same as that for the virtual impactor inlet (Figures 22 and 23). Setting the flow rate of the reference sample to that of the virtual impactor, and by using reference filter geometry with minimal losses, the reference aerosol sample was representative to that entering the test device. For most experiments, three or more pairs of reference and test configuration samples were collected for each particle size studied to ensure repeatability of the results. For a few scoping experiments, a single long-duration test was run in order to accumulate visible quantities of possible wall losses, and any scoping tests are noted as such in the results section. The filters were placed in solutions containing 50% isopropyl alcohol and 50% distilled water (v/v) to elute the fluorescent tracer. The total solution volume varied between 20 mL and 80 mL, where less liquid was used for smaller test particles to increase the fluorescent concentration of the solution. The relative concentrations of fluorescent tracer in the solutions were measured with a fluorometer (Turner/Barnstead Thermolyne Model 450, Dubuque, IA). By dividing the relative concentration of fluorescent tracer in the test filter solution by the relative concentration of the reference filter, and correcting for any differences in sample volume, the percentage of particulate mass collected in the major and minor flows relative to total test particulate was determined.

Polystyrene Latex Particles with Aerodynamic Particle Sizer

For tests with particles smaller than 2 microns a different test aerosol was used. For small particle tests, a suspension of solid monodisperse polystyrene latex (PSL)

microspheres (Nanosphere Size Standards, Duke Scientific, Palo Alto, CA; Estapore Uniform Microspheres, Bangs Laboratories, Inc., Fishers, IN) in distilled water was injected continuously into an airblast atomizer of custom design. During the atomization process, the water component of the atomized suspension evaporated, leaving an aerosol composed of the test microspheres and a number of condensation nuclei resulting from the evaporation of water droplets not containing a PSL microsphere. The test aerosol was conveyed through an aerosol delivery duct to an Aerodynamic Particle Sizer (APS Model 3310, TSI, Inc., St. Paul, MN). Five, one-minute samples were collected by the APS and the average PSL aerosol concentration in the aerosol delivery duct was determined (Figure 24). Next, the virtual impactor was inserted between the duct and the APS. In one set of tests, the major flow path was connected in line with the APS and in another set the minor flow was connected to the APS. Five samples at each of several flow rates were then taken for both the major and minor flow configurations. Reference configuration tests were repeated during the change from major to minor flow configuration to ensure consistency in aerosol output of the atomizer. By assumption of constant particle generation and low particle losses in the straight tube test section, the collection efficiency of the major and minor flow path was determined from the ratio of aerosol concentration in the test configuration relative to the reference configuration.

In order to operate the APS at the different vacuum loads found in the inlet, major and minor flow configurations, a calibration of APS sample flow rate was necessary. As the APS manufacture provides calibration values of flowmeter voltage for only unloaded APS inlet conditions (no vacuum pressure), serious flow deficiencies (and

hence particle concentration errors) occurred if these voltage values were applied to the loaded inlet conditions that occurred during minor and major flow concentration measurements. In order to prevent measurement errors of this kind, the true APS sample flow rate was measured over the range of vacuum loads that occurred in the aerosol tests and the appropriate voltage values for constant sample flow rate were determined. These flowmeter voltage values corresponding to constant APS sample rate were then used to configure the APS during the aerosol tests.

Acoustic Measurements

In the course of conducting aerosol tests on the LSVI and CSVI units, an acoustic ‘ringing’ of the virtual impactor nozzle was observed for all flowrates above threshold value. In order to characterize the nature of the phenomenon, sound recordings were made on the prototype virtual impactors at various flow rates. To make the sound measurements, the virtual impactor outlets were connected to the same flow measurement and control systems used during the aerosol tests and the inlet was left open to the ambient environment. No difference in the ringing phenomenon was observed whether the virtual impactor inlet was connected to the aerosol duct or if left open to the ambient environment. The vacuum pump or blower used to operate the flow system was located in a sound isolation chamber to minimize the background noise in the sound recording. An electret unidirectional condenser microphone (Radio Shack Model 33-3007, Fort Worth, Texas) was placed approximately 2 cm ($\frac{1}{2}$ ”) from the virtual impactor inlet with the axis of the microphone coincident with the inlet axis. At each of several flow rates an approximately three second sound recording was made.

The recording was made directly to a PC through the microphone input on the PC sound card. The sampling frequency of the A/D conversion was either 22.050 kHz or 44.100 kHz, and with a resolution of 16 bits. Five, 5000-point sub-samples were extracted from each recording and a Discrete Fourier Transform (DFT) was performed on each sub-sample for power spectrum analysis. Comparison of the five sub-samples allowed for the discrimination of acoustic signal emanating from the virtual from variable background noise.

Monodisperse Liquid and Polystyrene Latex Fluorescent Aerosol Tests

Upon completion of preliminary analysis of liquid and solid particles tests on the LSVI and CSVI units, and after identification of the problems associated with nozzle misalignment and acoustic ringing of the virtual impactors, a final set of characterization tests was conducted on the ultimate prototype of the two virtual impactor configurations (LSVI Unit 8 and CSVI Unit 2) at the maximum flow rate for each device that avoided acoustic ringing.

Monodisperse aerosol tests using both liquid fluorescent particles and solid fluorescent PSL microspheres were conducted. For the liquid particle experiments, wall losses were directly measured by disassembling the virtual impactor units between each set of three test runs at a given particle size and recovering deposited particles. The particle losses were recovered from the critical region by wetting a cotton swab with isopropyl alcohol and swiping the nozzle throat. Four swipes of the nozzle throat were made to ensure maximum particle recovery. Following the swabbing procedure, the nozzles were rinsed with isopropyl alcohol to remove any trace of unrecovered deposits

and to establish a zero base line for the next experiment. The cotton swabs containing the fluorescent deposits were immersed in the same solution as for the aerosol filters, and the fluorescent concentration was analyzed as described above.

In the case of the solid fluorescent PSL microspheres, a suspension of PSL microspheres and distilled water was atomized using a Collison nebulizer (BGI Inc. Model CN31I, Waltham, MA). The mass concentration of PSL in the suspension varied between 0.02% and 0.08% and was well below the limit proposed by May (1972) to prevent significant numbers of doublet PSL particles due to two microspheres occupying the same water droplet during atomization. The particle size spectrum generated by the nebulizer was periodically sampled throughout the tests to identify any potential doublet particles. In addition to aerodynamic particle size spectra, the PSL microsphere size spectrum was analyzed in the hydrosol state with a coulter counter (Beckman Coulter, Inc., Model Multisizer 3, Miami, FL).

As in the liquid aerosol tests, a reference filter was used to determine the relative concentration of the test aerosol entering the virtual impactor. However, unlike the liquid aerosol tests, the duration of the aerosol sample collected was not determined by length of time in which flow was drawn through the virtual impactor or the reference filter. Rather, for each test the vacuum pump was first activated on the device (either the virtual impactor or reference filter). Next, 138 kPa (20 psi) was applied to nebulizer by means of a pressure regulator and solenoid valve (Figure 25). The pressure was maintained constant and for a fixed duration (usually ten minutes), thus producing an approximately constant aerosol generation rate. At the end of the test, the solenoid valve

was closed halting aerosol generation. The vacuum pump of the reference filter or virtual impactor was allowed to run for an additional minute at the end of particle generation to fully evacuate the aerosol delivery duct. APS samples taken at the test section of the delivery duct confirmed that all test aerosols were removed from the delivery duct within approximately the first ten seconds of shut-down of the nebulizer. Conducting experiments in this manner allowed for approximately six to eight consecutive tests (either reference or test configuration) to be run before re-filling of the nebulizer was required. This equates to a liquid consumption rate of about 20 mL/hour and was also consistent with the observations of May (1972). The configuration of aerosol delivery system and nebulizer are seen in Figures 20 and 21.

The glass fiber filters containing the fluorescent microspheres (Pall Gelman Sciences Model A/E 102mm, Ann Arbor, MI) were immersed in 20 mL of ethyl acetate to dissolve the polystyrene latex and liberate the encapsulated dye. The filters were immersed for a minimum of eight hours. The relative fluorescent concentration of the solutions was measured with a digital fluorometer (Turner/Barnstead Thermolyne Quantech Model FM109515, Dubuque, IA) using optical filters appropriate for the excitation and emission wavelength of the fluorescent dye of the PSL (Table 4). It was discovered that a moderate agitation of the filter solutions by swirling the liquid was sufficient to uniformly mix the solution. Multiple samples (~ 5 mL) taken from the same original solution mixed in this manner were indistinguishable from multiple fluorometric readings of the same sample. Thus, it was necessary to only measure one sub-sample extracted from each mixed solution.

Nozzle wall losses were not recovered in the fluorescent PSL experiments. Wetting a cotton swab or tissue wipe with either isopropyl alcohol or water failed to remove the PSL deposits. Due to its relatively high volatility, swabs wetted with ethyl acetate did not recover deposits sufficiently for analysis. More aggressive use of ethyl acetate (i.e. a squirt bottle) resulted in the loss of rivulets containing the dissolved PSL. In principle, one could recover wall losses by complete immersion of the virtual impactor, but the volume of ethyl acetate required in this study would have resulted in solutions too dilute to give fluorescent readings sufficiently greater than the background fluorescence of the ethyl acetate reagent.

Quality Assurance

To ensure reproducibility of the results of the study, efforts were made to identify and correct any potential problems in experimental procedure. First, all devices used in for aerosol collection (the virtual impactor units, the reference filter holders and the flow system used for gas flow measurement and control) were checked for leaks by a pressure decay test. The outlets of each device were sealed and then the component was subjected to a vacuum of 10 kPa (40" H₂O). The time required for the pressure to decay to 7.5 kPa (30" H₂O) was observed. All devices maintained vacuum above the threshold for at least 30 seconds, but typical results were more than a minute. Pressure decay tests on the virtual impactors and reference filter holders were periodically run during the aerosol tests to ensure that gaskets and seals maintained integrity throughout the study.

To determine the possible influence of any ambient background aerosol on the fluorescent measurements, several "blank" reference filter samples were taken from the

aerosol delivery duct. Additionally, the fluorescence level of the liquid reagents (isopropyl alcohol and water for liquid aerosol tests, ethyl acetate for PSL tests) were explicitly determined by setting the fluorometer “zero” using an optical block in the measurement section. The ambient background samples were indistinguishable from the fluorescent level of the blank reagents, and the reagent fluorescent reading was never more than 0.75% of the average reference filter fluorescent reading (greater than 100:1 signal-to-noise ratio) for the liquid aerosol tests. For the fluorescent PSL experiments, limits on mass concentration and duration of particle generation of the Collison nebulizer (May, 1972) as well as a limit on the minimum volume of ethyl acetate reagent (20 mL) necessary to fully wet the filter limited the maximum signal-to-noise ratio to 20:1 for some of the experiments. The maximum background reading relative to reference reading was 4.5%. Consideration of background fluorescence is discussed in the uncertainty analysis below.

When particle sizes were changed in the nebulizer, the nebulizer was first rinsed with ethyl acetate and refilled with distilled water prior to introducing the new PSL particles. A background reading of the nebulizer output was taken to ensure that no particles or residual fluorescent dye (which would be a component in the condensation nuclei) remained from previous tests. It was observed that rinsing the nebulizer with alcohol or water was not sufficient to remove the PSL or fluorescent dye deposits, however when the nebulizer was washed with ethyl acetate, no particle “carry-over” was detected.

Uncertainty Analysis

Measurement errors can be divided into three categories (Beckwith and Marangoni, 1990):

- Bias or systematic errors
- Precision or random error
- Mistakes or blunders

The approach that was taken with respect to the error types was to reject any test data containing a mistake (repeating the measurement as necessary) and apply Pythagorean summation to determine total uncertainty for precision error and estimated bias errors. Some of the parameters potentially contributing to a source of bias error were derived from stochastic sources (e.g. nozzle width measurements). In these cases, the estimated systematic error level was taken as two times the variance observed of the stochastic quantity.

The two data parameters treated for uncertainties were the measured Stokes number (for each test particle) and measured minor collection efficiency. These measured quantities were reduced to their fundamental measured or reference quantities:

$$Stk_{measured} = \frac{\rho_p \cdot [D_f \cdot F_f]^2 \cdot C_c \cdot Q_{avg}}{9 \cdot \mu_f \cdot L \cdot W^2}$$

$$\eta_{measured} = \left[\frac{FIC_{test}}{FIC_{ref}} \right] \cdot \left[\frac{V_{test}}{V_{ref}} \right] \cdot \left[\frac{t_{test}}{t_{ref}} \right] \cdot \left[\frac{Q_{avg,test}}{Q_{avg,ref}} \right]$$

where:

ρ_{pc} = test particle density

D_f = diameter of impacted and flattened test particle

F_f = flattening factor of impacted test particle

C_c = slip correction factor

Q_{avg} = average total flow rate over duration of the test

μ_f = air viscosity

L = slot length

W = slot width

FIC = ‘fluorescent intensity units’ defined by manufacturer for the fluorometer
output proportional to fluorescent concentration

V = fluorescent solution volume

t = duration of test

Applying the uncertainties and precision error estimates for each quantity in the measured values of the Stokes number and efficiency, and adding any additional terms gives the total uncertainties of the measured quantities:

$$\mu_{Stk} = \sqrt{\mu_{\rho_p}^2 + 2\mu_{D_f}^2 + 2\mu_{F_f}^2 + \mu_{Q_{avg,u}}^2 + \mu_{Q_{avg,p}}^2 + \mu_{\mu_f}^2 + \mu_L^2 + 2\mu_W^2}$$

$$\mu_{\eta} = \sqrt{\mu_{FIC,lin}^2 + s_{FIC,p}^2 + n\mu_V^2 + \mu_t^2 + \mu_{Q_{avg,u}}^2 + \mu_{Q_{avg,p}}^2 + s_{Gen}^2}$$

where:

$\mu_{\rho p}$ =	relative uncertainty in particle density
μ_{Df} =	relative uncertainty in the measured diameter of flatten particle
μ_{Ff} =	relative uncertainty in the flattening factor
$\mu_{Q_{avg,u}}$ =	relative uncertainty in flowmeter due to bias error
$\mu_{Q_{avg,p}}$ =	relative uncertainty in flowmeter due to reading error (precision error)
$\mu_{\mu f}$ =	relative uncertainty in air viscosity (due to temperature variations)
μ_L =	relative uncertainty in nozzle length measurement
μ_W =	relative uncertainty in nozzle width measurement
$\mu_{FIC,lin}$ =	relative uncertainty in fluorometric reading due to non-linearity error
$s_{FIC,p}$ =	variance in fluorometric reading due to repeatability (precision error)
n =	number of strokes of dispenser used to prepare solutions
μ_V =	relative uncertainty in volume delivered by dispenser
μ_t =	relative uncertainty in timing mechanism
s_{gen} =	variance in aerosol generator output

The uncertainties of the various parameters were determined from manufacturer reported data, from observations of repeatability of measured quantities, or from reasonable assumptions of error when no data was available. For particle density (0.957 g/cm³ for oleic acid with 10% sodium fluorescein), an uncertainty of ± 0.01 g/cm³ was assumed to allow for any variances in fluorescein concentration. An uncertainty of ± 0.01 (dimensionless) was assumed for the flattening factor (Olan-Figueroa et al., 1982). The value for μ_{Df} was determined from the average variance of the flattened particle measurements over all tests (1.21 microscope hairline units). The uncertainty in the flowmeter measurement was taken from the manufacturer (Dwyer Instruments, Inc., Models RMC Ratemaster 102 and 104, Michigan City, IN) as $\pm 2\%$ of full scale, and an additional error equivalent to $\frac{1}{4}$ of the minimum scale division of the flowmeter was applied to account for precision errors resulting from reading the flowmeter. Possible error in the viscosity value was taken to be the variance associated with a ± 3 °C temperature change from the reference temperature. Hinds (1982) gives the variation of the viscosity of air with temperature as the power 0.74, implying a relative variance of 0.74% over the assumed temperature variance. The uncertainty in the nozzle length was assumed as ± 0.127 mm (0.005") due to precision limits of the caliper. The nozzle width uncertainty was taken as two times the variance of the 48 circumferential measurements for CSVI Unit 2 (2.37%) and the maximum deviation of the three measurements of LSVI Unit 8 (6.13%). The value for μ_t was determined by the precision of the timing device (± 1 sec) divided by total test time. The value for μ_v was given by the manufacturer of the dispenser used to measure liquids for the fluorescent solutions

(Barnstead Thermolyne Model 3020A, Dubuque, IA) as 0.1%. The precision error of the fluorescent intensity readings was determined from the average variance of replicate readings of the same sample observed over the whole study; 0.13% for the liquid fluorescein-tagged particles (Turner Model 450 Fluorometer) and 0.19% for the fluorescent PSL particles (Turner Quantech Model FM109515). The non-linearity error estimate in the fluorometer reading was given by the fluorometer manufacture as 0.1% of full scale for both models. The potential non-linearity error was relatively small as the maximum difference between the test and reference readings was never more than a 10:1 ratio.

One final source of precision error estimation bears discussion, and that was random error due to the non-constant aerosol generation rate (a manageable but inevitable error source with the use of either the VOAG or Collison nebulizer). One explanation for the change in observed aerosol generation rate for the VOAG may be due to the change in concentration of the non-volatile liquid (oleic acid in the present study) supplying generator when changing particle sizes due to contamination of the fluid lines and filtration from prior tests. For the Collison nebulizer, one should expect a slight change in aerosol production due to the fact that the atomization rates are not the same for the solid particles and distilled water that make up the source suspension, hence the suspension becomes either more or less concentrated with time, depending upon the relative atomization rates of the components. It was observed that submicrometer particles tended to atomize more readily than the water, while the reverse was true for particles larger than one micron.

The fact that the observed variances for some sets of reference and test filter particle concentration measurements were larger than that predicted from precision error analysis was taken to be a result of non-constant aerosol generator output. This assumption was supported by the fact that for some VOAG test particle experiments, a linear change in generator aerosol output was observed ($R^2 > 0.9$ to a linear fit of measured reference filter concentration vs. elapsed time). It should be noted that the average change in aerosol generator output was relatively small, averaging 5.6% per hour over all tests conducted, and that the change across two consecutive test and reference configurations (~ 20 minutes turnaround time) was less than 2%.

The temporal variation of the Collison nebulizer tests was somewhat higher than the VOAG (9.3% per hour), but had the advantage over the VOAG in that the temporal variation was more consistent (always either increasing or decreasing for the same particle size), so that applying a linear fit to the reference data produced a reliable comparison to the test measurements.

For all tests the value of minor collection efficiency was calculated from the ratio of averaged reference filter concentration to averaged test filter concentration. This averaging technique was different than that used in other studies in which the ratio of test/reference filter concentration for consecutive tests was averaged. This second method potentially introduces a bias error if the aerosol generator output is monotonically increasing or decreasing.

Although the efficiency measurements were not effected by the temporal variance of aerosol generation, the apparent precision of the measurements was unduly

exaggerated for the tests when the variance of the data was determined from the averaged quantity. For three cases of VOAG tests ($R^2 = 0.82, 0.94, 0.99$ for the linear fit equations) and all Collison nebulizer tests, the precision was estimated from the residuals of the linear fit. An 'aerosol generation' variance, s_{gen} , was estimated from this procedure, and was found to be 2.98% for the VOAG tests and 2.29% for the Collison nebulizer tests. The generator variance was treated as a precision error for the purposes of total error estimation.

RESULTS AND DISCUSSION

Preliminary Monodisperse Liquid Fluorescent Aerosol Tests

LSVI

Contrary to the numerical predictions, the initial experimental results showed significant particle deposition within the LSVI units. When operated at total flow rates required for a 0.8 μm AD cutpoint (75 L/min), LSVI Units 0 to 6 have collection efficiencies below 50% for particles larger than 2.5 microns (Table 5). After significant modifications to blade profile and manufacturing process, LSVI Unit 7 was shown to have collection efficiency of 50% and 67% for 2.2 and 6.8 μm AD particles, respectively. However, at flow rates well below that rate required for a 0.8 μm AD cutpoint, efficiencies were greater than 80% for two single-run tests conducted at those off-design flow rate conditions.

Besides qualitative fluorometric analysis, each LSVI was inspected for particle deposition following each liquid particle test. Regions of significant deposition of the fluorescent particles produced a stain visible under UV illumination. Three significant sources of deposition were identified; on the outlet taper plane of the receiver nozzle, on the port cover plates, and irregular spots of deposition on the nozzle throats associated with blade irregularities.

It was discovered early in the study that much greater deposition occurred on the receiver nozzle than on the acceleration nozzle (Figure 26). In the earliest LSVI units with simple taper receiver nozzles, the deposition was seen to begin at a point almost immediately below the vertex of the tapered wall. For this reason, a 0.508 mm (0.020")

abrupt expansion was incorporated to the receiver blade profile. All LSVI units after LSVI Unit 5 retained this feature. After adding this feature, the deposition pattern was observed to move to a location about 5 mm (3/16") below the vertex of the taper angle, possibly corresponding to the reattachment length of the receiver jet. A second abrupt expansion was added to the receiver nozzle in LSVI Units 7 and 8 to reduce the influence of this deposition mechanism (Figure 27). The second expansion began at the point 3.2 mm (0.125") below the taper angle vertex in the aligned direction. After incorporation of this compound expansion receiver nozzle profile, visible particle deposition was almost eliminated from the receiver nozzle (see Figures 8 to 13 for a comparison of the nozzle profiles).

Another source of particle losses was associated with the blade irregularities and imperfections. An example of these losses was deposition observed on LSVI Unit 7 at one end of the receiver nozzle due to a burr in the opposed acceleration nozzle (Figure 28). On the acceleration nozzle, a burr approximately 2 mm (1/16") long and protruding into the flow path about 60 μm (0.005") was found at one end of the acceleration nozzle (but several nozzle diameters above the nozzle throat). Particle deposition was observed on the receiver nozzle directly below this burr, but not on the opposite end of the LSVI unit. This result demonstrated the sensitivity of wall losses to nozzle geometry in the critical region.

CSV I

Monodisperse liquid particle tests were conducted on the CSV I unit as well. As in the LSVI, significant deposition losses were observed on the receiver throat (Figure

29). The total collection efficiency was measured to be 10% for 6.6 μm AD aerosol particles at a nozzle Reynolds number of 430, and 20% for a nozzle Reynolds number of 165 for CSVI Unit 1.

Polystyrene Latex Particles with Aerodynamic Particle Sizer

The collection efficiency curves from the PSL test showed two distinct regions of behavior for LSVI Unit 7. For flow rates below 35 L/min (1.2 CFM), classical virtual impactor performance was observed with the estimated value of Stk_{50} equal to about 0.7 (Figure 30). For flow rates above 35 L/min (1.2 CFM), a departure from classical behavior was observed and the LSVI asymptotically approached the behavior of a high-loss mixing element. At a nozzle Reynolds number of 1000 (90 L/min or 3.2 CFM total flow), the highest flow rate tested, the aerosol concentrations in the major and minor flow paths were approximately equal and independent of particle size; i.e. there was no concentration of particles in the minor flow stream even at particle Stokes numbers significantly greater than unity, contrary to normal virtual impactor behavior (Figure 31). Furthermore, the sum of the collection efficiencies of the major and minor flow path was observed to decline with increase in total flow rates beyond 35 L/min (1.2 CFM), evidence of increasing particle losses.

Acoustic Measurements

During the course of the PSL testing, a previously undetected acoustic “ringing” of LSVI Unit 7 was observed. When the virtual impactor was connected to the vacuum system and the flow rate gradually increased, a distinct audible tone was observed to emanate from the LSVI units for all flow rates above about 45 L/min (1.6 CFM),

corresponding to acceleration nozzle Reynolds number of 540. As the flow was increased above 45 L/min (1.6 CFM), the intensity of the tone increased with flow rate up to the highest flow rate tested, 90 L/min (3.2 CFM). Below 45 L/min (1.6 CFM), no “ringing” was observed (Sound Media Files 1 to 4). For the CSVI Unit 2, with nozzle width of 0.508 mm (0.020”), a similar trend was observed where the critical flow rate corresponding to the onset of ringing was 140 L/min (5 CFM), corresponding to nozzle Reynolds number of 310. For CSVI Unit 1, with nozzle width 0.190 mm (0.0075”), no critical flow rate associated with the onset of ringing was identified, and intermittent ringing was observed for all flow rates from 20 to 220 L/min.

For the LSVI Unit 8 and CSVI Unit 2, the power spectrum analysis of the sound recordings agreed well with qualitative observation. For the LSVI, no distinct frequency in the sound power spectrum was observed over the five sub-samples analyzed for flow rates below 45 L/min (Figures 32 and 33). At every flow rate above 45 L/min, a consistent ring tone was observed having a fundamental frequency of 2850 Hz (Figures 34 and 35). A consistent ringing tone was also measured at the first octave of the fundamental. Further increases in flow rate above the critical flow rate did not change the frequency of the tone, but did increase the relative intensity of the tone by a factor of ten when the flow increased from 50 L/min to 70 L/min (Figures 36 and 37). The tone of greatest sound intensity was observed to be the second octave of the fundamental for LSVI Unit 8. For the CSVI Unit 2, similar sound spectra were observed for flow rates just below and above the critical flow value (Figures 38 to 41). The frequency of the fundamental tone was observed to be 1310 Hz, but the power spectrum analysis did not

show as great of a change in sound intensity at the onset of resonance for CSVI Unit 2 as for LSVI Unit 8 (Figures 42 and 43).

In an attempt to restrict any possible motion of the blade tips of the LSVI nozzle, the acoustic experiments were repeated after fitting five 0.6 mm diameter (0.020") wire segments between the acceleration and receiver nozzle. The wire diameter and material (copper) was such that the wires were firmly compressed between the acceleration and receiver nozzle, effectively clamping the nozzle tips at five points along the nozzle length. The sound measurements of this 'clamped' LSVI virtual impactor were identical to those obtained with the unclamped unit, further indication that the ringing phenomenon was not associated with the elastic properties of the nozzles (Figures 36 and 37).

The non-dimensional parameter associated with periodic fluctuations of a fluid is the Strouhal number, S :

$$S = \frac{nW}{U_o}$$

where:

n = the characteristic frequency (fundamental tone of resonance)

W = the nozzle width

U_o = mean nozzle velocity

For the LSVI, the Strouhal number associated with the onset of ringing was 0.032 and for the CSVI Unit 2 it was 0.069. For flow-induced vibrations or

phenomenon associated with vortex shedding or other period flow disturbances, the Strouhal number usually has a value within an order of magnitude of unity. For example, the Strouhal number associated with vortex shedding behind a cylinder in cross flow is 0.17 to 0.25 for Reynolds numbers from 10^2 to 10^7 (Roberson and Crowe, 1993), implying near-proportionality between frequency and velocity over a wide range of Reynolds number. Because in the present case $S \ll 1$ and the frequency was observed independent of flow rate, vortex shedding or periodic flow fluctuations were not likely the source of the resonant tone.

A more probable explanation for the ringing phenomenon is that described by the Helmholtz resonator. In basic form a Helmholtz resonator consists of a relatively small mass of air in a throat or aperture oscillating, due to an applied agitation, in resonance with a larger cavity of air fluidly connected to the aperture. An example of a Helmholtz resonator is the whistle produced when blowing air across the inlet of a bottle. Fletcher and Rossing (1998) give the resonance frequency of the Helmholtz resonator, f_o , as:

$$f_o = \frac{c}{2\pi} \cdot \sqrt{\frac{A}{V \cdot L}}$$

where:

c = speed of sound in air

A = area of the aperture

V = volume of the cavity behind the aperture

L = throat depth of the aperture

Using the throat length of the receiver nozzle as L , and the volume of the minor flow channel in LSVI Unit 8 predicted a fundamental frequency of 650 Hz, significantly lower than the resonance tone observed. However, it should be noted that the impingement of the fluid jet on the receiver throat may have lowered the effect depth of the oscillating fluid mass and hence raised the frequency of the fundamental tone.

Liquid and Polystyrene Latex Fluorescent Monodisperse Aerosol Tests

When the characterization tests were conducted with LSVI Unit 8 and CSVI Unit 2 at flow rates below the onset of ringing for the respective concentrators, classical virtual impactor performance was observed. The data for all tests, along with uncertainty estimates determined from the methods described above, are seen in Table 6.

LSVI Unit 8

The collection efficiency in the minor flow of LSVI Unit 8 at 38 L/min (1.3 CFM) corresponding to nozzle Reynolds number 445 is seen in Figure 44. The particle cutpoint corresponding to 50% collection efficiency was 1.1 $\mu\text{m AD}$. The collection efficiency peaks at a value of 95% at a particle size of 3.5 $\mu\text{m AD}$. The collection efficiency reduced with particle size to a value 72% for 9.6 $\mu\text{m AD}$ particles.

The total major flow collection efficiency shows a complimentary reduction in collection efficiency for particle sizes near the cutpoint as expected (Figure 45). One interesting result was the skewness observed between the left and right major flow collection efficiencies (Figure 46). As noted above, LSVI Unit 8 retained some skewness in nozzle geometry, and the pressure drop across the left and right major flow

path was not identical when the flow rates were held identical. At particle sizes below the cutpoint, the relative difference between the left and right collection was low (35% right, 45% left for 0.6 μm AD particles). As the particle size increased above the cutpoint, the reduction in particles entering the respective flow streams was nearly the same, so that for particles larger than about 1.7 μm AD, all particles that entered the major flow (16%) entered only on the left major flow stream.

The wall loss analysis of LSVI Unit 8 shows losses approximately constant nozzle wall losses between 5 and 10% for particle sizes between 2 and 7 μm AD (Figure 47). Losses were at a maximum of 26% for the largest particle size tested (9.6 μm AD).

CSVI Unit 2

The collection efficiency in the minor flow of CSVI Unit 2 at 122 L/min (4.3 CFM) is seen in Figure 48. The particle cutpoint corresponding to 50% collection efficiency was 2.2 μm AD. The collection efficiency peaks at a value of 96% at a particle size of 4.7 μm AD. Further increases in particle size reduced the efficiency to a value of 77% for the largest particle size tested (9.8 μm AD). As for LSVI Unit 8, the reduction in minor flow efficiency was attributed to particle losses. However, for CSVI Unit 2, wall losses in the critical zone were significantly less than for the LSVI unit (Figure 49). These reduced losses in the critical zone were attributed to the lower Stokes number of the corresponding particle size of the CSVI unit relative to the LSVI unit, and the relative superiority of the nozzle precision of CSVI Unit 2 over LSVI Unit 8. The sum of the measured wall losses and minor flow collection did not account for all the particulate mass for the CSVI Unit 2 tests. A likely explanation for the observed mass

defect was losses that occurred in regions other than the critical zone due to the relatively more torturous flow path required of the aerosol entering the CSVI unit compared to the LSVI unit. Aerosol entered the CSVI device through a 50.8 mm (2") diameter tube and was then deflected radially outward by a blunt deflection cone. The aerosol was then aspirated into one of ten oblong cross-section entrance ports in the entrance annulus of the CSVI unit (Figures 4 and 6). Once aspirated, the flow was again diverted radially inward through an aerodynamically smoothed transition and accelerated in the impinging nozzle.

Despite the similarity in minor collection efficiency results at large particle sizes, it should not be assumed that there would be equal performance of the LSVI and CSVI units having the same nozzle width and total flow rate. The several LSVI units would be required to provide the total slot length of a single CSVI unit, and additional particle losses due to nozzle end effects and flow splitting/diversion in the LSVI array could be expected.

Modeling

When the minor flow collection efficiency data of the LSVI and CSVI units were compared on the common basis of particle Stokes number, near equivalent particle concentration behavior was observed for all particles sizes except those well above the cutpoint due to the differences particle loss mechanisms described above (Figure 50). Within experimental uncertainty, the cutpoint and collection efficiency curves were identical despite the differences in nozzle Reynolds number (445 for the LSVI and 270 for the CSVI unit). In order to describe the collection efficiency for a long-slot virtual

impactor for Reynolds numbers between 445 and 270, the following model was proposed:

$$\eta_{\text{minor}} = 1 - \frac{(1-r)}{1 + \left[\frac{Stk}{Stk_{50}} \right]^b}$$

where:

η_{minor} = minor flow collection efficiency

Stk = particle Stokes number (the independent variable)

Stk_{50} = the particle Stokes number corresponding to the cutpoint

b = coefficient determining sharpness of collection efficiency curve

r = minor/total flow ratio

The model has only two parameters; Stk_{50} , which is determined from particle cutpoint and the exponent, b . Although the data in the present study covered a range of Stokes numbers from 0.04 to 38, the model has the proper asymptotic behavior in the respective limits of Stokes number, namely that the minor flow concentration approaches the minor flow splitting ratio as $Stk \rightarrow 0$ and approaches 100% as $Stk \rightarrow \infty$. The proposed model was intended to describe the inertial separation characteristics of the virtual impactor and not include effects of the particle losses on the nozzle wall or due to other mechanisms that were observed at Stokes numbers well above the cutpoint.

For this reason, the experimental data was corrected to remove the effect of particle losses when determining the best-fit values of the model parameters.

To remove particle loss effects for the purposes of fitting data to the model, a simple linear fit to minor collection efficiency curve for $Stk \gg 1$ was determined. Because wall losses were not the same for the LSVI and CSVI units, a separate wall loss equation was fit to each data set. The wall loss correction was significant only for the largest particles tested (25% for $Stk = 38$) and was 0.3% at the cutpoint. The losses predicted from the linear fit were then added to the measured minor flow collection efficiencies and a single data set was generated (Figure 51). The model parameters were then fit to the common data set by minimization of the squares of the residuals (least-squares fit). The values obtained for the model parameters were $Stk_{50} = 0.568$ and $b = 1.79$ (Figure 52).

Treatment of Polydisperse Test Aerosols

As described above, APS particle size samples were taken of the monodisperse test aerosols generated in the characterization experiments. In addition to the aerodynamic spectra of the liquid particles, coulter-counter samples of the solid PSL microspheres were taken. For all ‘monodisperse’ test aerosols, a small but finite variance in particle size distribution was observed. Because inertial classifiers often have sensitive dependence on particle size for particles near the cutpoint, errors can potentially result from assigning measured collection efficiency values to a discrete particle size. In order to properly account for the variance in particle size of the test

aerosols, an iterative procedure for fitting the model parameters to the measured collection efficiency data was applied.

For each test aerosol, a discrete fractional mass spectrum was computed from particle the count data. Based upon assumed values for the model parameters (Stk_{50} , b), the integrated product of fractional efficiency and mass fraction was computed. This integrated mass percentage was compared with the measured mass fraction (efficiency) and the residual computed ($[\text{computed value} - \text{measured value}]^2$). The residuals of all tests were summed, and an iterative procedure was applied to determine the values of model parameters that minimized the total residual. The value of Stk_{50} was nearly identical for each procedure- 0.577 for the polydisperse treatment and 0.568 for monodisperse assumption, but the coefficient b was 1.56 for the polydisperse analysis and 1.79 for the monodisperse assumption. A comparison of the calculated collection efficiency curve and the size distribution of three representative test aerosols is seen in Figure 53.

SUMMARY

Two linear nozzle virtual impactor/concentrators were constructed and characterized. Both devices were longer-slot (L/W), lower Reynolds number, and lower pressure drop than previous studies of such virtual impactors (Table 7). The value of Stk_{50} was 0.577 for both devices, corresponding to a particle cutpoint size of 1.1 $\mu\text{m AD}$ for the LSVI configuration and 2.2 $\mu\text{m AD}$ for the CSVI. The collection efficiency was greater than 72% for all particle sizes larger than three times the cutpoint up to the largest particle size tested ($\approx 10 \mu\text{m AD}$). The peak collection efficiency for both concentrators was greater than 95%.

An acoustic resonance was observed at Reynolds numbers above 500 for the LSVI configuration, and above 300 for the CSVI configuration. The Strouhal number was 0.03 and 0.07, respectively, and attempts to fix the blade tip position had no effect on the resonance, an indication that the phenomenon was not associated with either periodic flow disturbances in the nozzle or mechanical motion of the blade tips. For flow conditions with acoustic resonance, normal virtual impactor behavior broke down, and high particle wall losses were observed.

REFERENCES

- Berglund, R. N., and Liu, B. Y. H. (1973). Generation of Monodisperse Aerosol Standards, *Environ. Sci. Technol.* 7:147-153.
- Beckwith, T. G., and Marangoni, R. D. (1990). *Mechanical Measurements*, Addison-Wesley Publishing Co., Reading, MA.
- Chang, M-C., Geller, M. D., Sioutas, C., Fokkens, P. H. B., and Cassee, F. R. (2001). Development and Evaluation of a Compact, Highly Efficient Coarse Particle Concentrator for Toxicological Studies, *Aerosol Sci. and Technol.* 36:492-501.
- Chein, H., and Lundgren, D. A. (1995). A High-Output, Size-Selective Aerosol Generator, *Aerosol Sci. and Technol.* 23:510-520.
- Chein, H., and Lundgren, D. A. (1993). A Virtual Impactor with Clean Air Core for the Generation of Aerosols with Narrow Size Distributions, *Aerosol Sci. and Technol.* 18:376-388.
- Chen, B. T., Cheng, Y. S., and Yeh, H. C. (1990). A Study of Density Effect and Droplet Deformation in the TSI Aerodynamic Particle Sizer, *Aerosol Sci. and Technol.* 12:278-285.
- Chen, B. T., and Yeh, H. C. (1987). An Improved Virtual Impactor: Design and Performance, *J. Aerosol Sci.* 18:203-214.
- Conner, W. D. (1996). An Inertial-Type Particle Separator for Collecting Large Samples, *J. Air Pollut. Control Assoc.* 1:35-38.

- Ding, Y., Ferguson, S. T., Wolfson, J. M, and Koutrakis, P. (2000). Development of a High Volume Slit Nozzle Virtual Impactor to Concentrate Coarse Particles, *Aerosol Sci. and Technol.* 34:274-283.
- Ding, Y., and Koutrakis, P. (2000). Development of a Dichotomous Slit Nozzle Virtual Impactor, *J. Aerosol Sci.* 31:1421-1431.
- Farthing, W. E. (1998). Problem Definition: Collection Requirements vs. Aerosol Fundamentals, *Proceedings of the Naval Surface Warfare Center Information Exchange on Bioaerosol Sample Collection*, March 16-18, 1998, Dahlgren, VA.
- Fletcher, N. H., and Rossing, T. D. (1998). *The Physics of Musical Instruments*, Springer-Verlag, New York, NY.
- Forney, L. J., Ravenhall, D. G., and Lee, S. S. (1982). Experimental and Theoretical Study of a Two-Dimensional Virtual Impactor, *Environ. Sci. Technol.* 16:492-497.
- Forney, L. J., Ravenhall, D. G., and Winn, D. S. (1978). Aerosol Impactor: A Study of a Fluid Jet Impinging Upon a Void, *J. Appl. Phys.* 49:2339-2345.
- Griffiths, W. D., Iles, P. J., and Vaughan, N. P. (1986). The Behavior of Liquid Droplet Aerosols in an APS 3300, *J. Aerosol Sci.* 17:921-930.
- Gussman, R. A. (1984). Note on the Particle Size Output of Collison Nebulizers, *Am. Ind. Hyg. Assoc. J.* 45:B8-B12.
- Haglund, J. S., Chandra, S., and McFarland, A. R. (2002). Evaluation of a High Volume Aerosol Concentrator, *Aerosol Sci. and Technol.*, 36:690-696.
- Hall, D. E. (1991). *Musical Acoustics*, Brooks/Cole Publishing Co., Pacific Grove, CA.

- Han, R., and Moss, O. R. (1997). Flow Visualization Inside a Water Model Virtual Impactor, *J. Aerosol Sci.* 28:1005-1014.
- Hari, S. (2003, December). Computational Fluid Dynamics (CFD) Simulations of Dilute Fluid-Particle Flows, Ph.D. dissertation, Department of Nuclear Engineering, Texas A&M University, College Station, TX.
- Hassan, Y. A., Jones, B. G., and Yule, T. J. (1979). An Analytical Study of Virtual Impactor Aerosol Separators, *Trans. Amer. Nucl. Soc.* 33:182-184.
- Hinds, W. C. (1999). *Aerosol Technology*, John Wiley and Sons, Inc., New York, NY.
- Hounam, R. F., and Sherwood, R. J. (1965). The Cascade Centripeter: A Device for Determining the Concentration and Size Distribution of Aerosols, *Amer. Ind. Hyg. Assoc. J.* 26:122-131.
- Kesavan, J., Doherty, R. W., Wise, D. G., and McFarland, A. R. (2001). Factors that Affect Fluorescein Analysis, Edgewood Chemical Biological Center, U.S. Army Soldier and Biological Chemical Command, Final report ECBC-TR-208, Edgewood, MD.
- Lide, D. R., (1992). *CRC Handbook of Chemistry and Physics*, D. R. Lide, Editor-in-Chief, CRC Press, Boca Raton, FL.
- Lin, H., and Heintzenberg, J. (1995). A Theoretical Study of the Counterflow Virtual Impactor, *J. Aerosol Sci.* 26:903-914.
- Loo, B. W., and Cork, C. P. (1988). Development of High Efficiency Virtual Impactors, *Aerosol Sci. and Technol.* 9:167-176.

- Marple, V. A., and Chien, C. M. (1980). Virtual Impactors: A Theoretical Study, *Environ. Sci. Technol.* 14:976-985.
- Masuda, H., Hochrainer, D., and Stober, W. (1979). An Improved Virtual Impactor for Particle Classification and Generation of Test Aerosols with Narrow Size Distributions, *J. Aerosol Sci.* 10:275-287.
- May, K. R. (1973). The Collison Nebulizer: Description, Performance and Application, *J. Aerosol Sci.* 4:235-243.
- Moshier, T. and Buonaugurio, T. (2000). Joint Biological Point Detection System (JBPDS) Requirements and Design Interplay, *Proceedings of the First Joint Conference on Point Detection for Chemical and Biological Defense*, October 23-27, 2000, Williamsburg, VA
- Olan-Figueroa, E., McFarland, A. R., and Ortiz, C. A. (1982). Flattening Coefficients for DOP and Oleic Acid Droplets Deposited on Treated Glass Slides, *Am. Ind. Hyg. Assoc. J.* 43:395-399.
- Peterson, C. M. (2003). President, SCP Controls, Inc., Minneapolis, MN, personal communication.
- Pilacinski, W., Ruuskanen, J., Chen, C. C., Pan, M. J., and Willeke, K. (1990). Size-Fractioning Aerosol Generator, *Aerosol Sci. and Technol.* 13:450-458.
- Ravenhall, D. G., Forney, L. J., and Jazayeri, M. (1978). Aerosol Sizing with a Slotted Virtual Impactor, *J. Colloid Interface Sci.* 1:108-117.
- Roberson, J. A., and Crowe, C. T. (1993). *Engineering Fluid Mechanics*, Houghton Mifflin Co., Boston, MA.

- Rosen, P. (1999). *Chemical and Biological Terrorism: Research and Development to Improve Civilian Medical Response*, Committee on R&D Needs for Improving Civilian Medical Response to Chemical and Biological Terrorism Incidents, P. Rosen, Committee Chair, National Academy Press, Washington, DC.
- Sioutas, C., Kim, S., and Chang, M. (1999). Development and Evaluation of a Prototype Ultrafine Particle Concentrator, *J. Aerosol Sci.* 30:1001-1017.
- Sioutas, C., Koutrakis, P., and Olson, B. A. (1994a). Development and Evaluation of a Low Cutpoint Virtual Impactor, *Aerosol Sci. and Technol.* 21:223-235.
- Sioutas, C., Koutrakis, P., and Burton, R. M. (1994b). Development of a Low Cutpoint Slit Virtual Impactor for Sampling Ambient Fine Particles, *J. Aerosol Sci.* 25:1321-1330.
- Sioutas, C., Koutrakis, P., and Burton, R. M. (1994c). A High-Volume Small Cutpoint Virtual Impactor for Separation of Atmospheric Particulate from Gaseous Pollutants, *Particle Sci. and Technol.* 12:207-221.
- White, F. M. (1994). *Fluid Mechanics*, McGraw-Hill, Inc., New York, NY.
- Wolf, W. P. and Hohe, D. R. (2000). JBPDS Block I EMD Program Overview and Summary, *Proceedings of the First Joint Conference on Point Detection for Chemical and Biological Defense*, October 23-27, 2000, Williamsburg, VA.

APPENDIX A
TABLES AND FIGURES

Table 1. Comparison of cutpoint Stokes numbers of virtual impactor studies at minor/total flow ratio of 10%.

Reference	Nozzle Type	Nozzle Width (mm)	L/W	Re	Pressure Drop (kPa)	$(Stk_{50})^{1/2}$	Stk_{50}
Hinds (1982)	Circular	*	*	*	*	0.49	0.24
"	Rectangular	*	*	*	*	0.77	0.59
Sioutas et al. (1994b)	Rectangular	0.35	43	2,370	12.20	0.55	0.30
"	Rectangular	0.23	65	1,110	8.50	0.50	0.25
"	Rectangular	0.23	65	1,780	18.10	0.48	0.23
Sioutas et al. (1994c)	Rectangular	0.33	170	4,460	30.00	0.45	0.20
Ding and Koutrakis (2000)	Rectangular	3.05	2.5	1,500	0.04	0.69	0.48
"	Rectangular	3.05	2.5	4,400	0.35	0.71	0.50
"	Rectangular	3.05	2.5	7,300	1.02	0.68	0.46
"	Rectangular	3.05	2.5	12,000	2.74	0.70	0.49
"	Rectangular	3.05	2.5	15,000	4.11	0.68	0.46

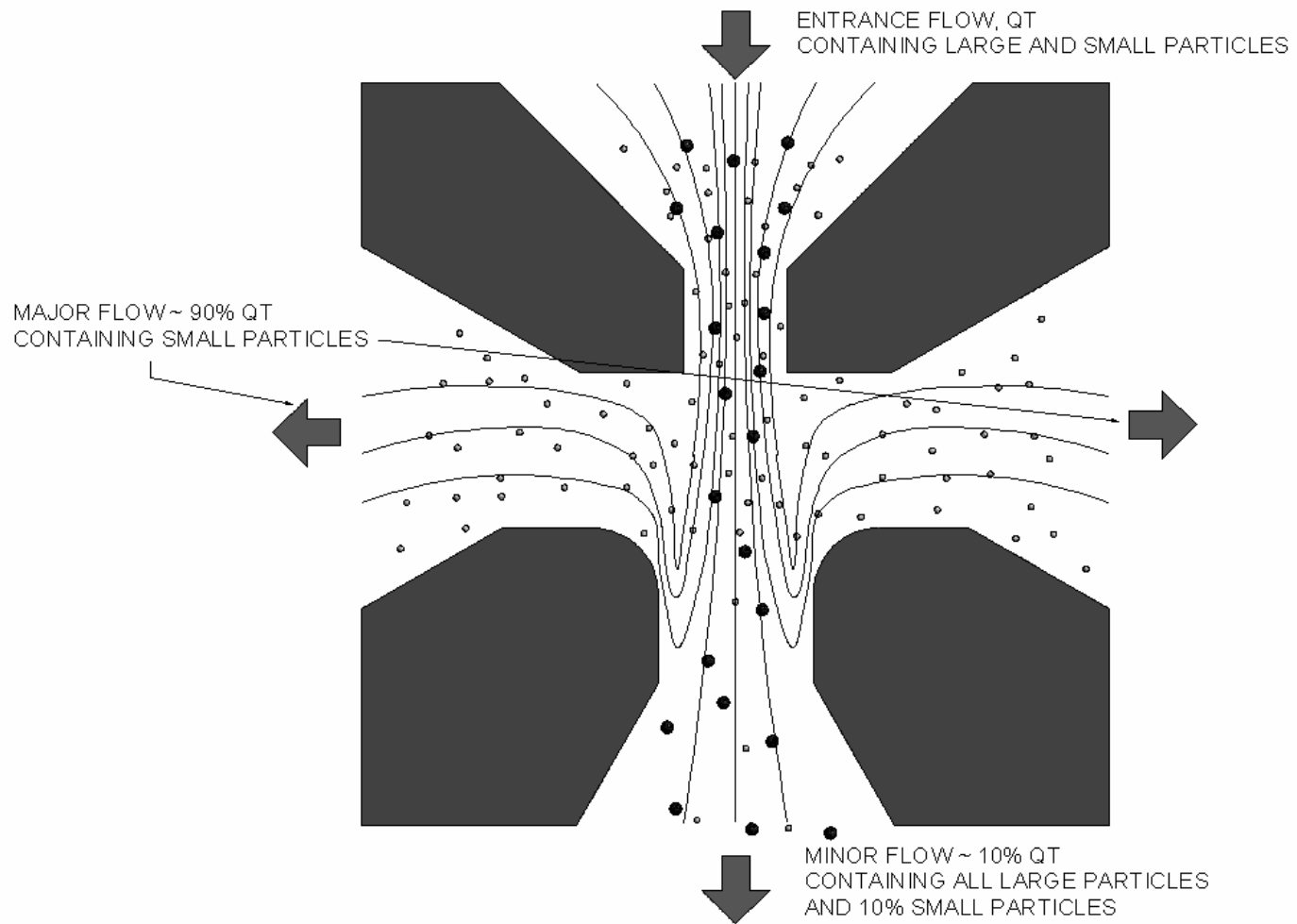


Figure 1. The concept of virtual impaction.

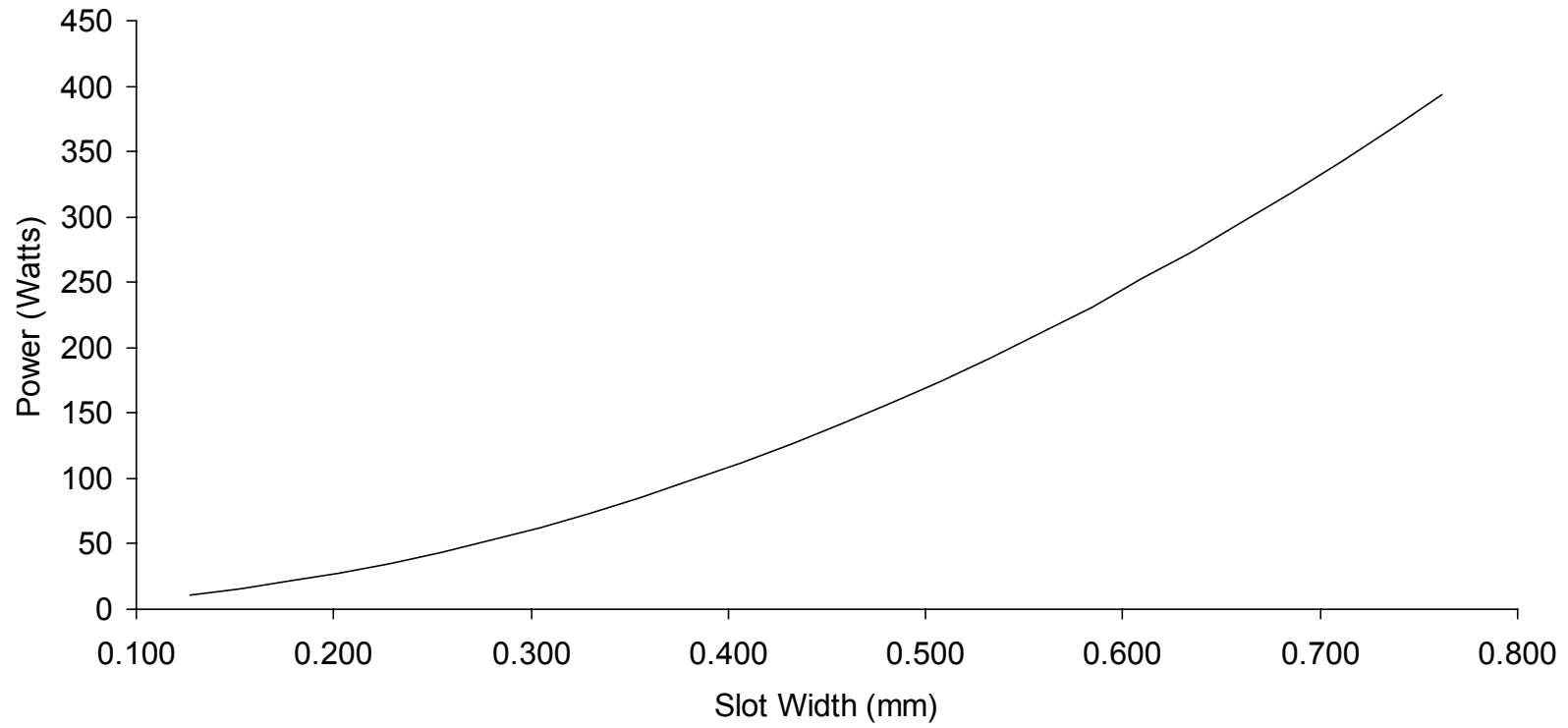


Figure 2. Theoretical power required for a slot nozzle virtual impactor/concentrator operating at 500 L/min with 0.8 μm AD cutpoint (minor loss coefficient, $K = 1$).

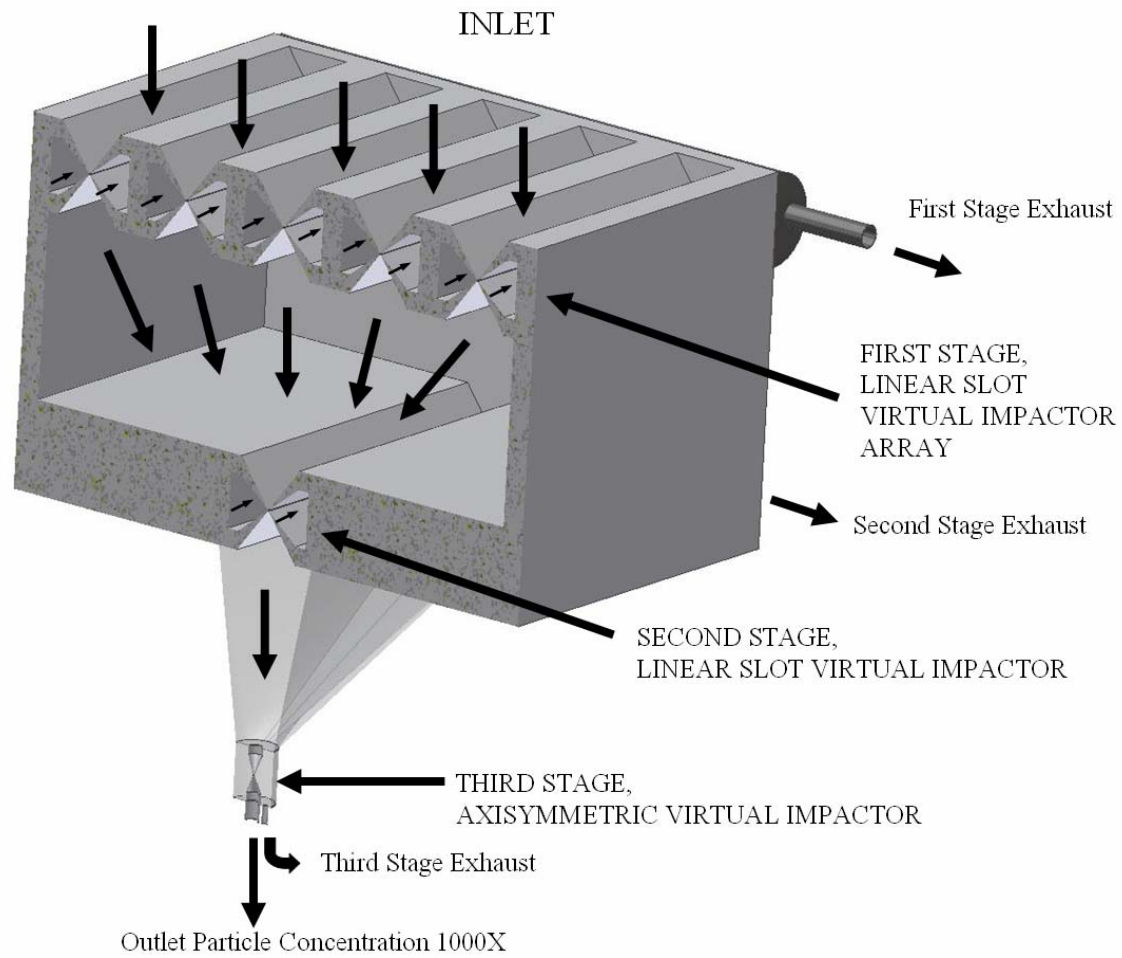


Figure 3. Conceptual design of a bioaerosol concentrator based on multiple stages of linear slot nozzle virtual impactors.

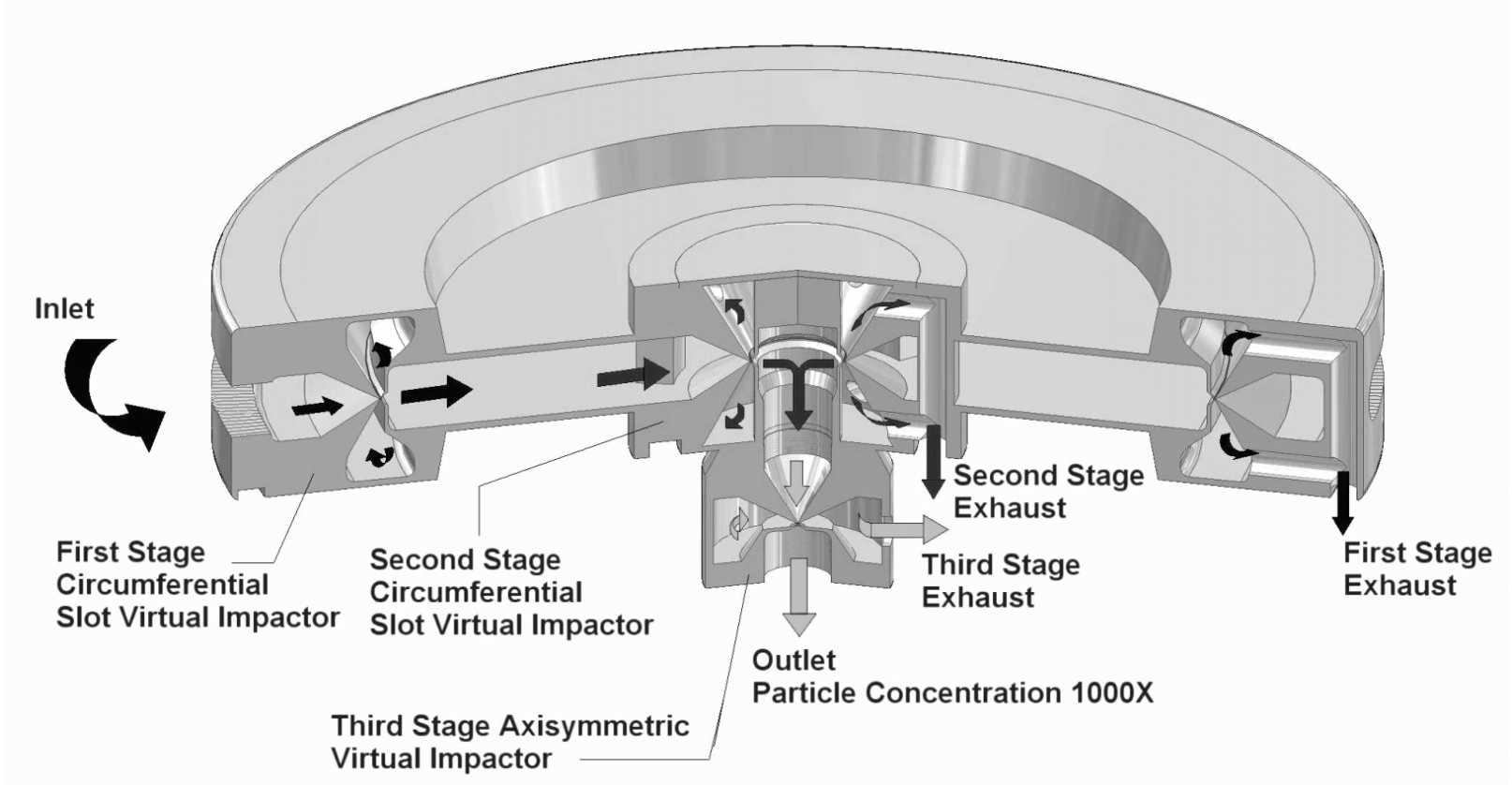


Figure 4. Conceptual design of a bioaerosol concentrator based on multiple stages of circumferential slot nozzle virtual impactors.

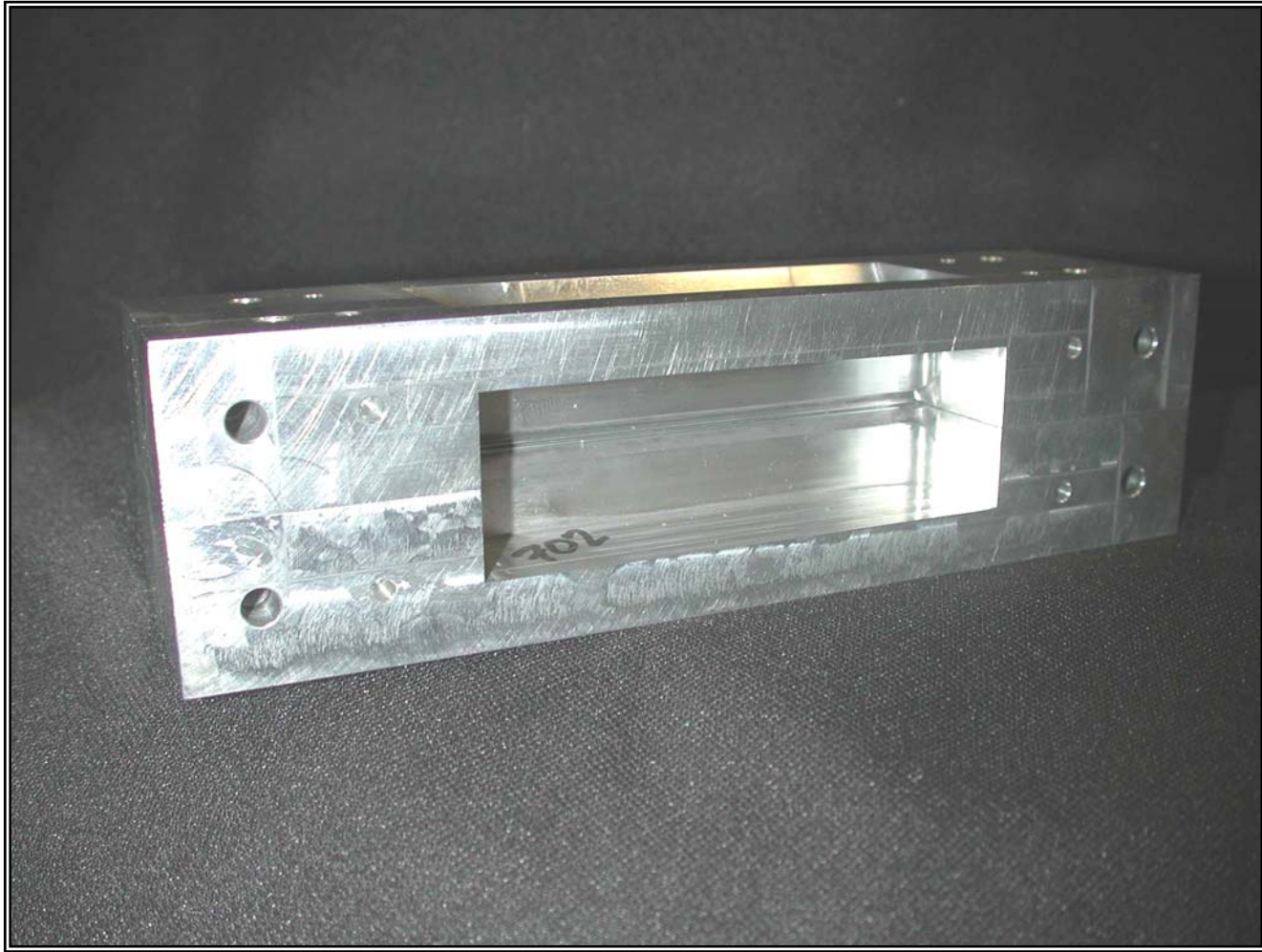


Figure 5. Photograph of prototype LSVI unit.



Figure 6. Photograph of prototype CSVI unit (split into half-assemblies).

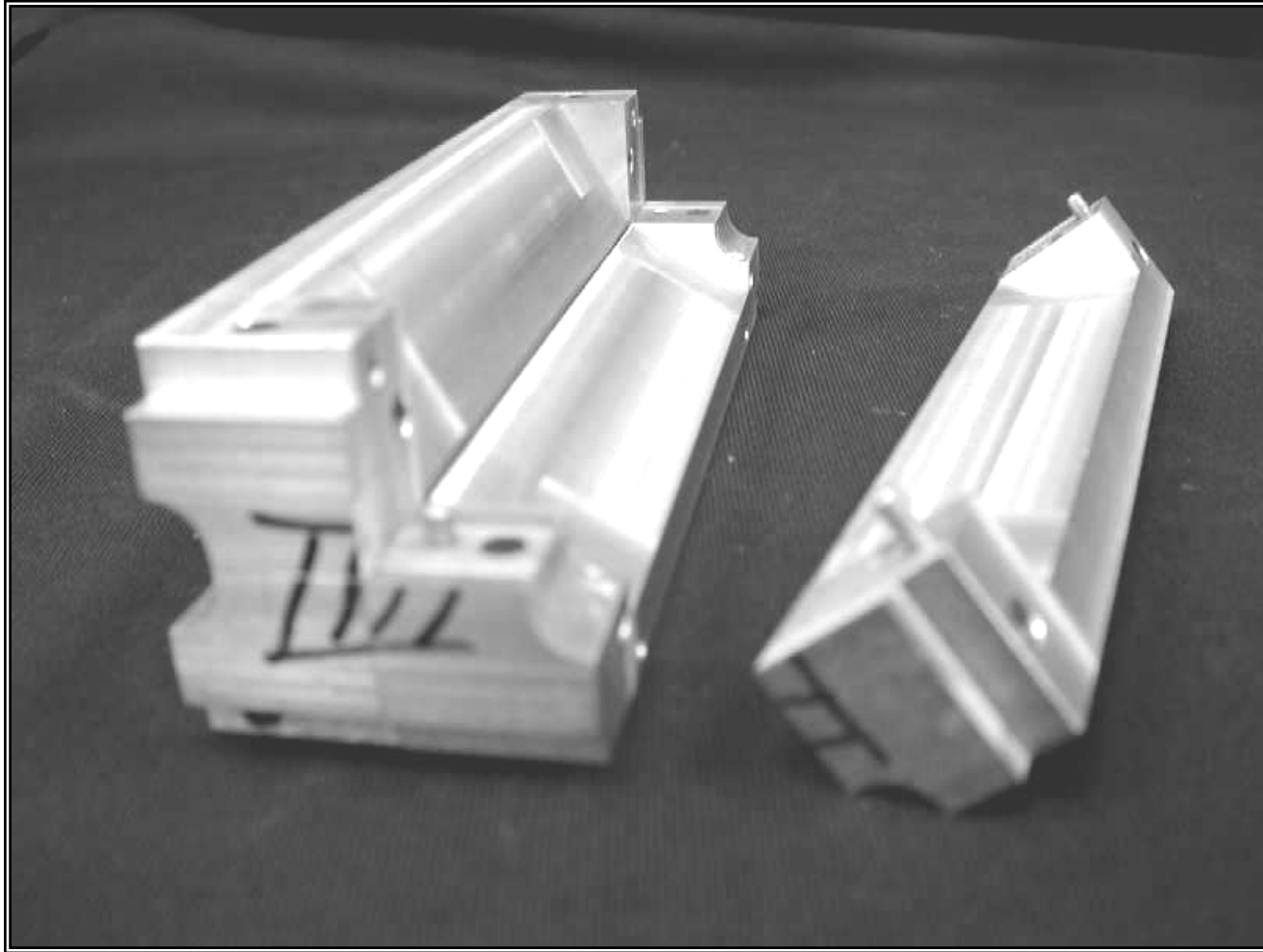
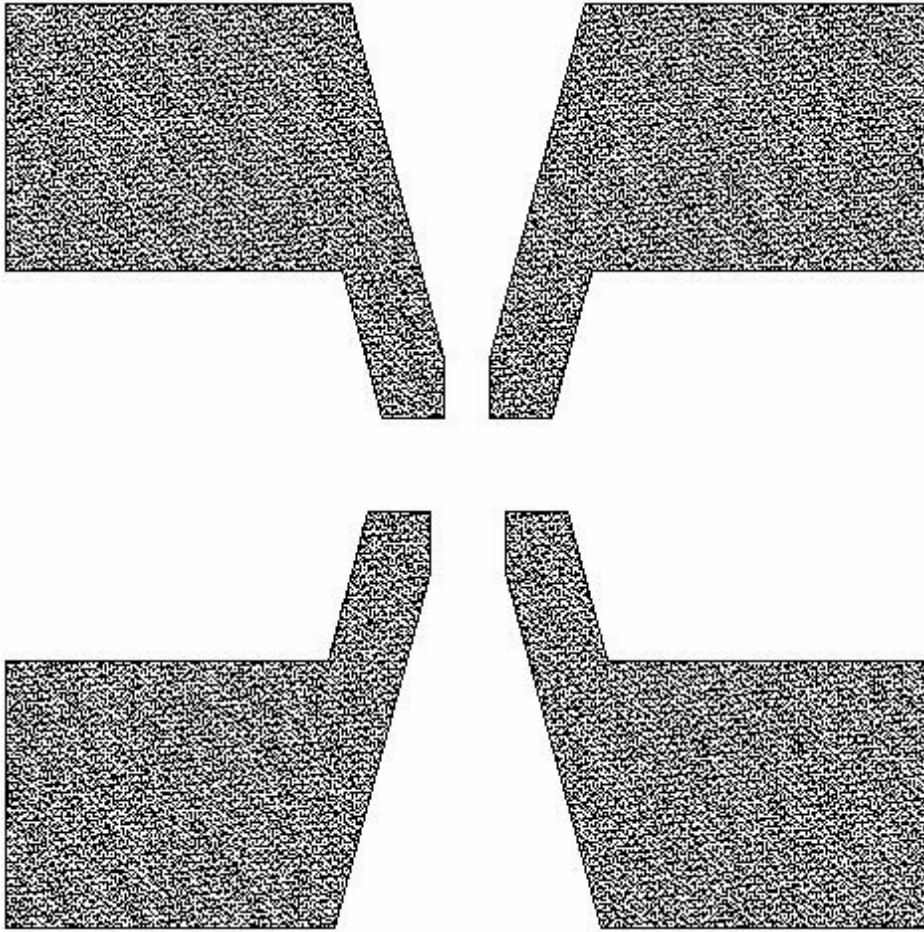


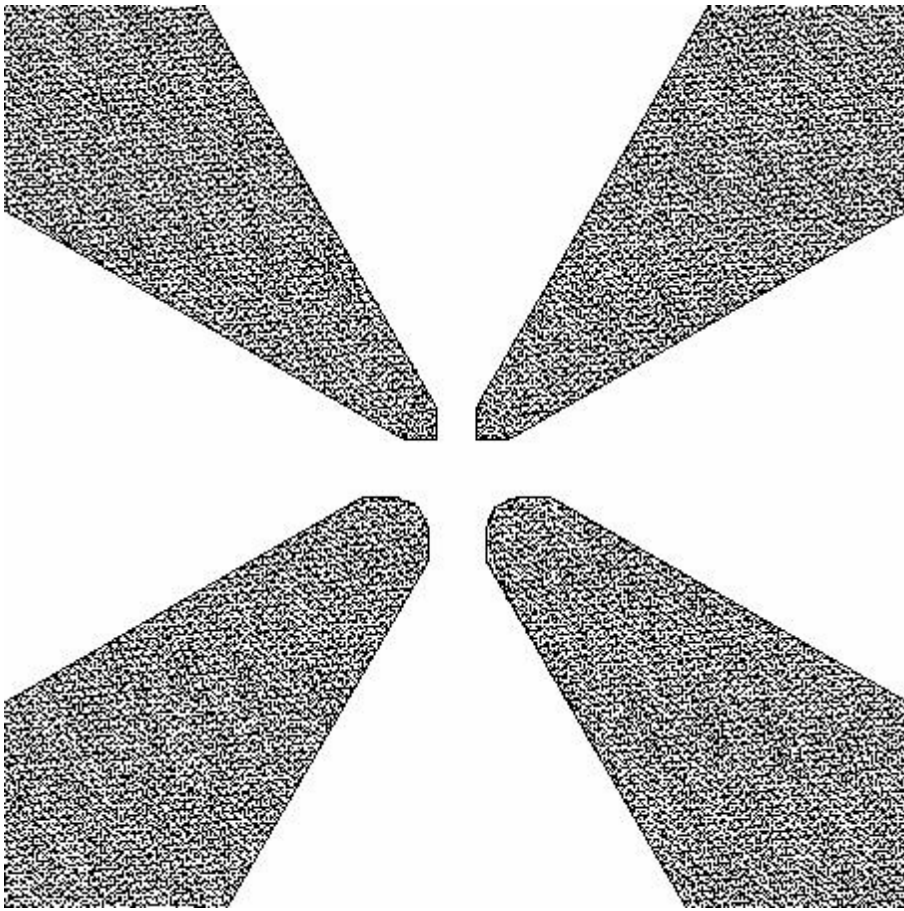
Figure 7. Four-block assembly of LSVI units (left acceleration blade detached).



Dimensions:

Acceleration nozzle width:	0.381 mm (0.015")
Receiver nozzle width:	0.635 mm (0.025")
Slot length:	127 mm (5.000")
Receiver nozzle taper:	30°
Material:	Al 6061

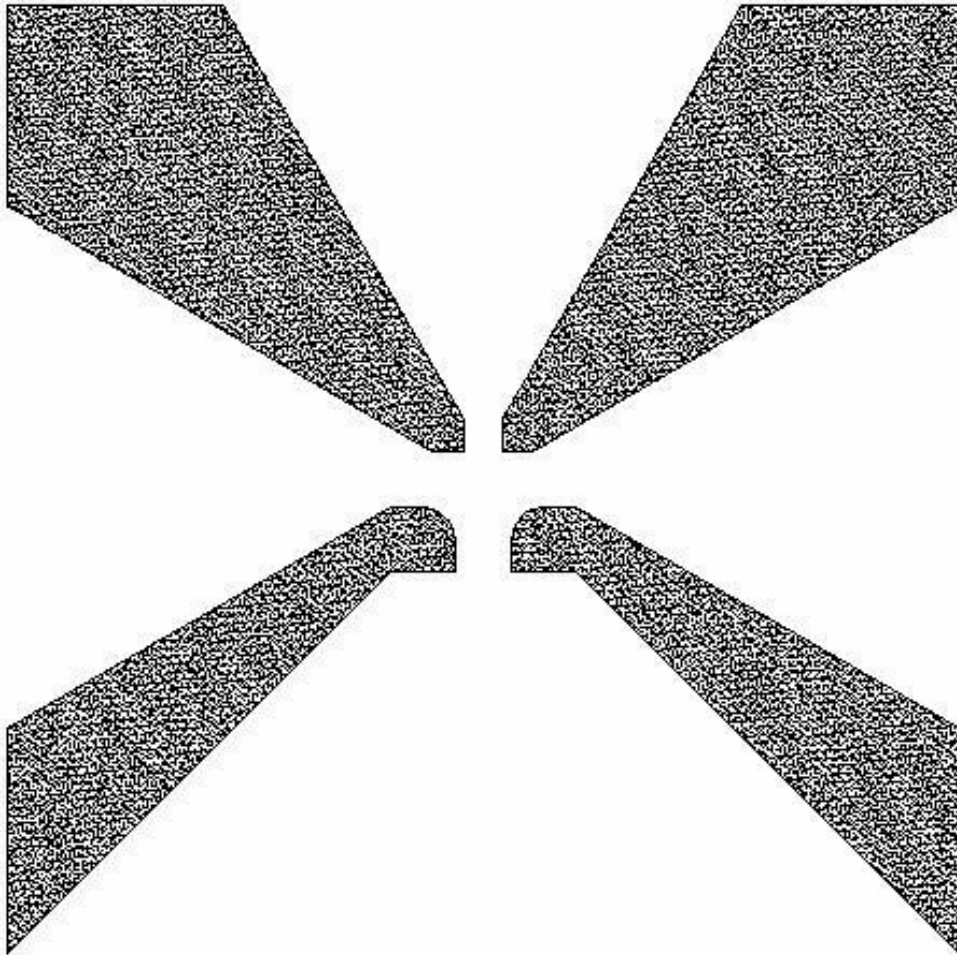
Figure 8. Nozzle cross-section of LSVI Unit 0.



Dimensions:

Acceleration nozzle width:	0.305 mm (0.012")
Receiver nozzle width:	0.457 mm (0.018")
Slot length:	127 mm (5.000")
Receiver nozzle taper:	60°
Material:	Al 7075 (LSVI Unit 2 304 Stainless Steel)

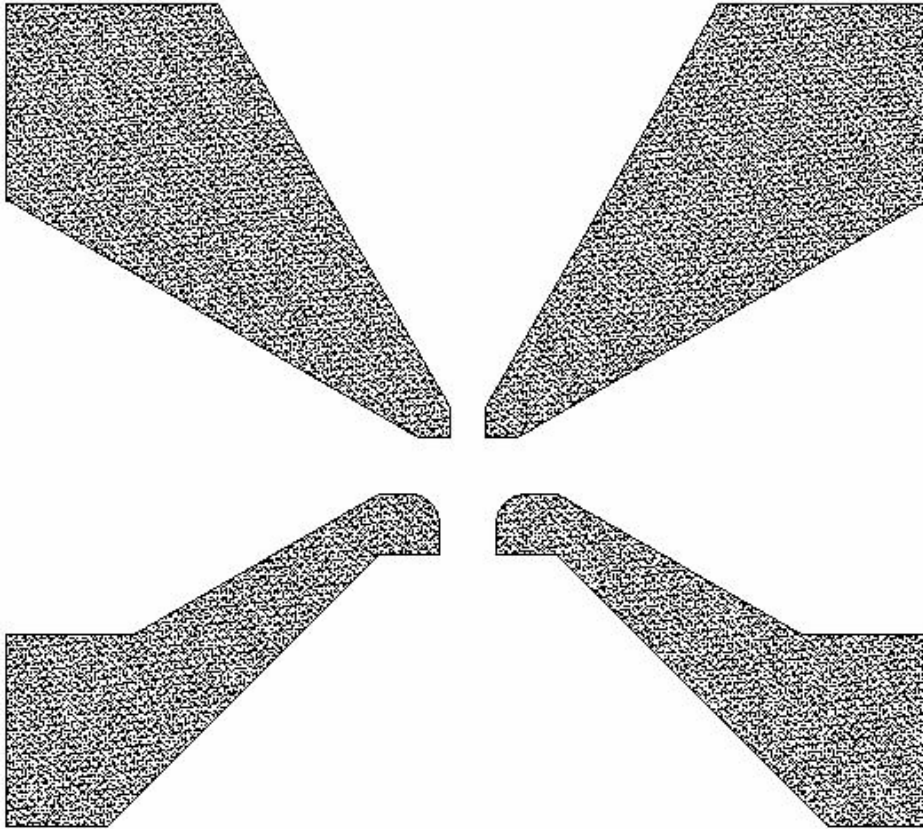
Figure 9. Nozzle cross-section of LSVI Units 1 to 4.



Dimensions:

Acceleration nozzle width:	0.305 mm (0.012")
Receiver nozzle width:	0.457 mm (0.018")
Slot length:	127 mm (5.000")
Receiver nozzle taper:	Compound; 0.508 mm (0.020") step, 60° taper
Material:	Al 7075

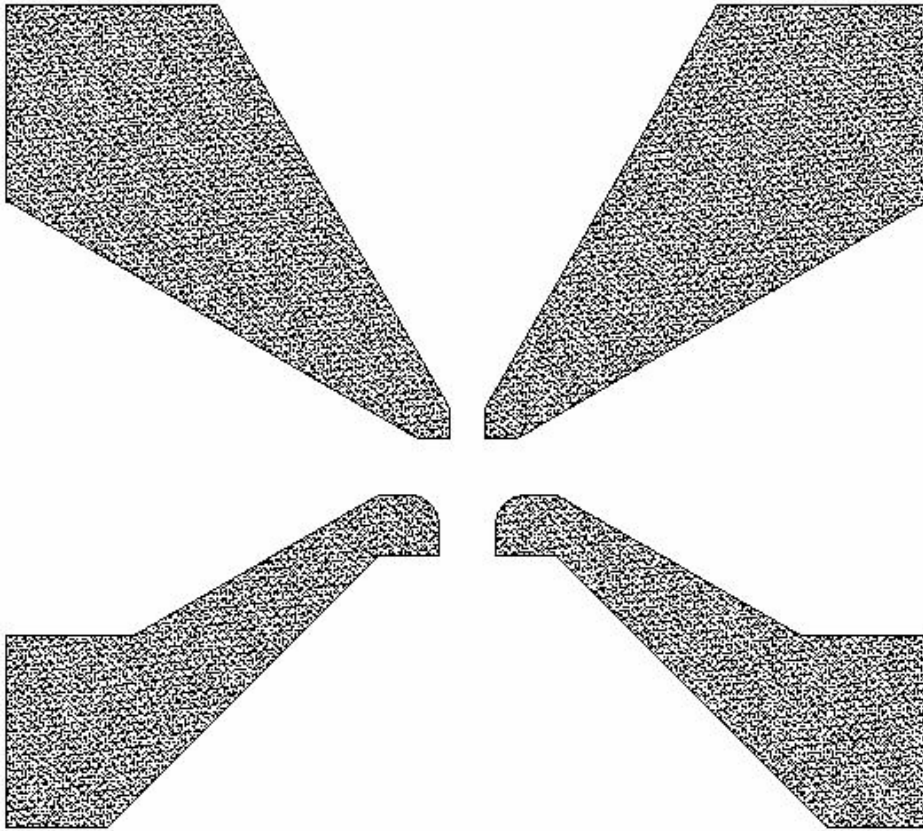
Figure 10. Nozzle cross-section of LSVI Units 5 and 6.



Dimensions:

Acceleration nozzle width:	0.305 mm (0.012")
Receiver nozzle width:	0.457 mm (0.018")
Slot length:	89 mm (3.500")
Receiver nozzle taper:	Compound; 0.508 mm (0.020") step, 60° taper, 13 mm (0.5") step
Material:	Al 7075

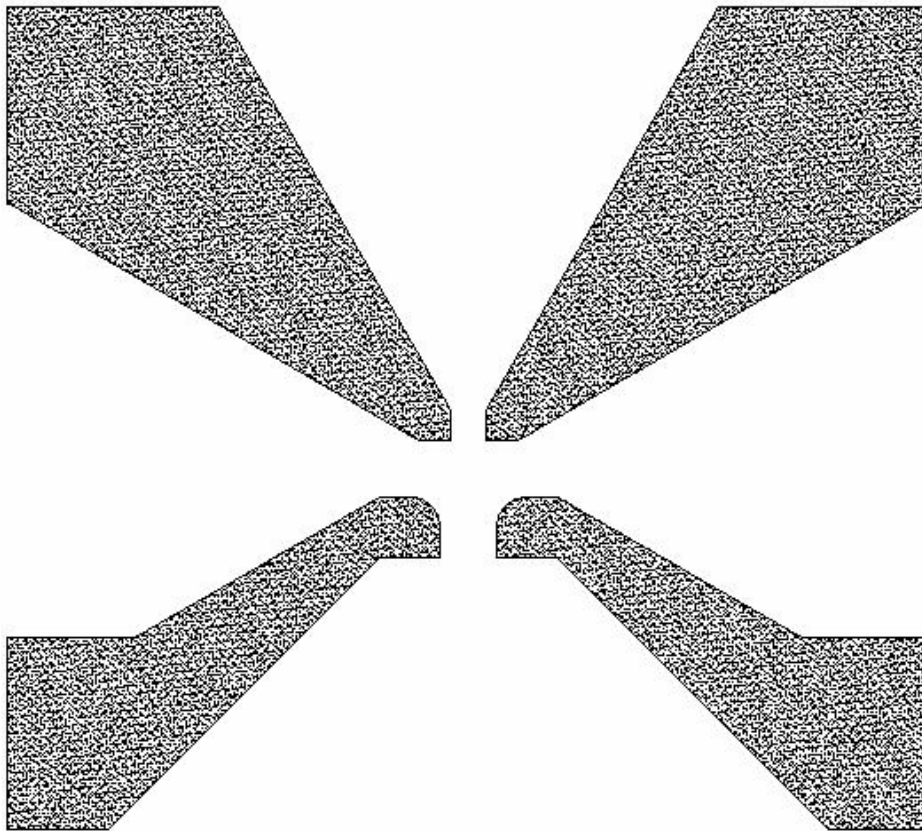
Figure 11. Nozzle cross-section of LSVI Units 7 and 8.



Dimensions:

Acceleration nozzle width:	0.203 mm (0.008")
Receiver nozzle width:	0.305 mm (0.016")
Slot length:	479 mm (18.8")
Receiver nozzle taper:	Compound; 0.508 mm (0.020") step, 60° taper, 13 mm (0.5") step
Material:	Al 7075

Figure 12. Nozzle cross-section of CSVI Unit 1.



Dimensions:

Acceleration nozzle width:	0.508 mm (0.020")
Receiver nozzle width:	0.762 mm (0.030")
Slot length:	479 mm (18.8")
Receiver nozzle taper:	Compound; 0.508 mm (0.020") step, 60° taper, 0.508 mm (0.020") step
Material:	Al 7075

Figure 13. Nozzle cross-section of CSVI Unit 2.

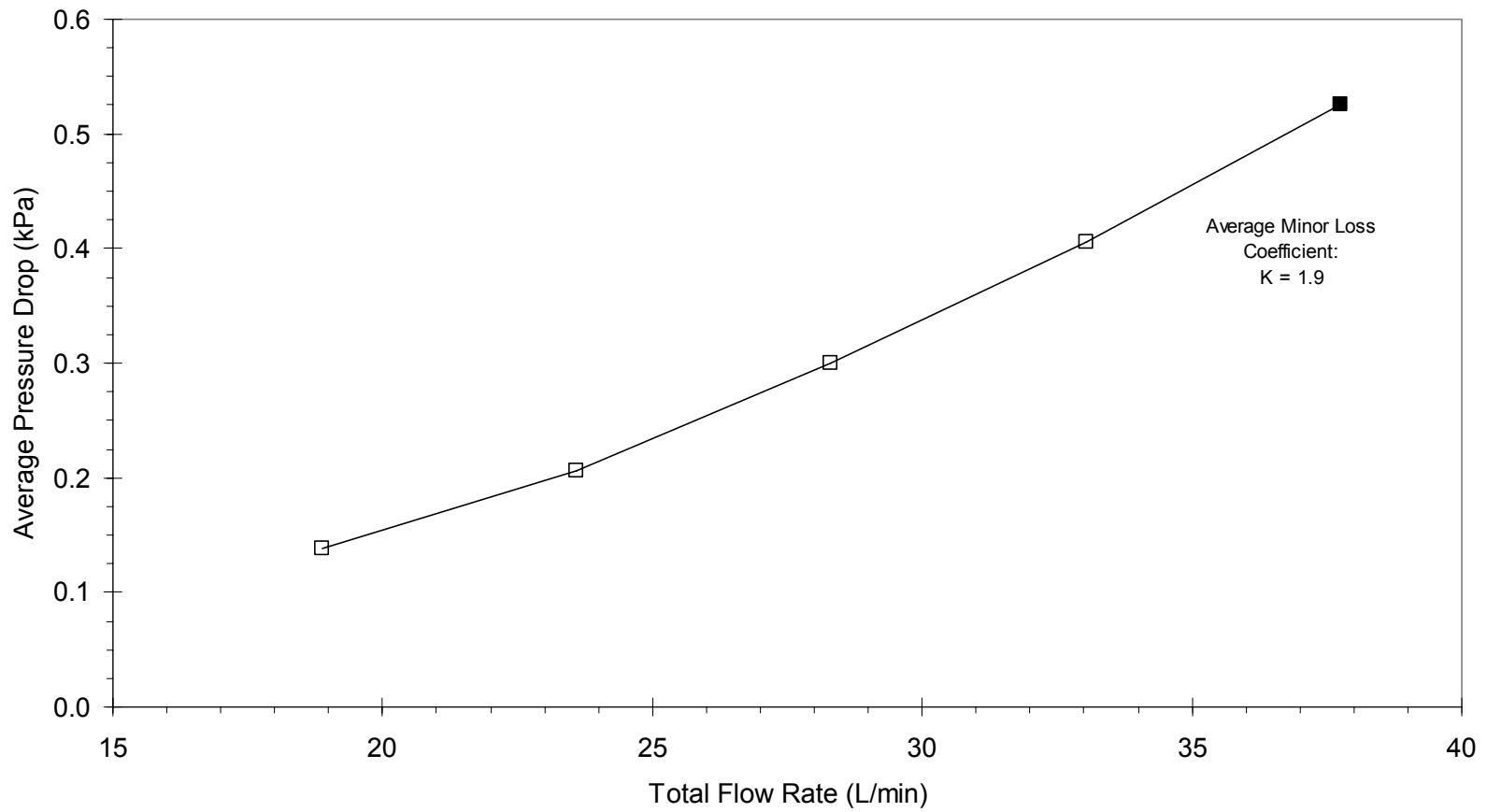


Figure 14. Pressure drop in major flow for LSVI Unit 8 at 10% minor/total flow ratio.

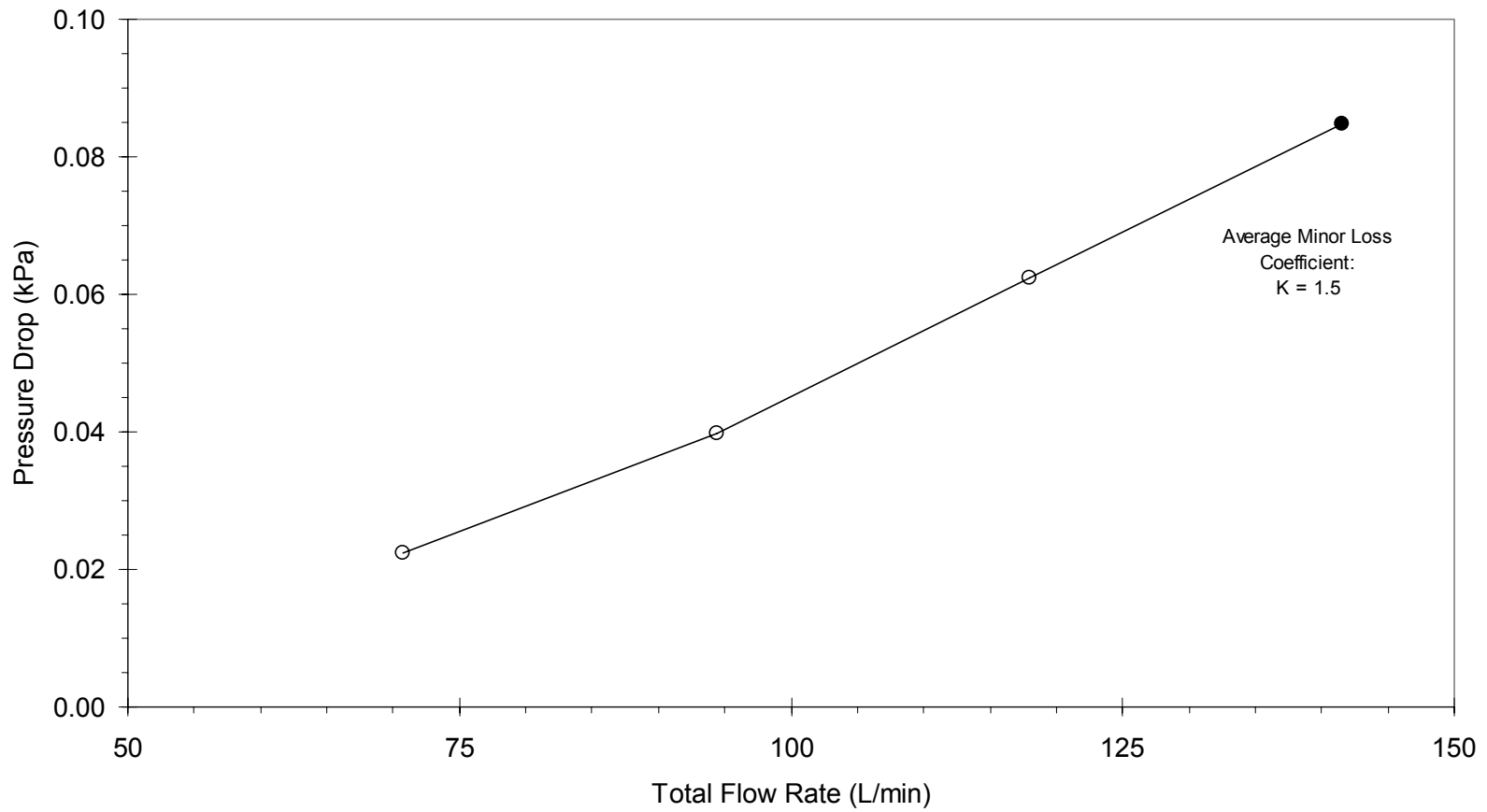


Figure 15. Pressure drop in major flow for CSVI Unit 2 at 10% minor/total flow ratio.

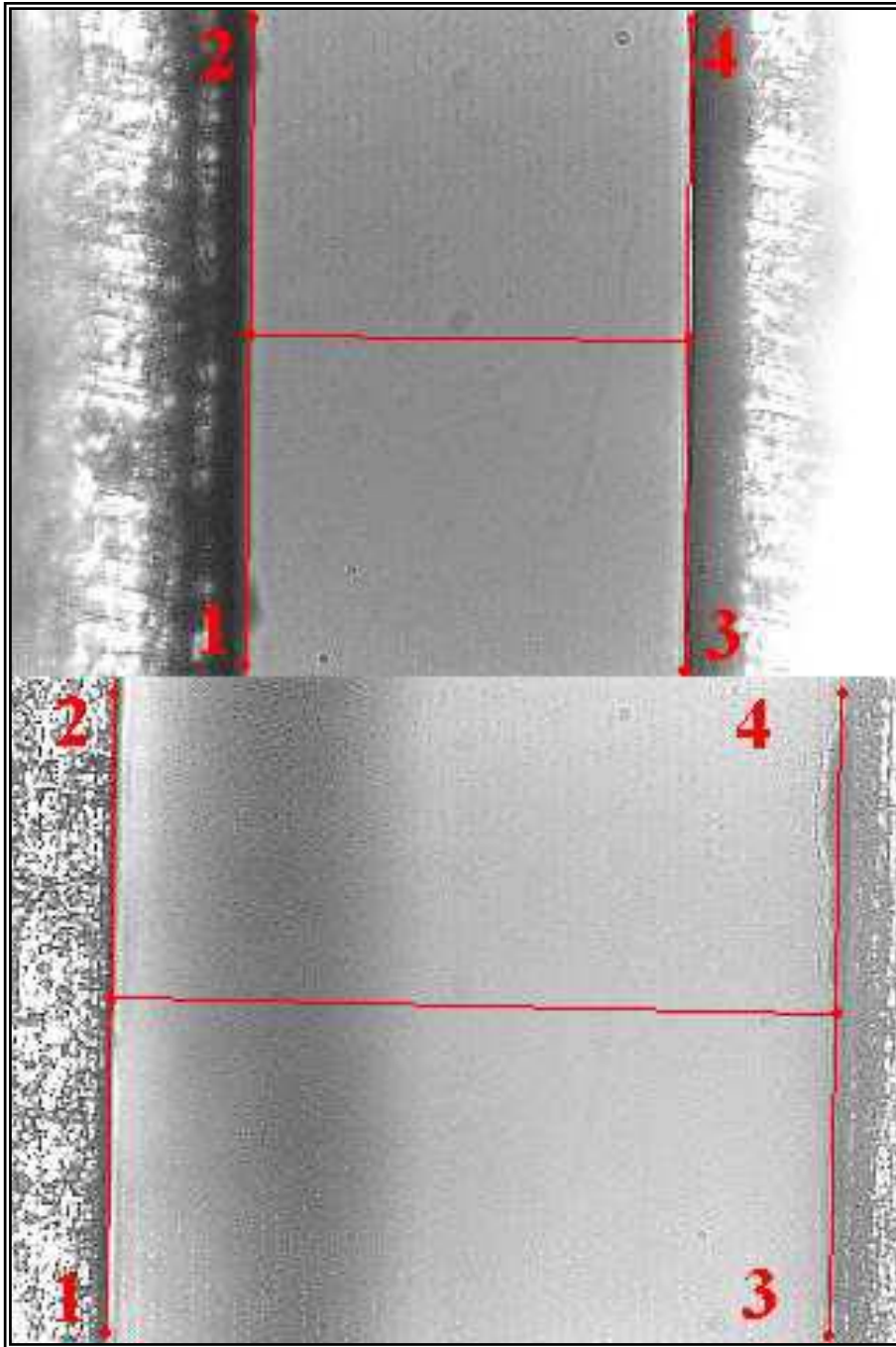


Figure 16. Image pair for LSVI nozzle width and alignment measurement (upper half acceleration nozzle, lower half receiver nozzle).

Table 2. Nozzle width and misalignment of LSVI units.

Position On Nozzle	LSVI 3	LSVI 4	LSVI 5 (mm)	LSVI 7	LSVI 8
Left End					
Acceleration Nozzle Width	0.316	0.294	0.289		0.316
Receiver Nozzle Width	0.415	0.402	0.376		0.482
Offset	0.016	0.007	0.014		0.006
Middle					
Acceleration Nozzle Width	0.234	0.260	0.259	0.300	0.319
Receiver Nozzle Width	0.413	0.363	0.342	0.495	0.483
Offset	0.003	0.008	0.038	0.011	0.009
Right End					
Acceleration Nozzle Width	0.310	0.291	0.279	0.303	0.338
Receiver Nozzle Width	0.417	0.398	0.393	0.479	0.476
Offset	0.006	0.004	0.035	0.010	0.004
Average					
Acceleration Nozzle Width	0.287	0.281	0.276	0.302	0.324
Receiver Nozzle Width	0.415	0.388	0.370	0.487	0.480
Offset	0.008	0.006	0.029	0.010	0.007
Average Relative Misalignment:	2.9%	2.3%	10.5%	3.4%	2.0%

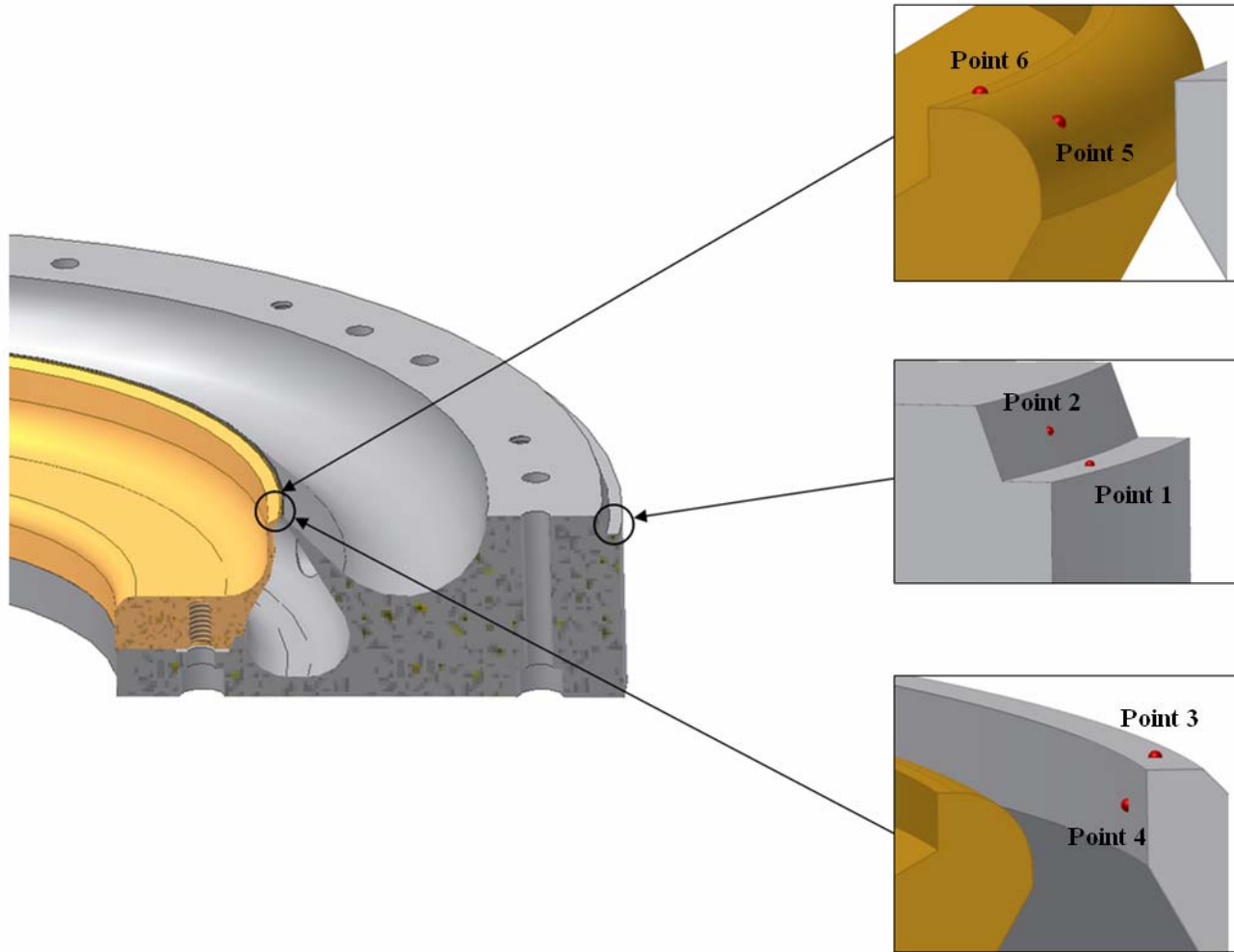


Figure 17. Locations of points measured by coordinate measurement machine for survey of CSVI nozzle geometry (receiver blade in gold, acceleration blade in gray).

Table 3. Nozzle width, variance and misalignment of CSVI units.

CSV I	Acceleration Nozzle Width (mm)	Acceleration Nozzle Variance (mm)	Receiver Nozzle Width (mm)	Receiver Nozzle Variance (mm)	Average Nozzle Alignment Deviation (mm)	Average Nozzle Misalignment (mm)
1	0.154	0.0144	0.257	0.0144	0.0028	0.0154
2	0.499	0.0029	0.762	0.0070	0.0088	0.0090

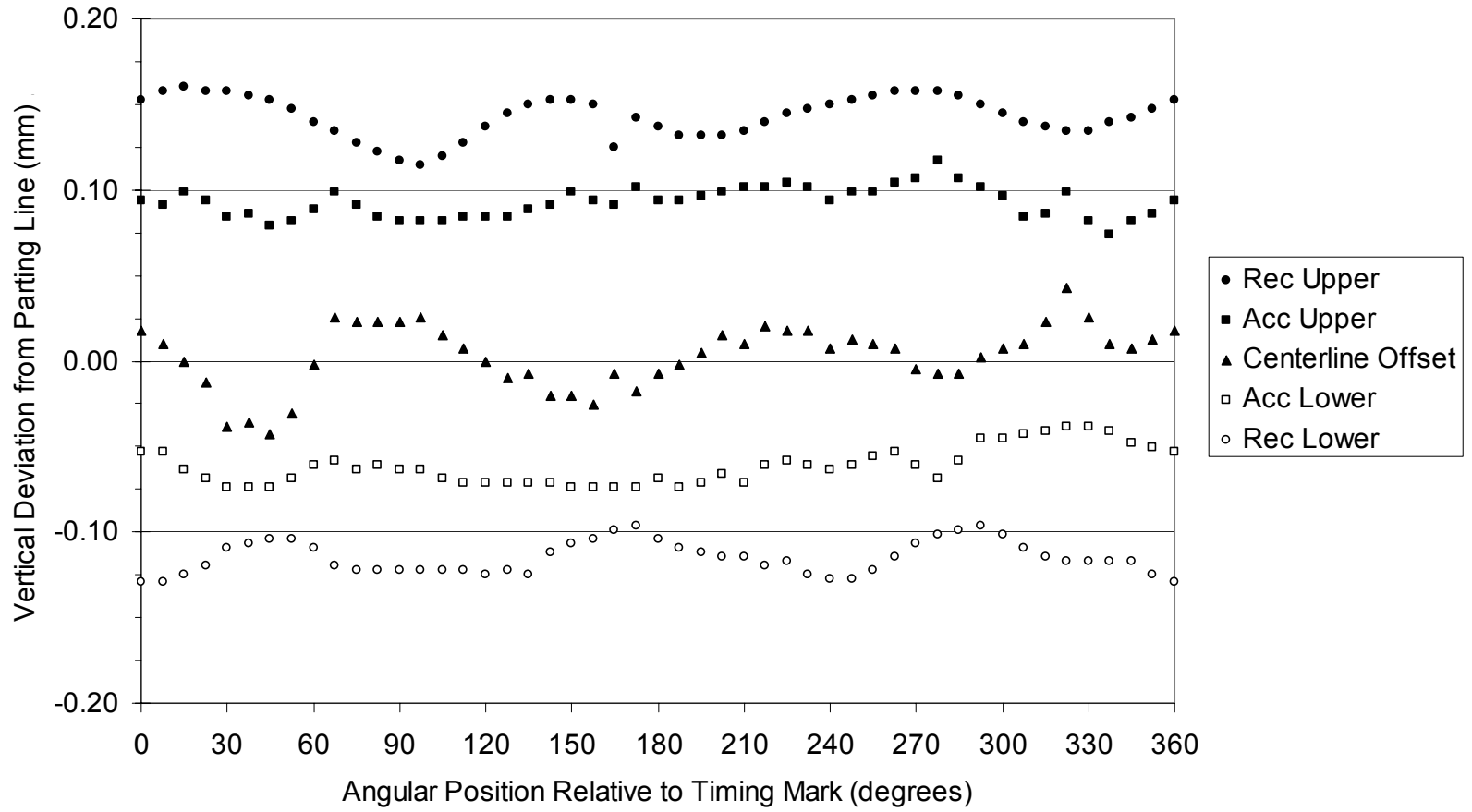


Figure 18. Nozzle width and alignment on circumference of CSVI Unit 1.

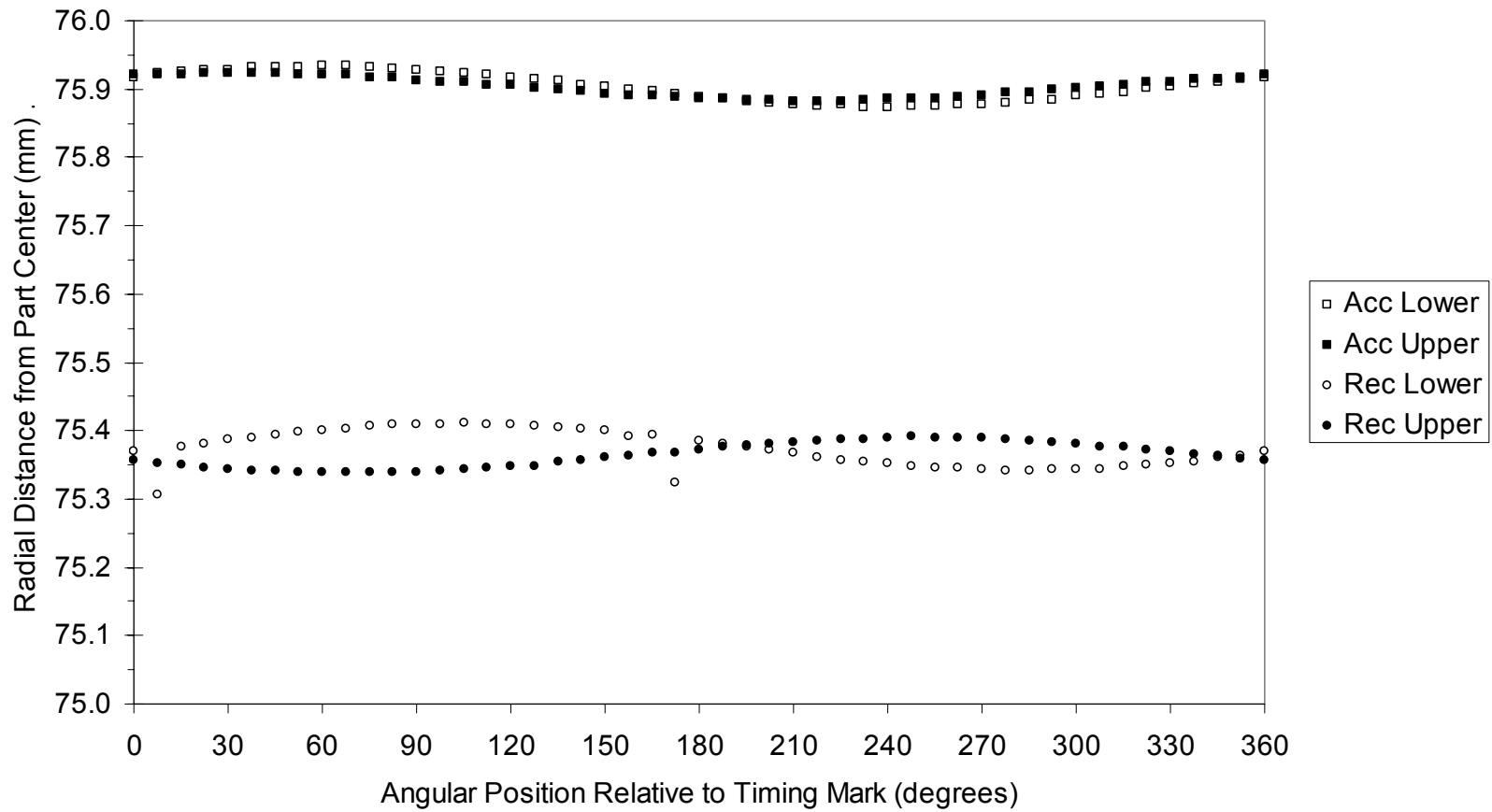


Figure 19. Radial position of nozzle tip on circumference of CSVI Unit 1.

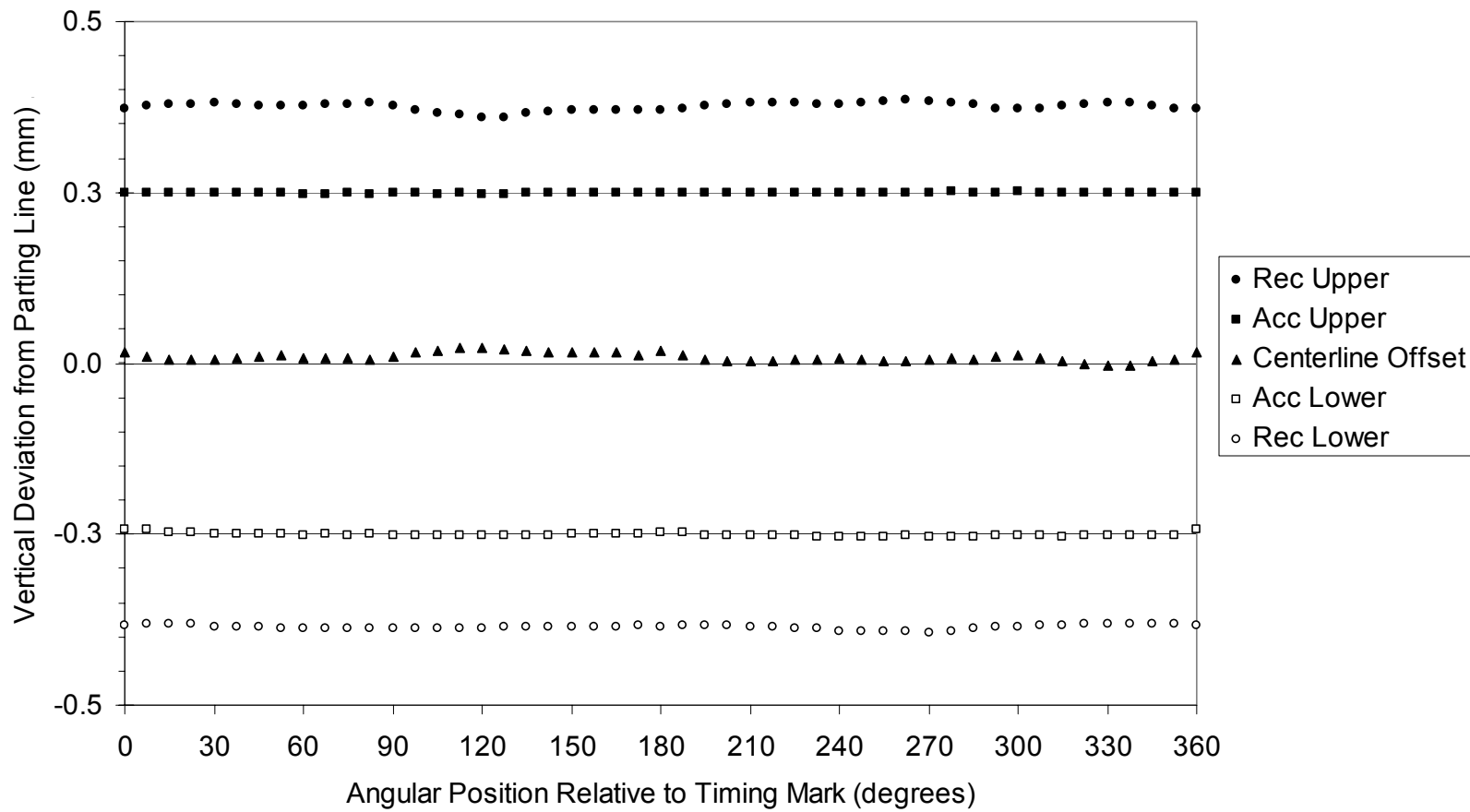


Figure 20. Nozzle width and alignment on circumference of CSVI Unit 2.

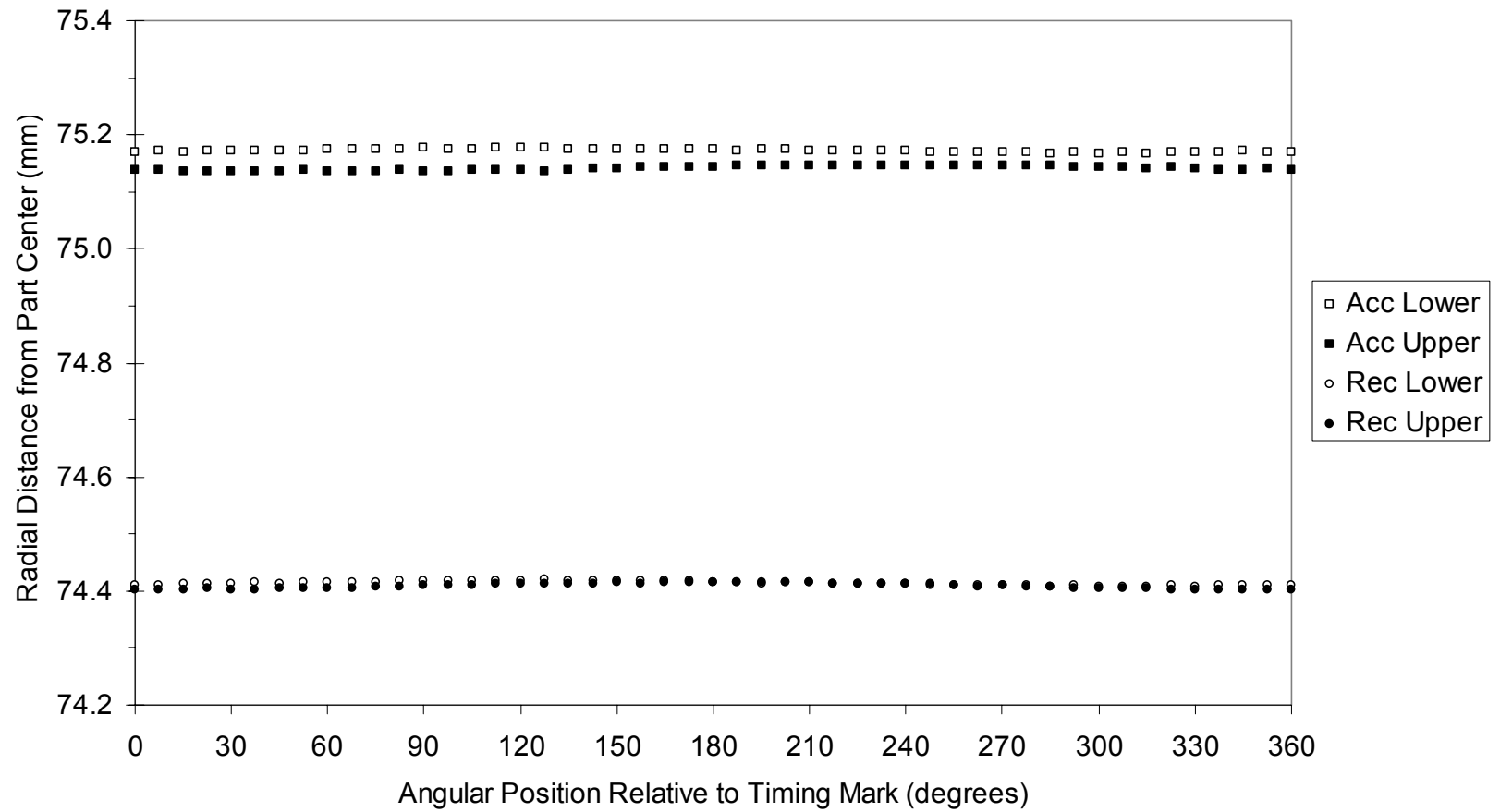


Figure 21. Radial position of nozzle tip on circumference of CSVI Unit 2.

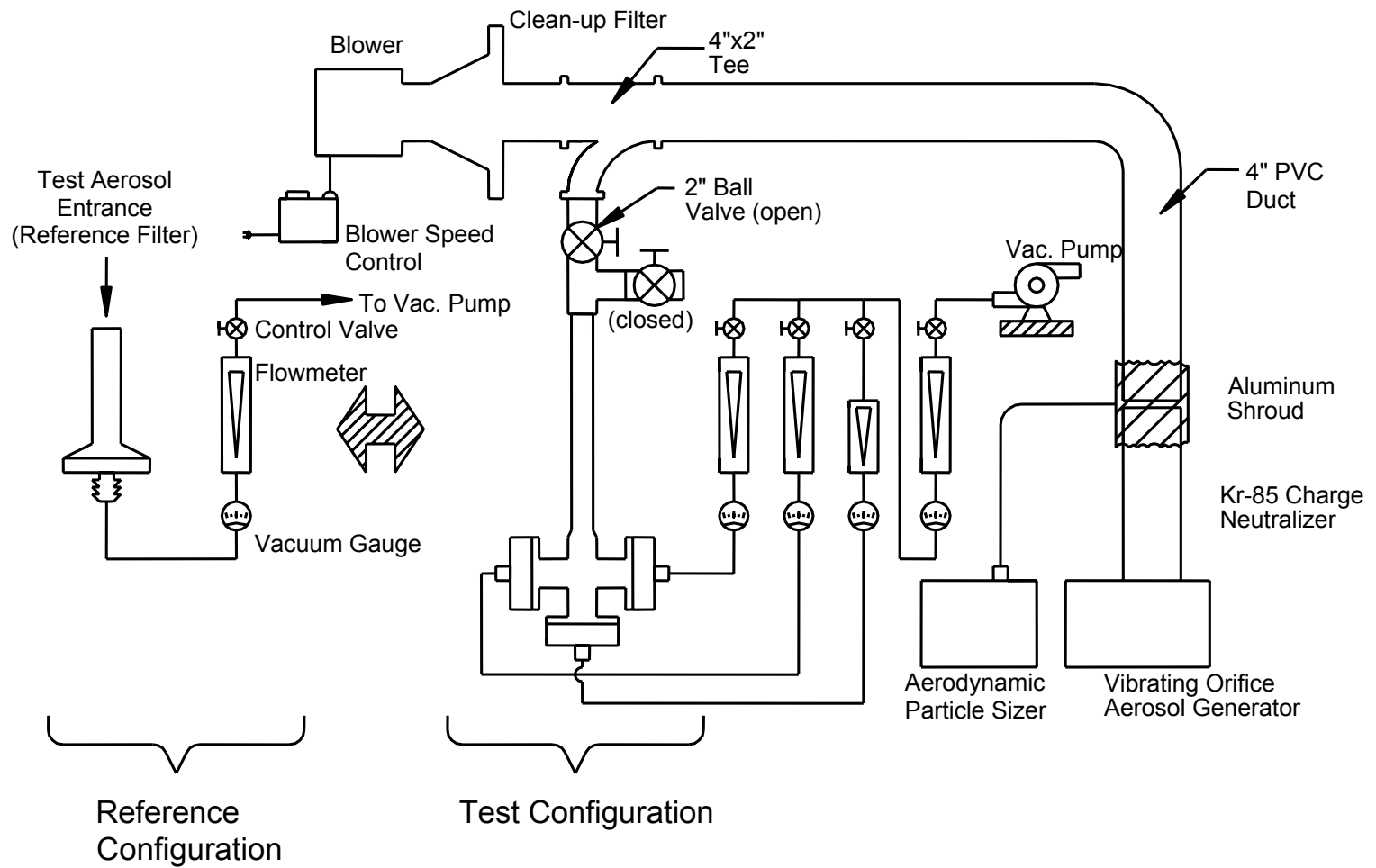


Figure 22. Test apparatus for liquid and solid PSL monodisperse aerosols for LSVI units.

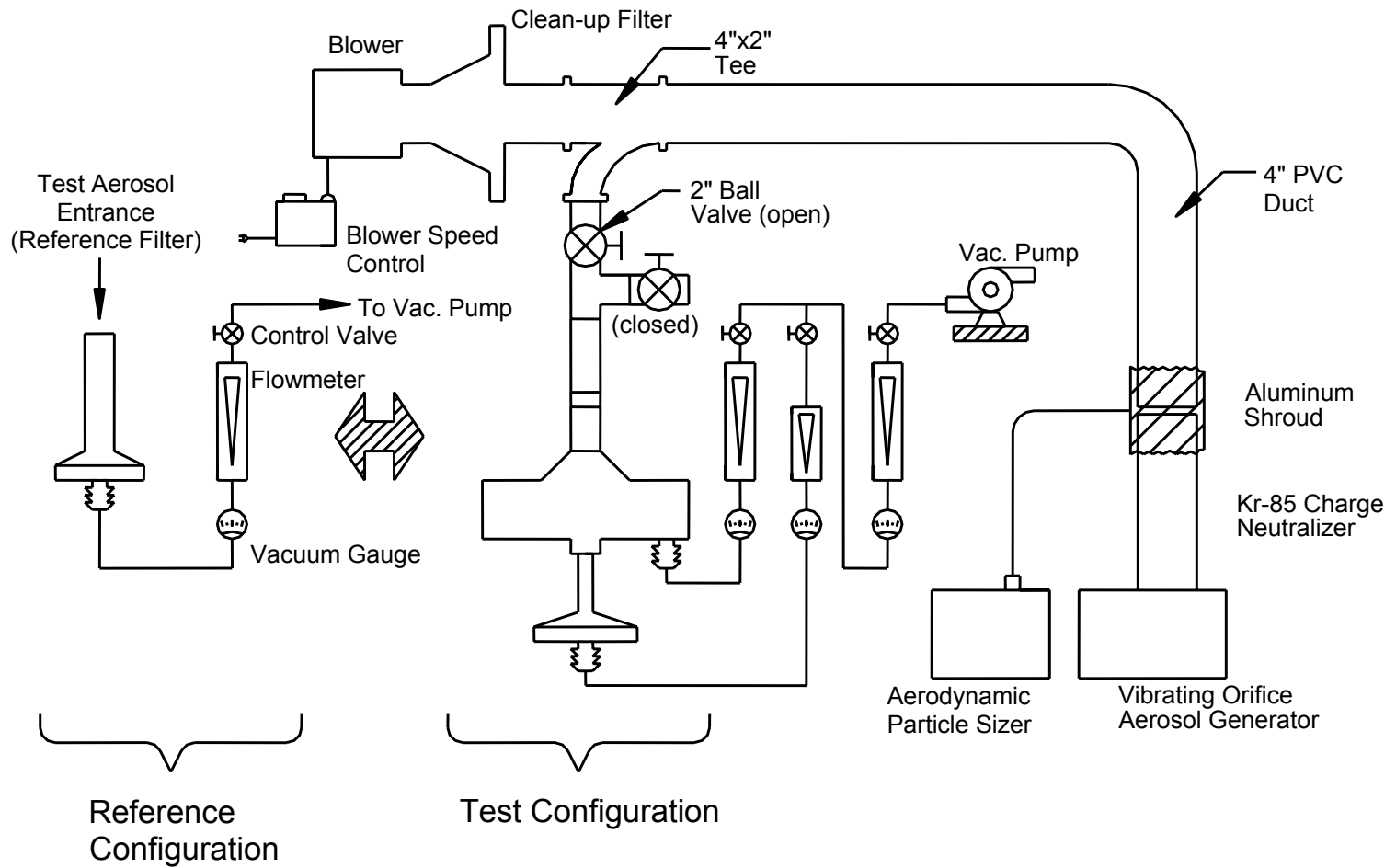


Figure 23. Test apparatus for liquid and solid PSL monodisperse aerosols for CSVI units.

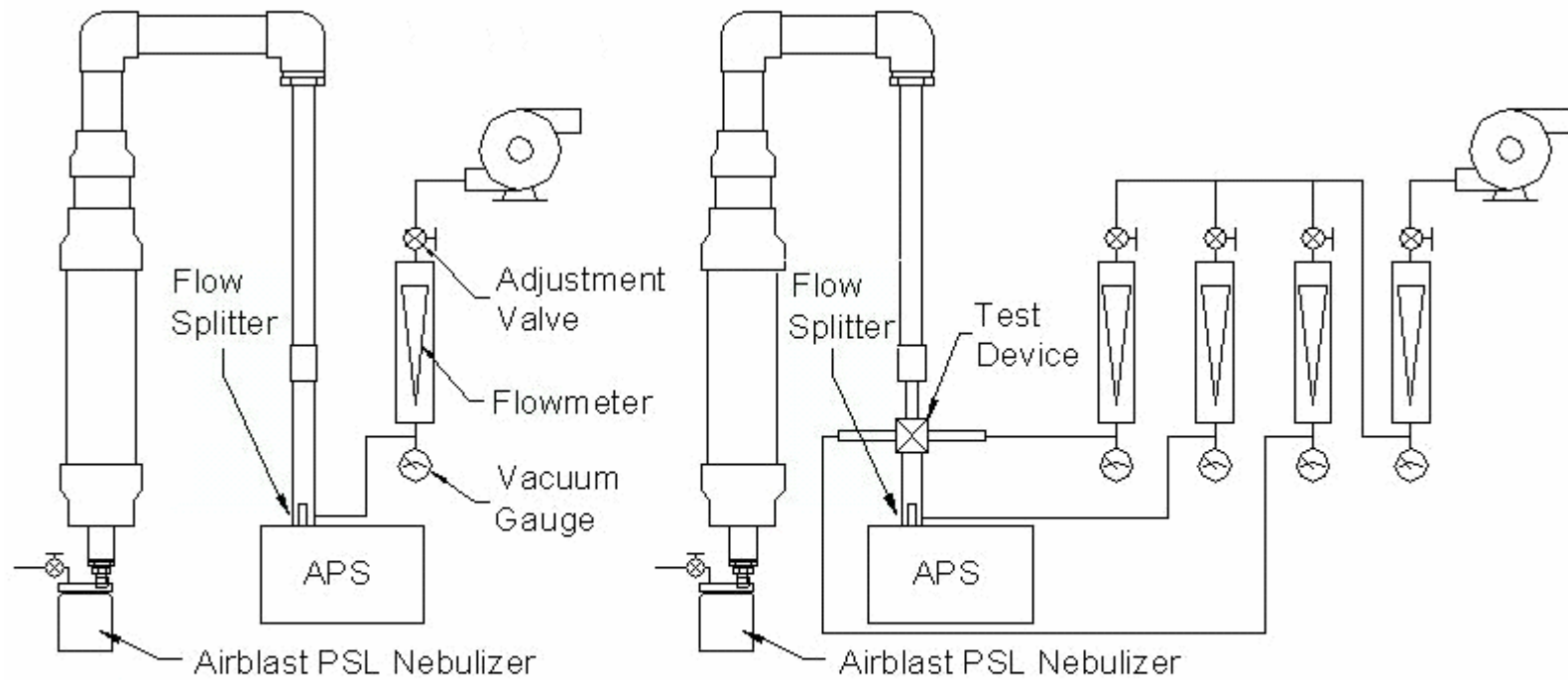


Figure 24. Test apparatus for LSVI units tested with PSL particles and aerodynamic particle sizer (APS).

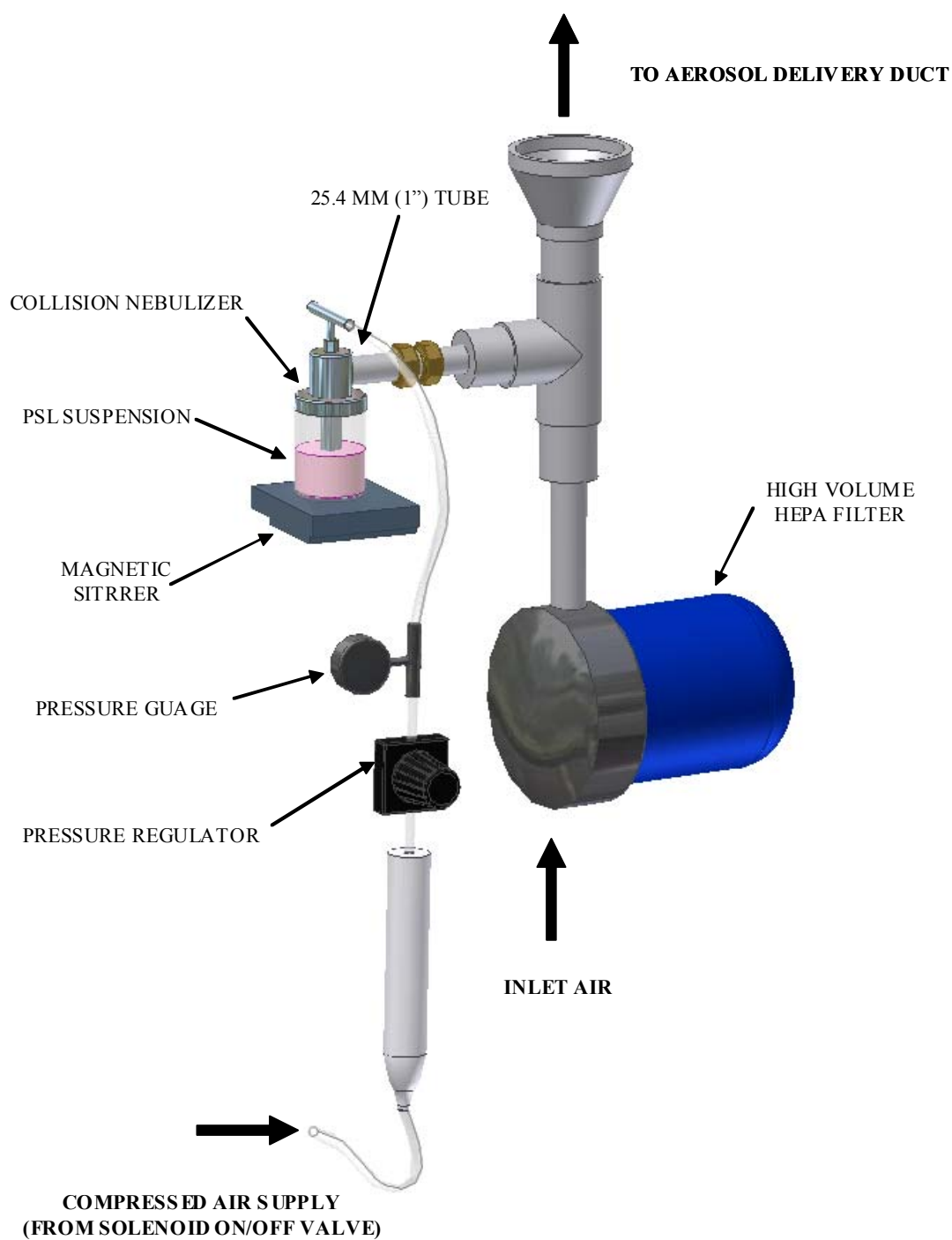


Figure 25. Configuration of Collision nebulizer and pressure control for constant generation of PSL particles for fixed duration.

Table 4. Optical filters and tracer dye used in fluorometric analysis of test aerosols.

Particle Type	Tracer	Excitation Peak (nm)	Emission Peak (nm)	Fluorometer	Excitation Filter (nm)	Emission Filter (nm)
Oleic Acid	Sodium Fluorescein	492	516	Turner Model 450	Narrow Band 490	High Pass 515
Polystyrene Latex	Duke Scientific, Green	468	508	Turner Quantech	Narrow Band 460	High Pass 500
Polystyrene Latex	Duke Scientific, Red	542	612	Turner Quantech	Narrow Band 540	High Pass 585

Table 5. Preliminary results of testing LSVI units with liquid monodisperse aerosols.

LSVI Unit No.	Test Replicates	Nominal Test Conditions			Efficiency		
		Total Flow Rate (L/min)	Flow Ratio (Minor/Total)	Particle Size ($\mu\text{m AD}$)	Minor	Major	Losses
0	3	28.3	10%	2.8	19%	52%	29%
3	1	42.5	10%	2.8	22%	34%	44%
3	3	75.5	100%	2.5	41%	0%	59%
3	3	75.5	10%	2.5	64%	7%	29%
3	3	18.9	10%	2.4	35%	56%	9%
3	1	37.7	10%	2.4	83%	6%	11%
3	1	18.9	20%	2.4	97%	3%	0%
6	3	75.5	10%	2.8	44%	6%	50%
6	3	75.5	10%	2.5	40%	10%	50%
6	3	75.5	20%	2.5	18%	46%	36%
6	3	75.5	10%	10.0	20%	0%	80%
7	5	75.5	10%	2.2	50%		
7	3	61.3	10%	6.8	67%		

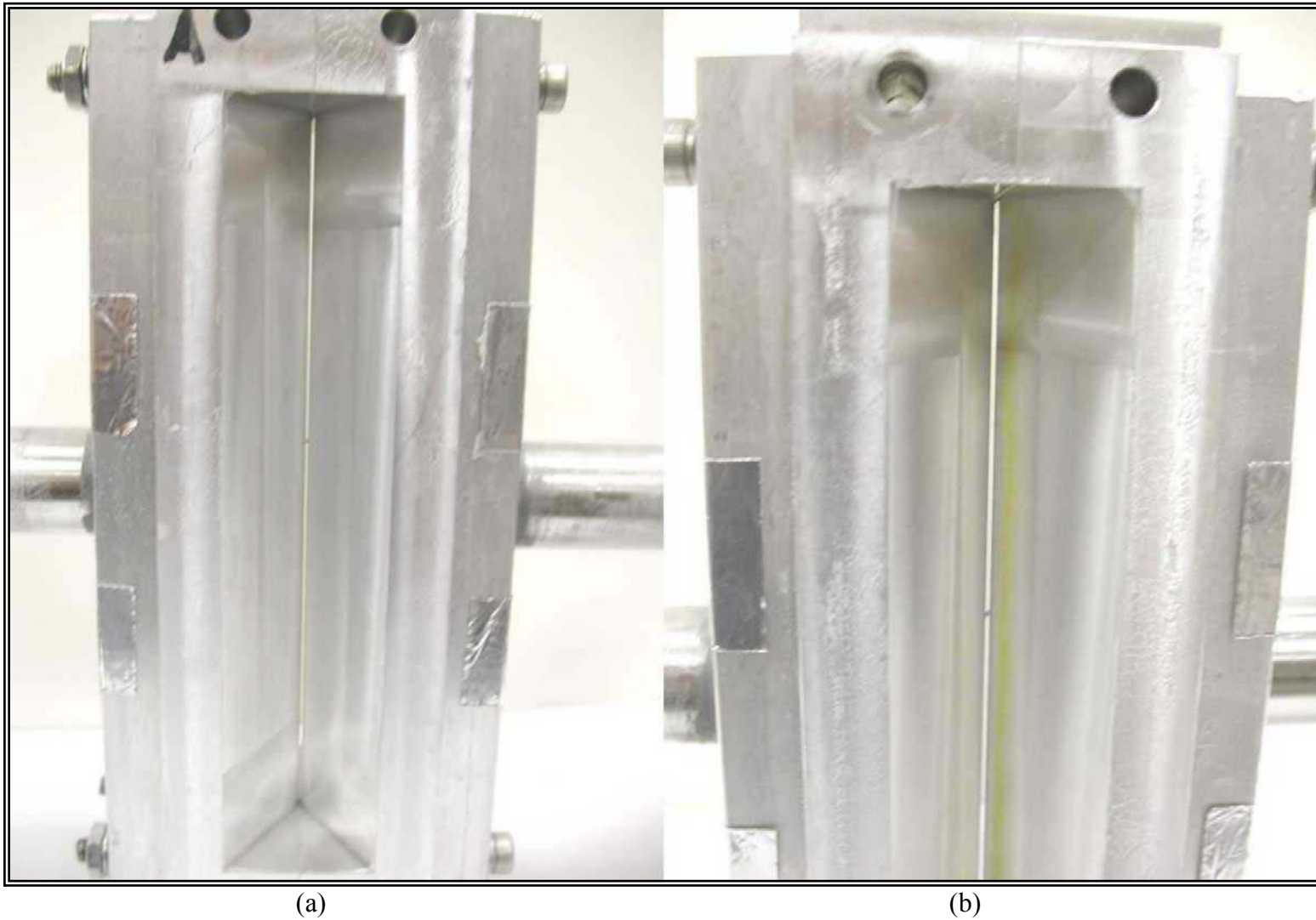


Figure 26. Comparison of particle deposition on LSVI Unit 3 on the acceleration nozzle (a) and the receiver nozzle (b) for 2.5 μm AD monodisperse liquid aerosol particles tagged with sodium fluorescein tracer.



Figure 27. Comparison of particle deposition on LSVI Unit 6 receiver nozzle WITHOUT secondary expansion (a) and LSVI Unit 7 receiver nozzle WITH secondary expansion (b) for monodisperse liquid aerosol particles tagged with fluorescent tracer.



(a)

(b)

Figure 28. Deposition of 6.8 μm AD monodisperse liquid aerosol particles on the receiver nozzle in LSVI Unit 7 (b) due to the presence of a burr on the opposed segment of the acceleration nozzle (a).



Figure 29. Deposition of 6.6 μm AD monodisperse liquid aerosol particles on the receiver nozzle throat in CSVI Unit 1.

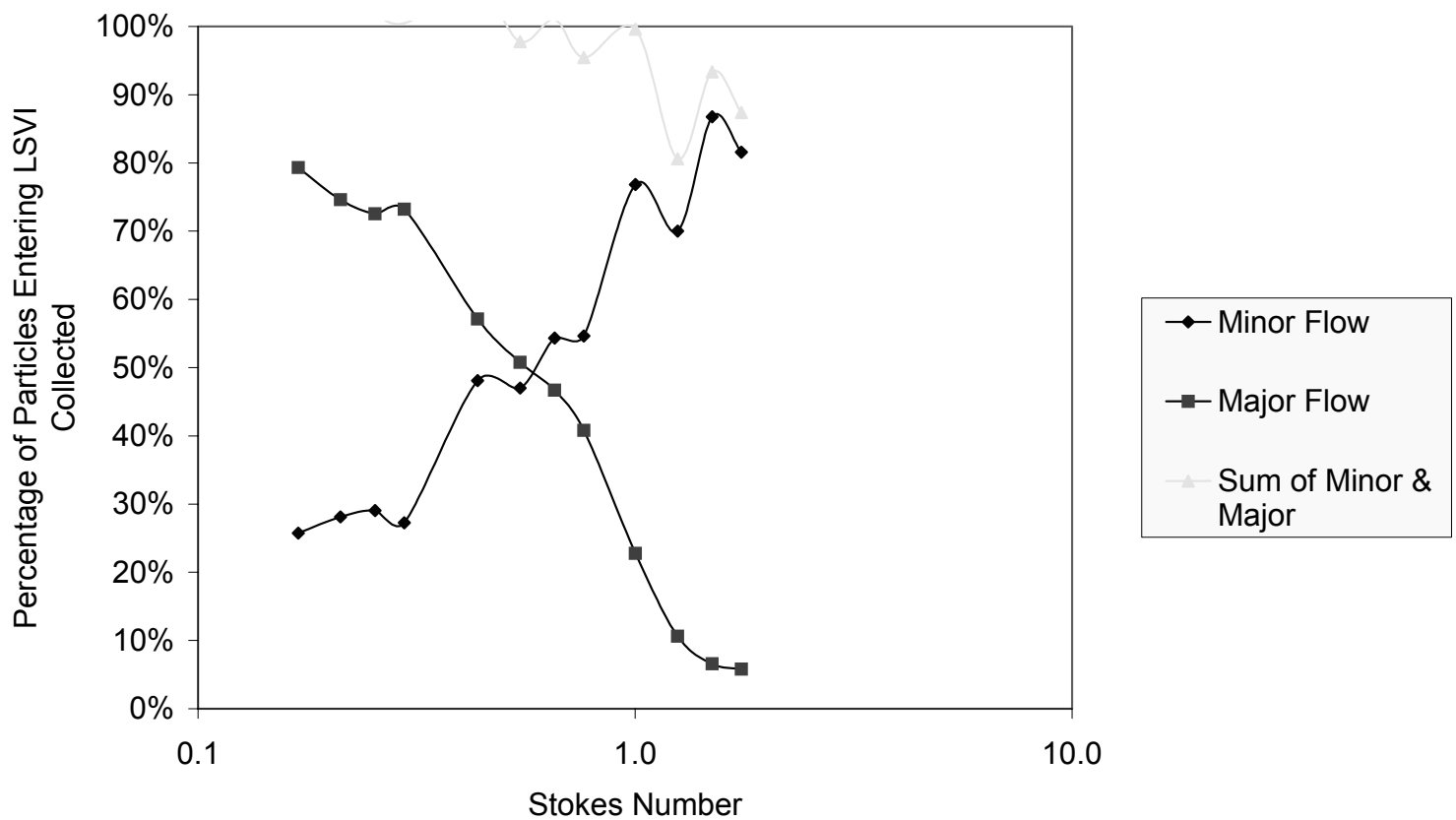


Figure 30. Collection efficiency of LSVI Unit 8 for solid monodisperse PSL particles sampled by APS for nozzle Reynolds numbers below 400 at 20% minor/total flow ratio.

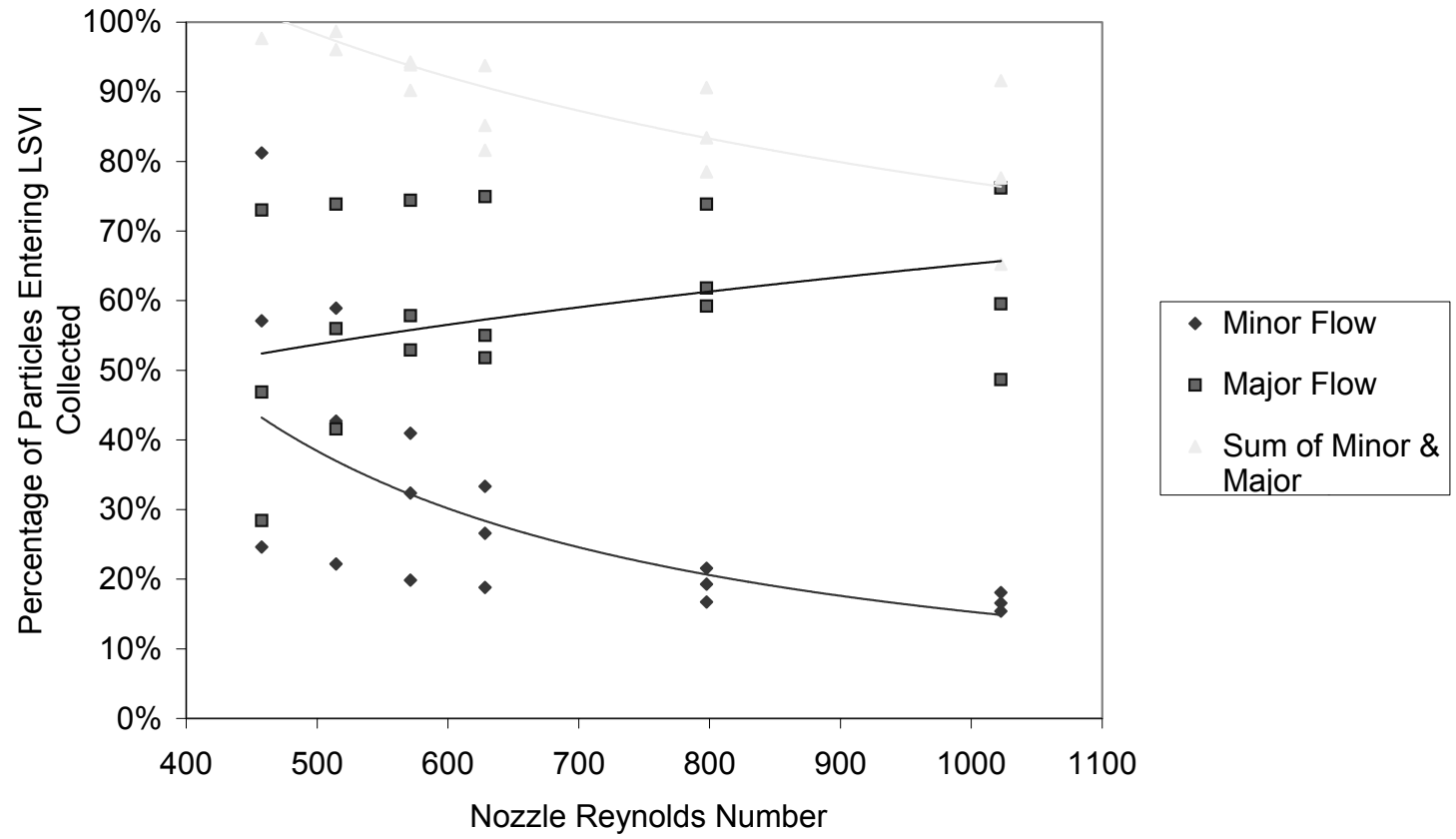


Figure 31. Collection efficiency of LSVI Unit 8 for solid monodisperse PSL particles sampled by APS for nozzle Reynolds numbers above 400 at 20% minor/total flow ratio.

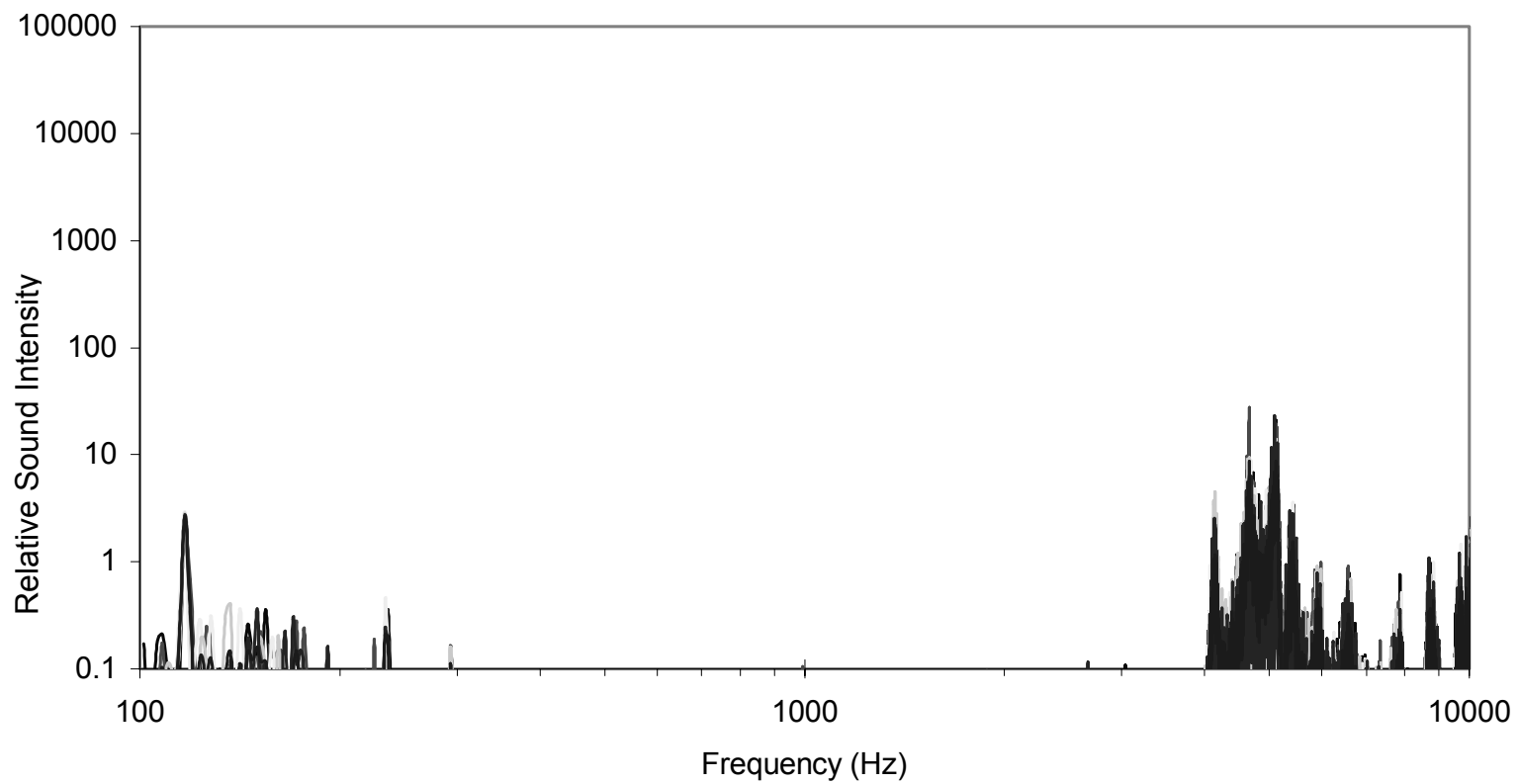


Figure 32. Sound power spectrum of LSVI Unit 8 at a total flow rate of 42.5 L/min.

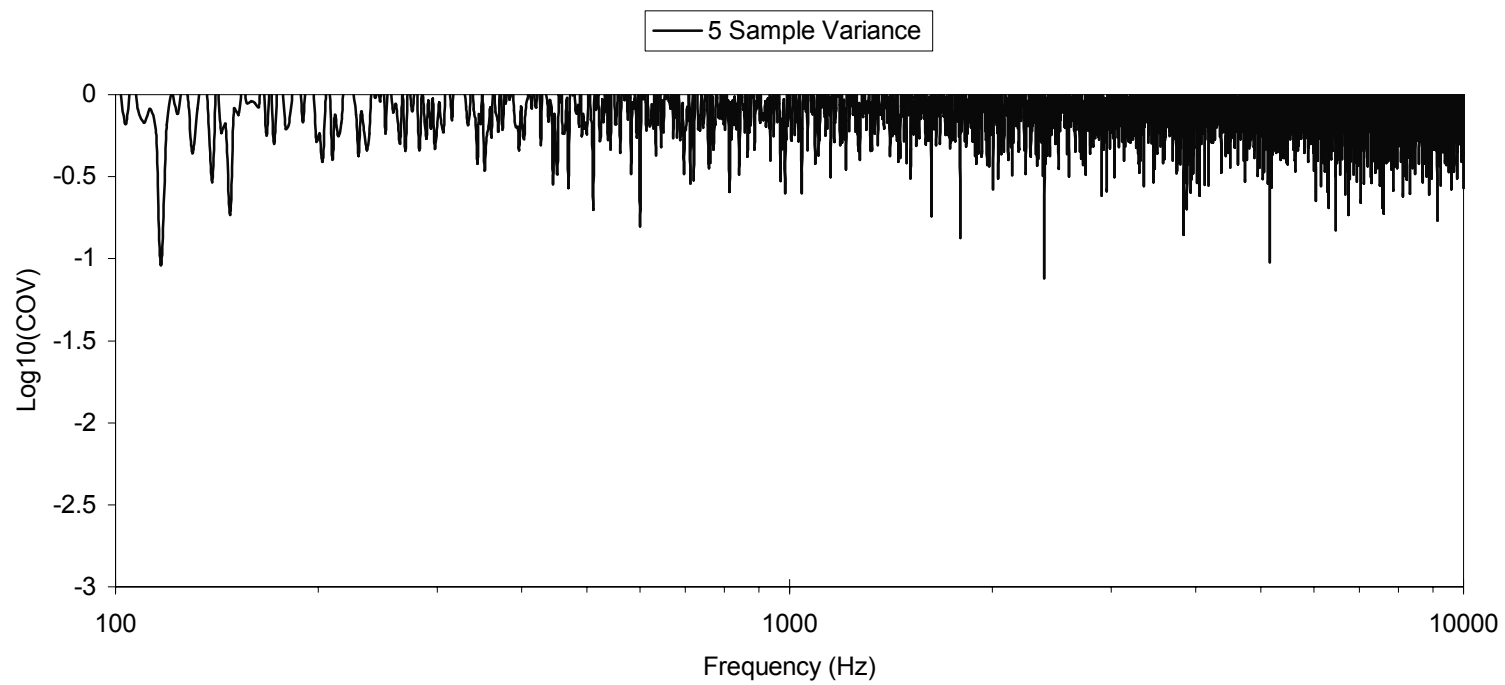


Figure 33. Variance of sound power spectrum of LSVI Unit 8 at a total flow rate of 42.5 L/min.

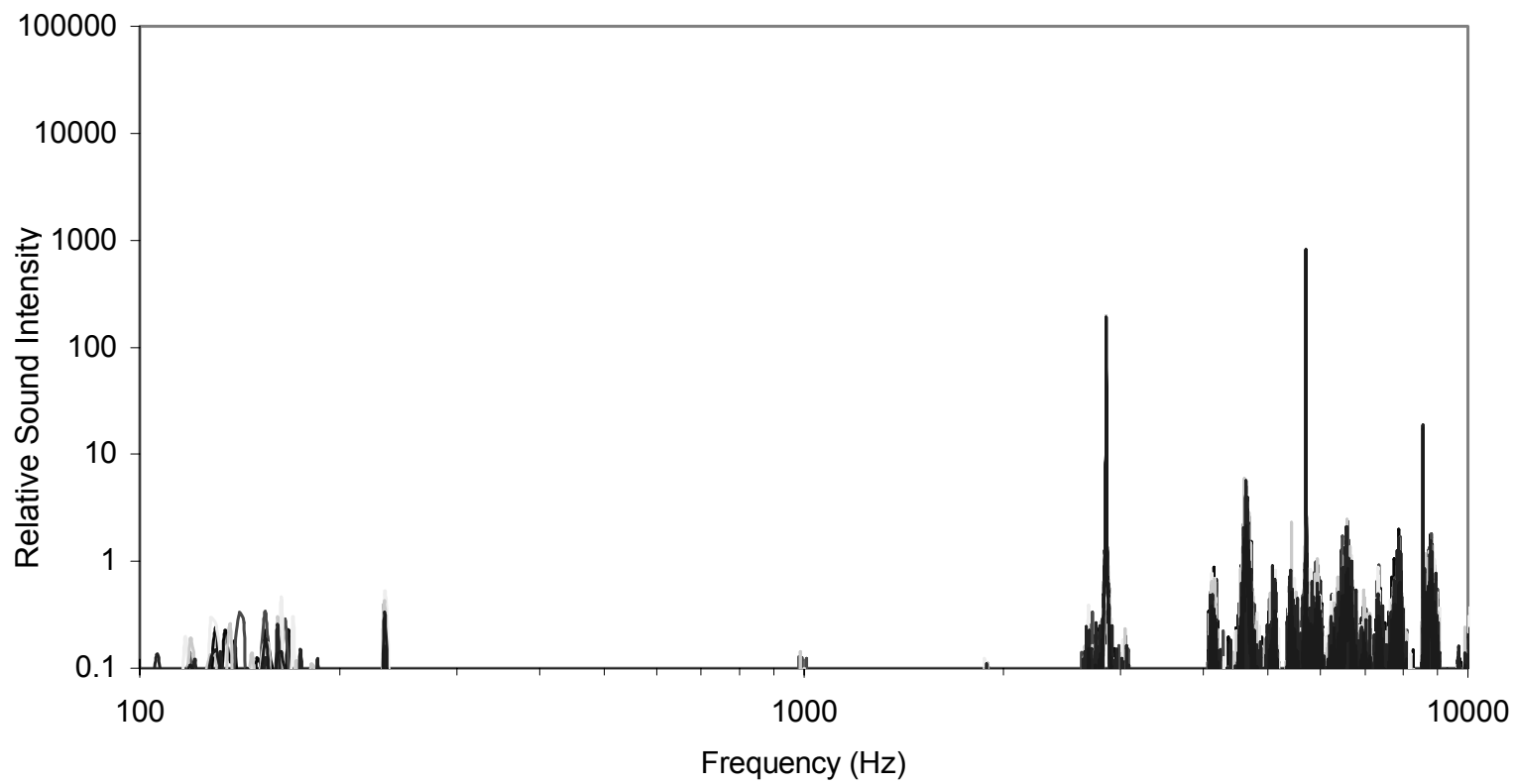


Figure 34. Sound power spectrum of LSVI Unit 8 at a total flow rate of 47.2 L/min.

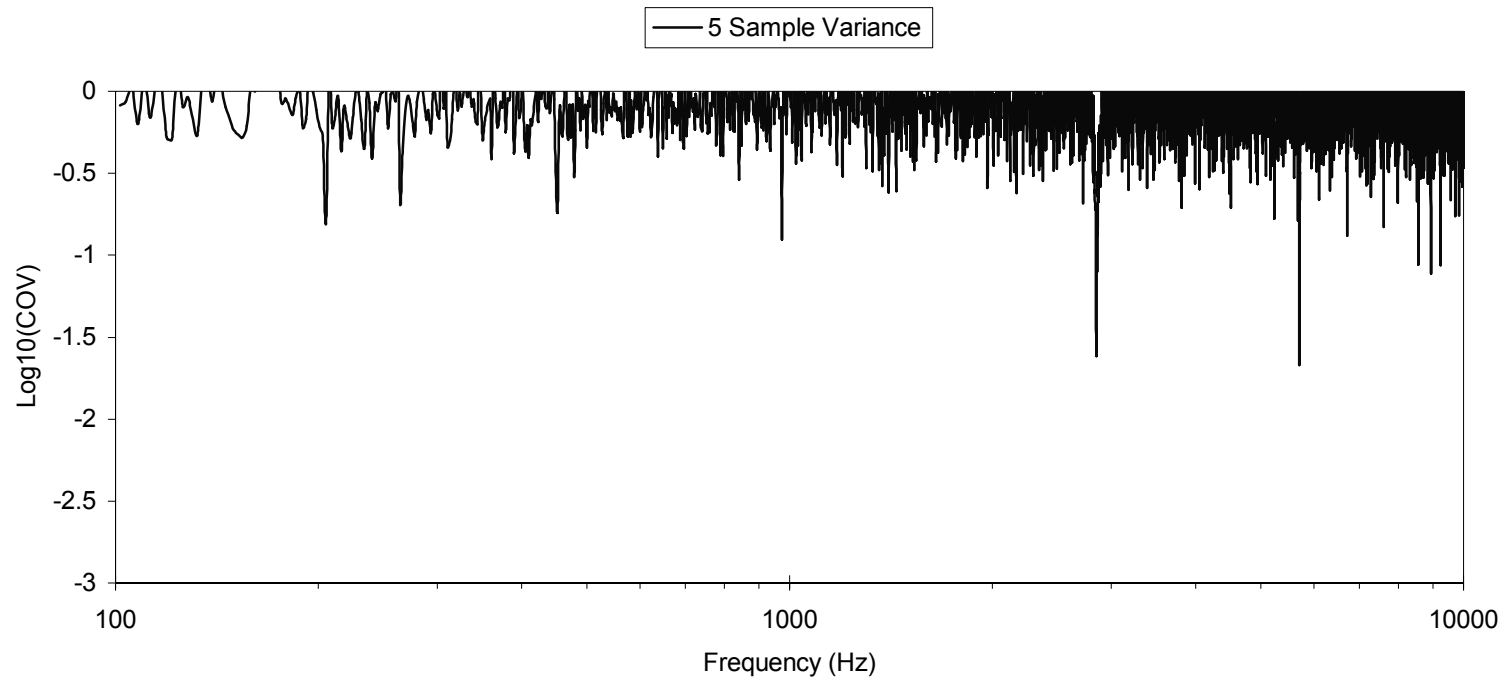


Figure 35. Variance of sound power spectrum of LSVI Unit 8 at a total flow rate of 47.2 L/min.

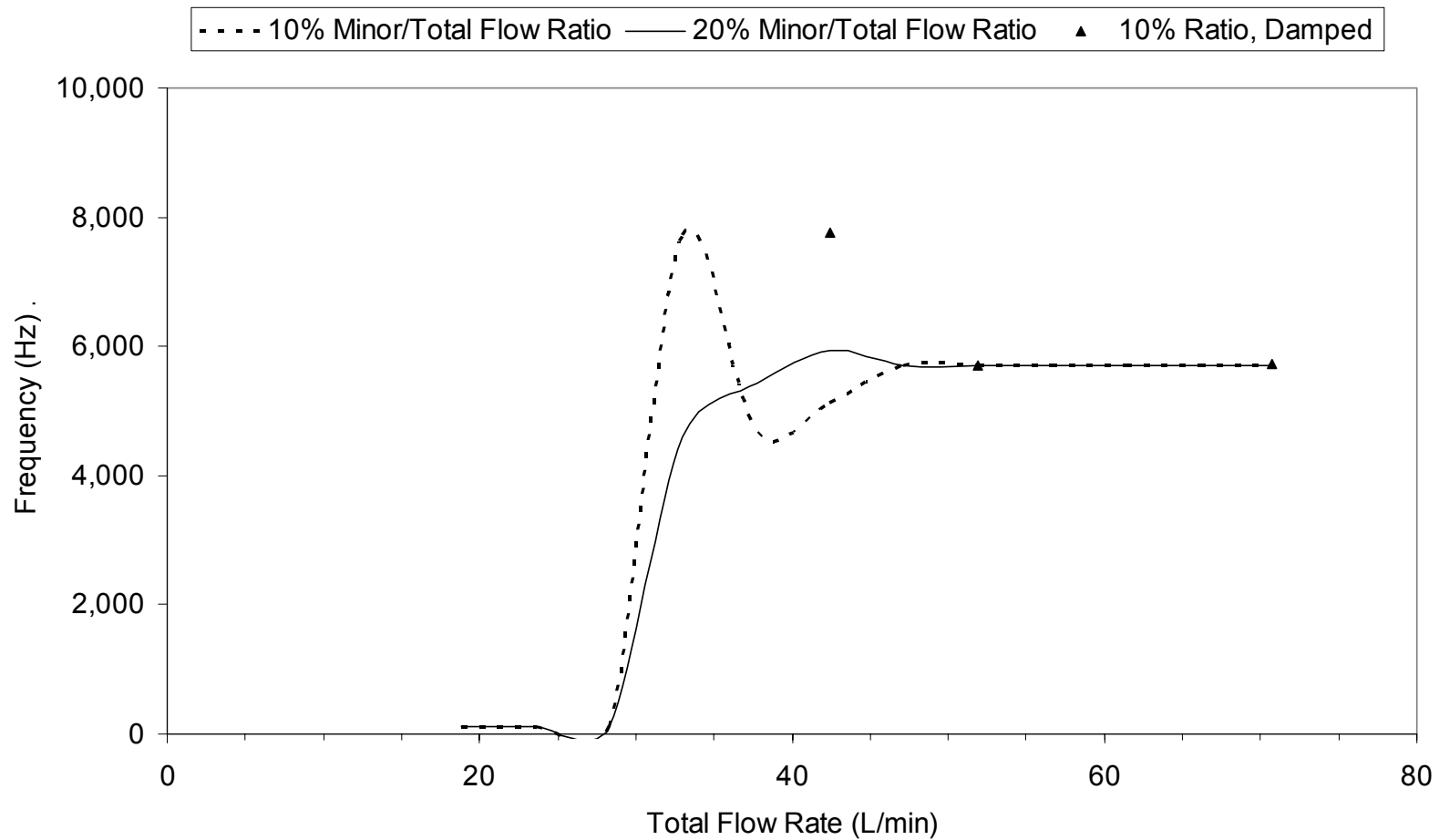


Figure 36. Frequency of maximum acoustic intensity for LSVI Unit 8.

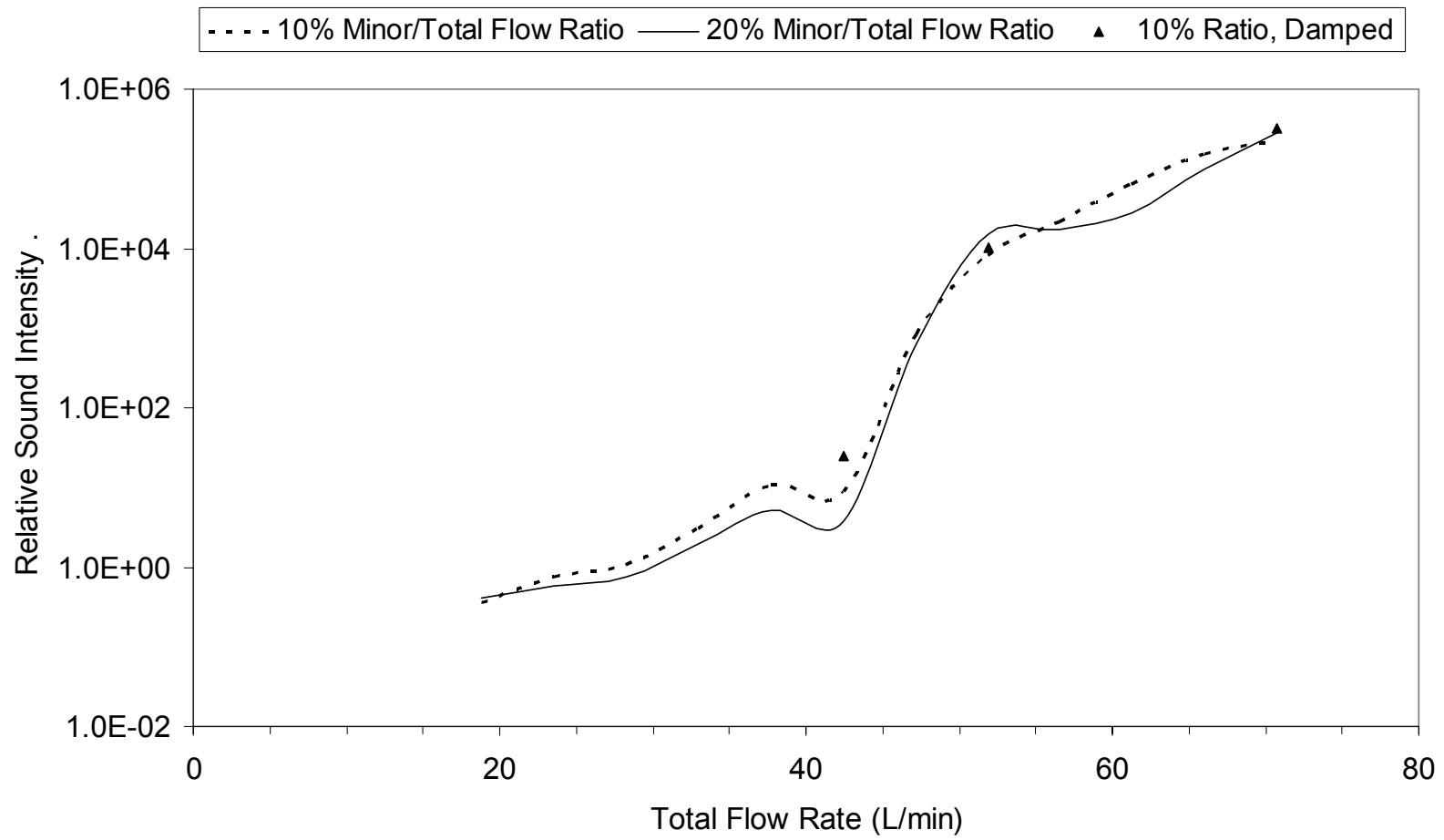


Figure 37. Amplitude of peak acoustic tone for LSVI Unit 8.

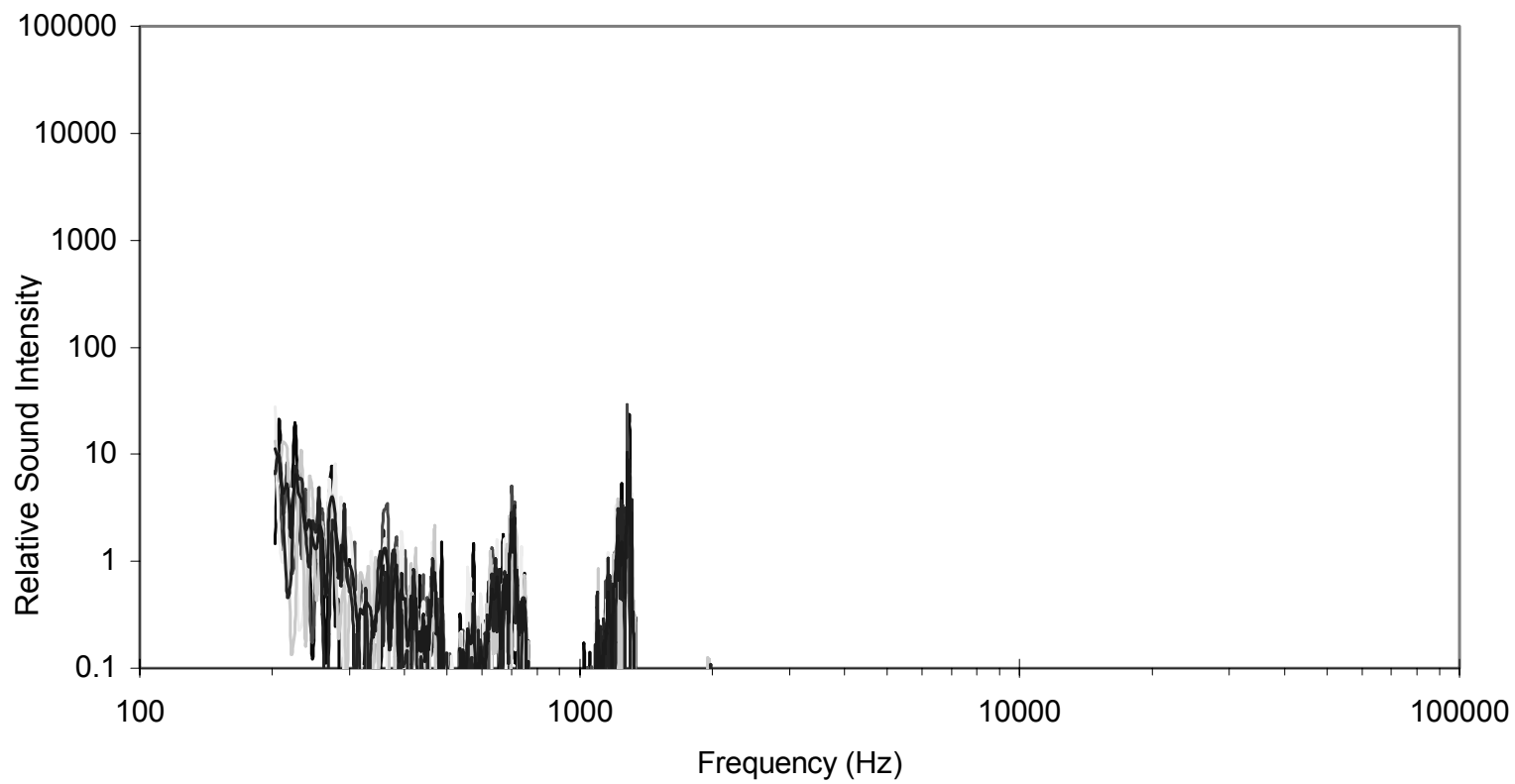


Figure 38. Sound power spectrum of CSVI Unit 2 at a total flow rate of 130 L/min.

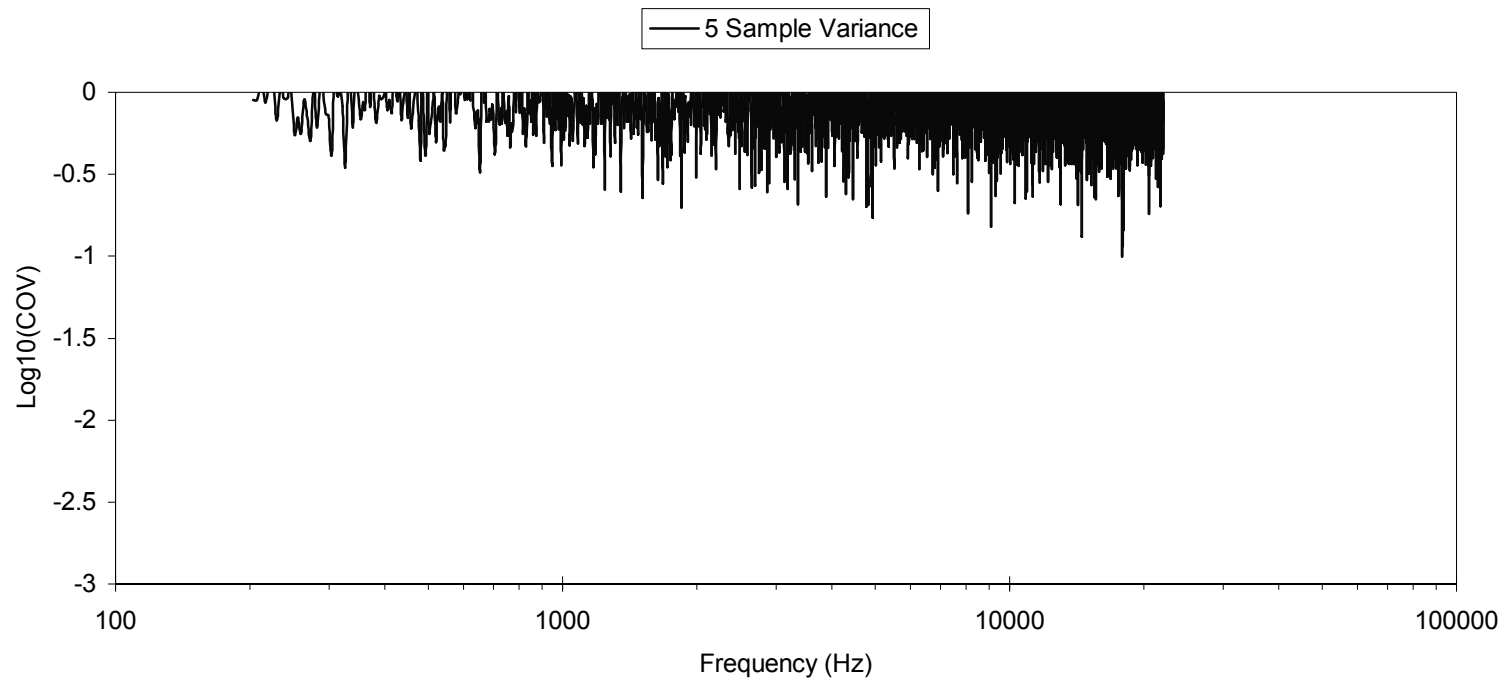


Figure 39. Variance of sound power spectrum of CSVI Unit 2 at a total flow rate of 130 L/min.

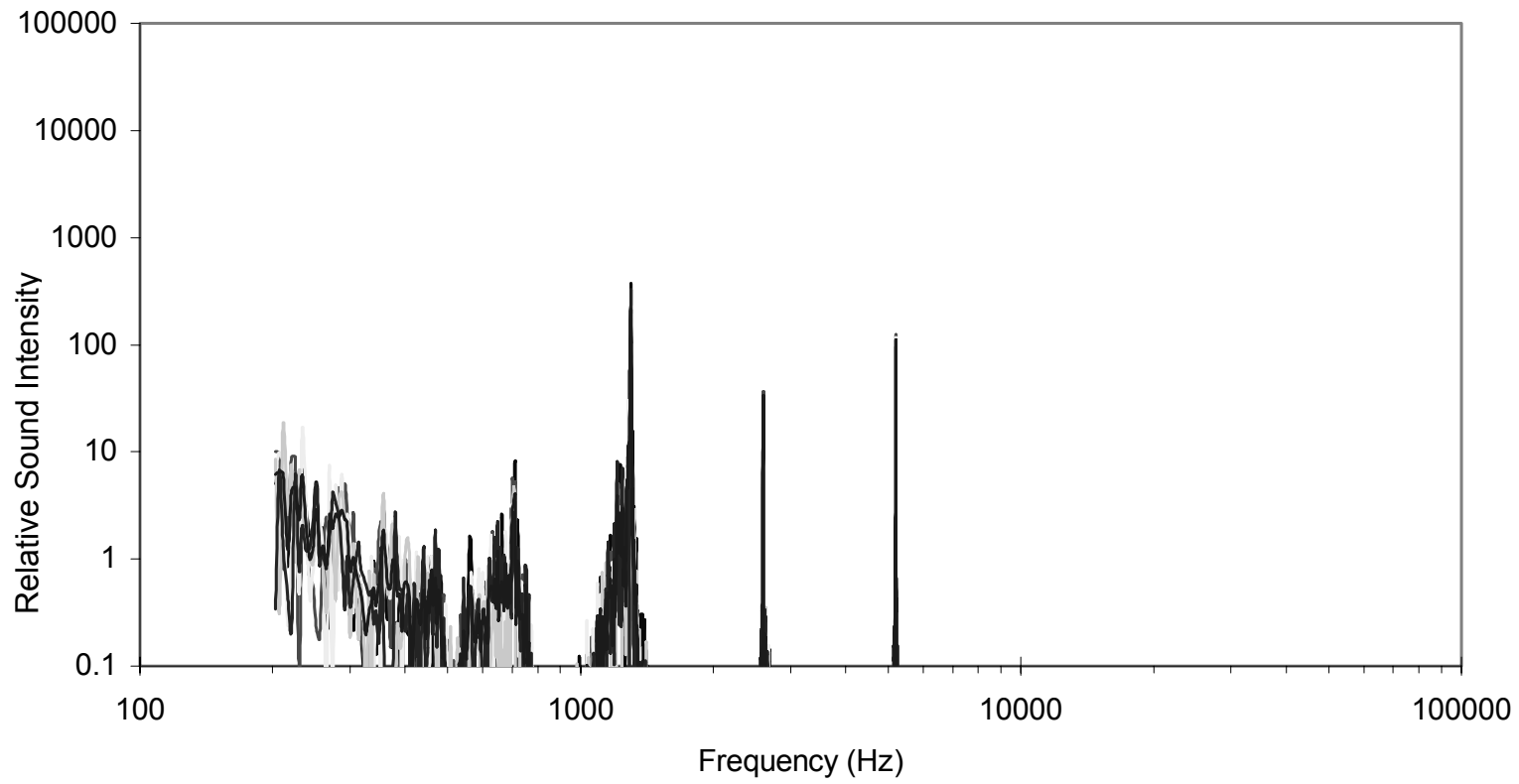


Figure 40. Sound power spectrum of CSVI Unit 2 at a total flow rate of 140 L/min.

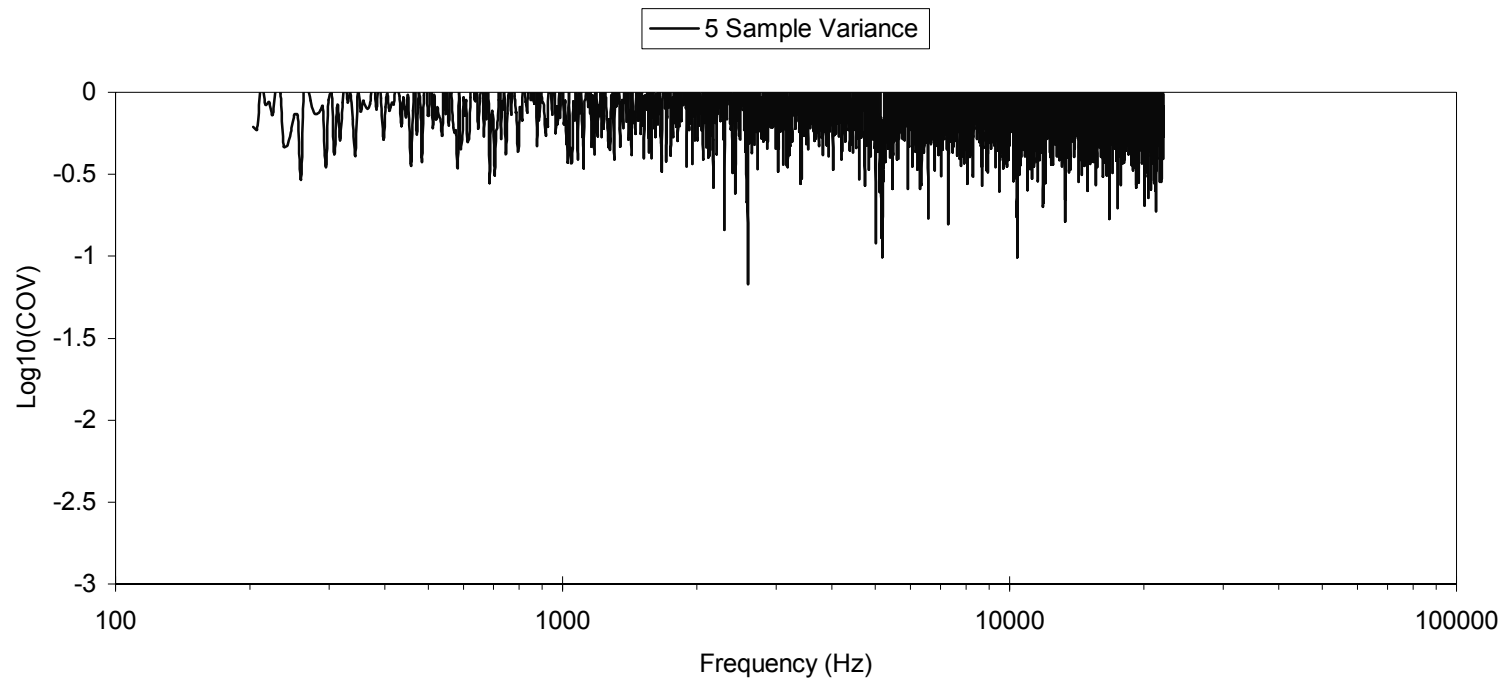


Figure 41. Variance of sound power spectrum of CSVI Unit 2 at a total flow rate of 140 L/min.

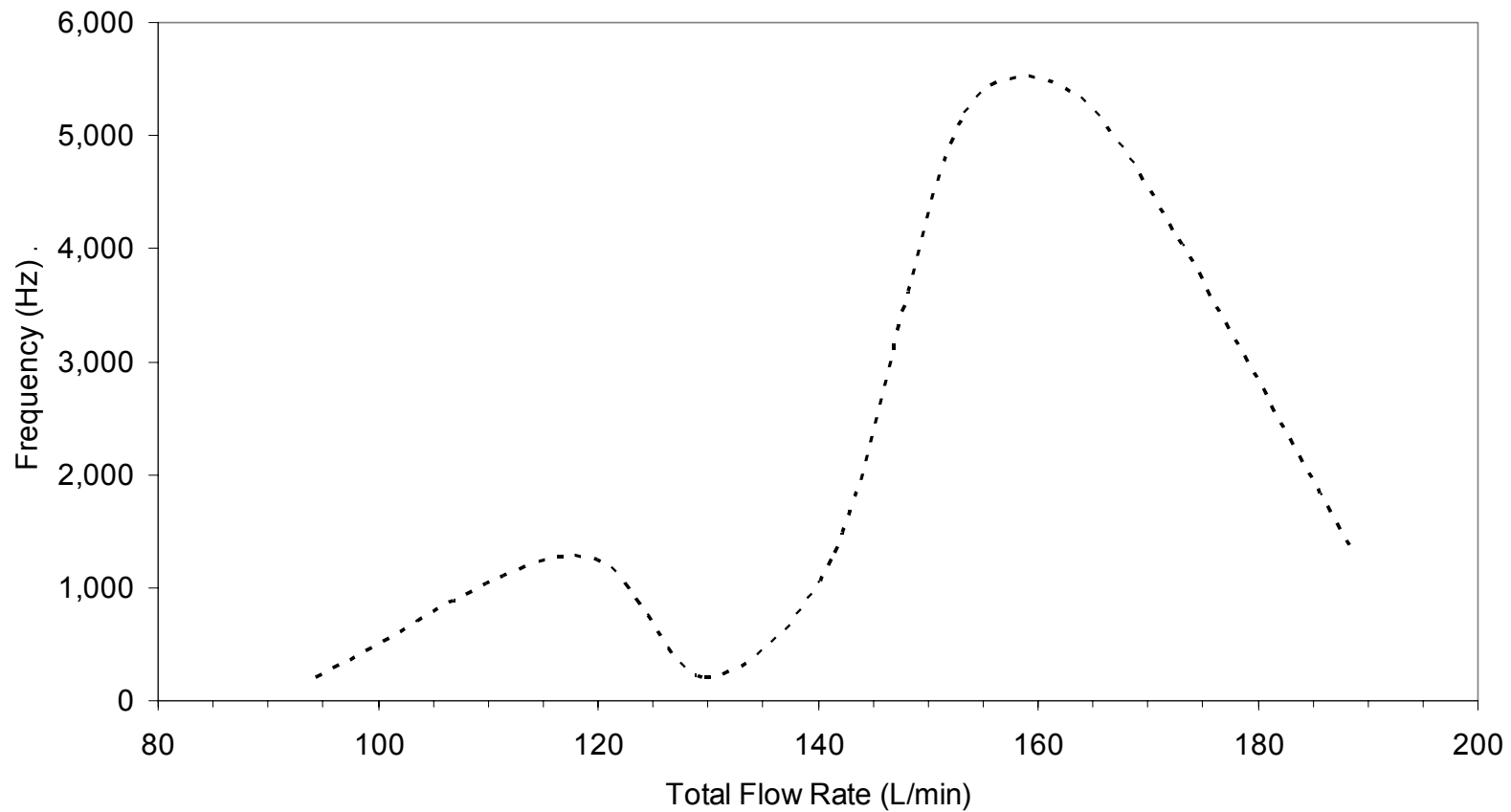


Figure 42. Frequency of maximum acoustic intensity for CSVI Unit 2 at a 10% minor/total flow ratio.

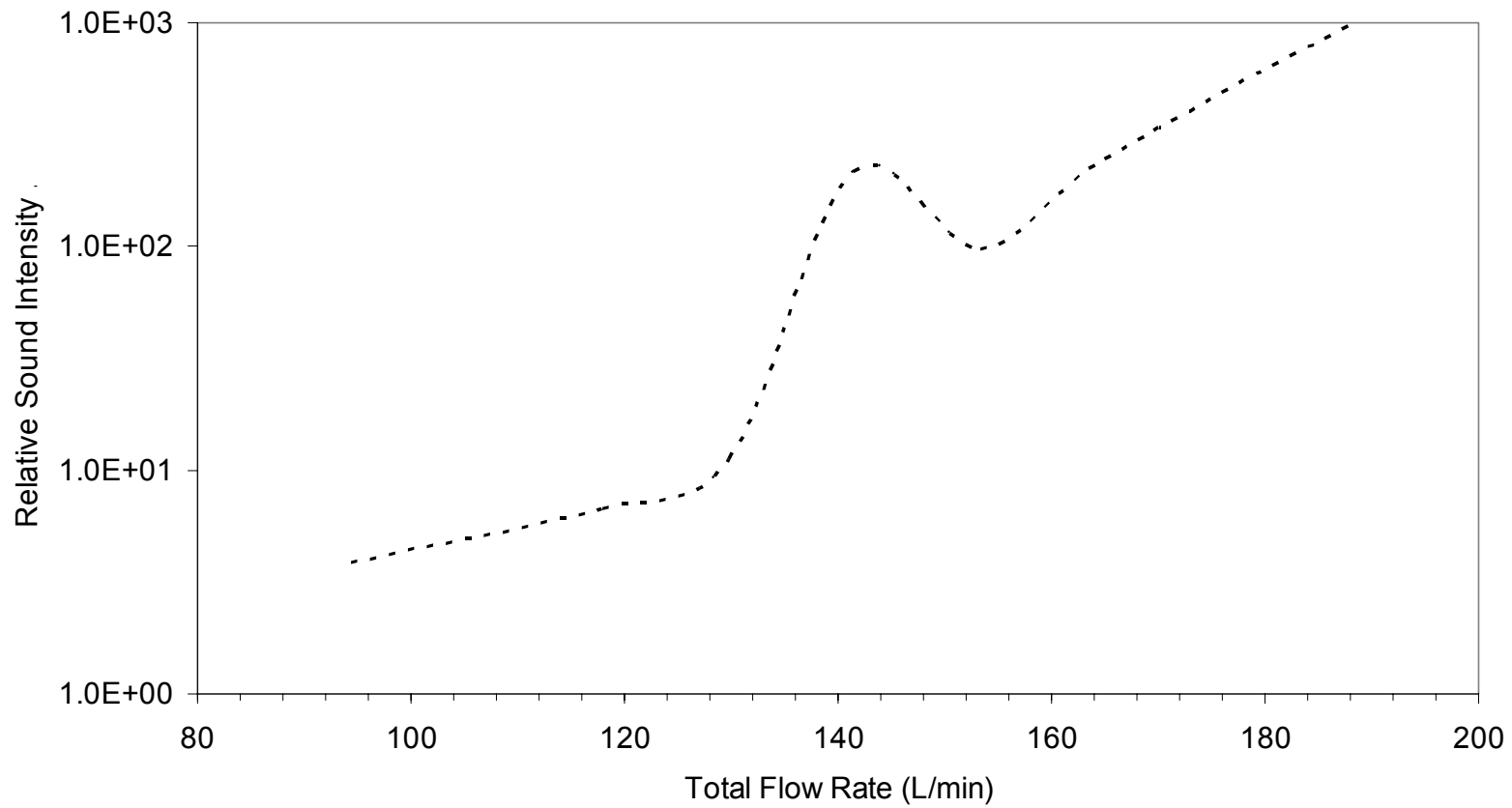


Figure 43. Amplitude of peak acoustic tone for CSVI Unit 2 at a 10% minor/total flow ratio.

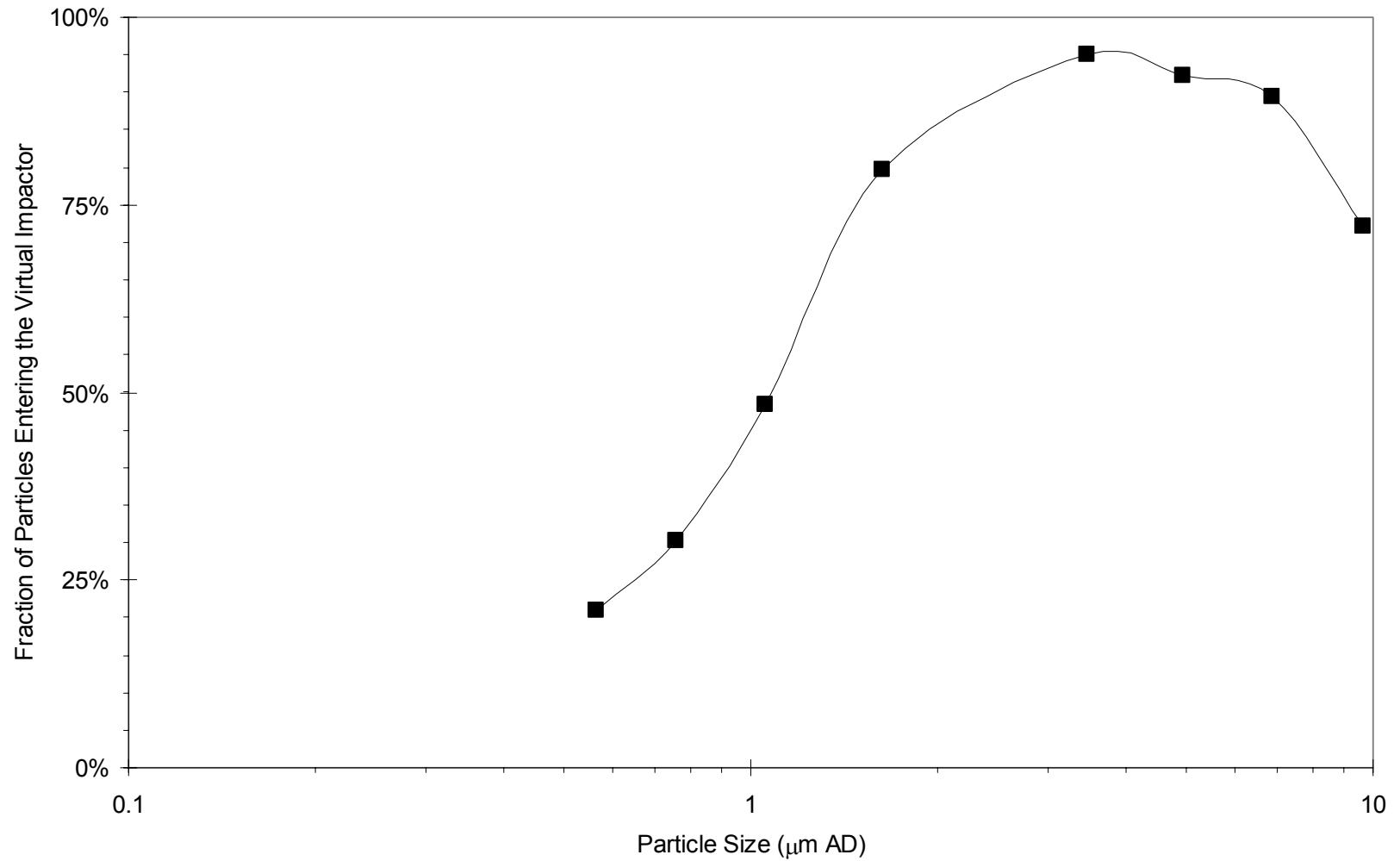


Figure 44. Collection efficiency in the minor flow of LSVI Unit 8 at a nozzle Reynolds number of 445 at 10% minor/total flow ratio.

Table 6. Final results of testing slot-nozzle virtual impactor units with monodisperse test aerosols.

Device	U_o (m/s)	Re	D_p ($\mu\text{m AD}$)	C_c	Stk (+/-)	Efficiency/Losses						
						Minor (%)	(+/-)	Major (%)	(+/-)	Wall Loss (%)	(+/-)	
LSVI Unit 8	21.78	444	9.63	1.018	38.17	2.01	72.1%	5.01%	0.0%	0.00%	26.6%	1.85%
LSVI Unit 8	21.80	445	6.88	1.025	19.63	1.27	89.5%	6.21%	1.1%	0.07%	7.3%	0.51%
LSVI Unit 8	21.80	445	4.96	1.034	10.30	0.78	92.2%	6.40%	0.9%	0.06%	7.3%	0.50%
LSVI Unit 8	21.80	445	3.47	1.049	5.11	0.55	95.1%	6.60%	1.8%	0.12%	6.7%	0.47%
LSVI Unit 8	21.80	445	1.63	1.104	1.18	0.21	79.8%	5.53%	19.3%	1.34%	9.5%	0.66%
LSVI Unit 8	21.79	444	1.05	1.160	0.52	0.02	48.3%	3.23%	56.5%	3.77%		
LSVI Unit 8	21.79	444	0.76	1.223	0.28	0.01	30.2%	2.02%	67.7%	4.52%		
LSVI Unit 8	21.79	444	0.56	1.299	0.17	0.01	21.0%	1.40%	79.0%	5.28%		
CSVI Unit 2	8.59	270	9.78	1.017	10.07	0.48	76.6%	2.76%			2.0%	0.1%
CSVI Unit 2	8.57	269	5.78	1.029	3.55	0.22	87.7%	3.15%			1.0%	0.0%
CSVI Unit 2	8.59	270	4.73	1.036	2.40	0.18	95.9%	3.44%			0.2%	0.0%
CSVI Unit 2	8.59	270	3.47	1.049	1.31	0.14	78.7%	2.82%			2.2%	0.1%
CSVI Unit 2	8.59	270	1.63	1.104	0.30	0.05	32.2%	1.15%			0.2%	0.0%
CSVI Unit 2	8.57	269	1.05	1.160	0.13	0.00	17.0%	0.52%				
CSVI Unit 2	8.57	269	0.76	1.223	0.07	0.00	14.3%	0.43%				
CSVI Unit 2	8.57	269	0.56	1.299	0.04	0.00	12.8%	0.39%				

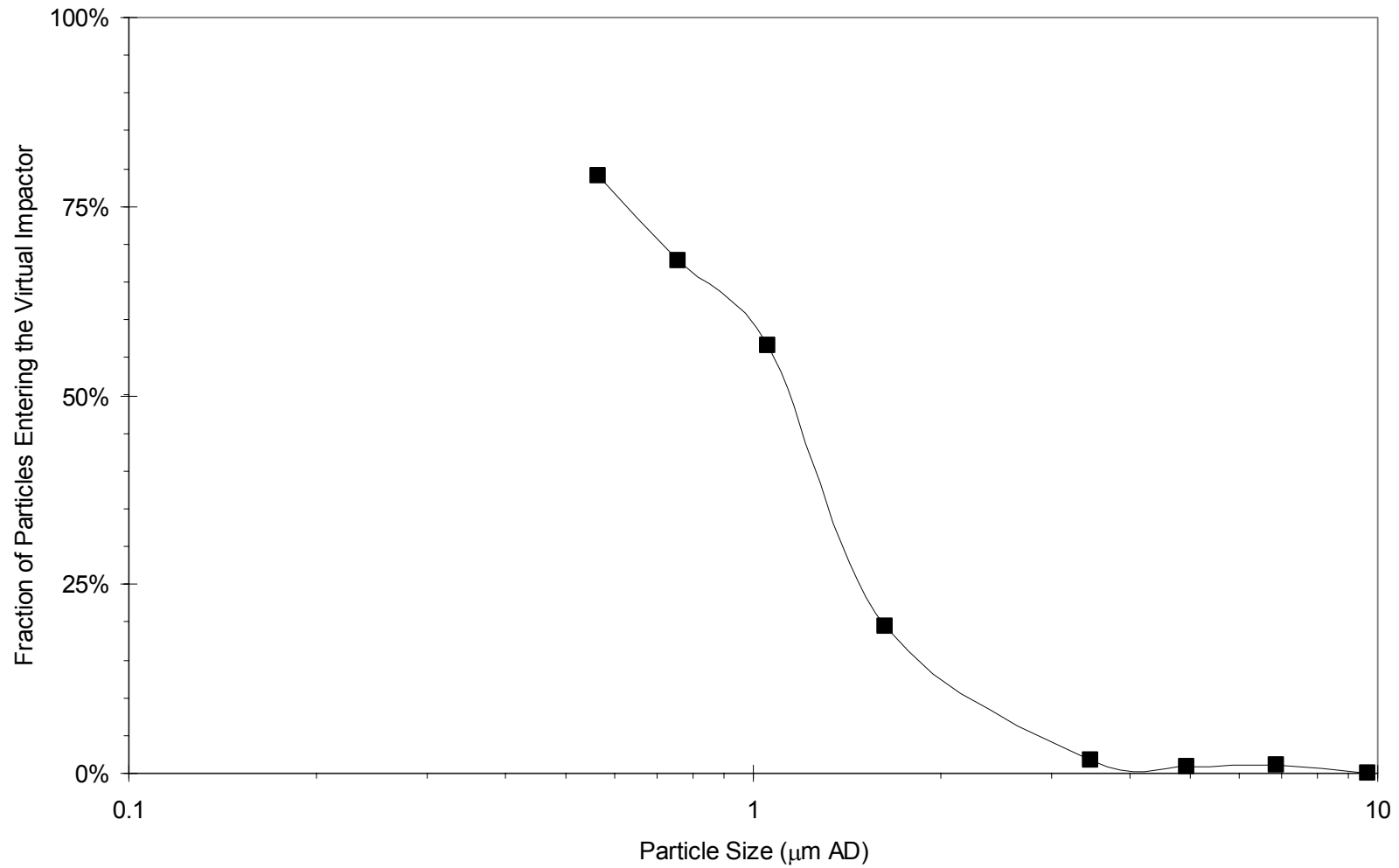


Figure 45. Collection efficiency in the major flow of LSVI Unit 8 at a nozzle Reynolds number of 445 at 10% minor/total flow ratio.

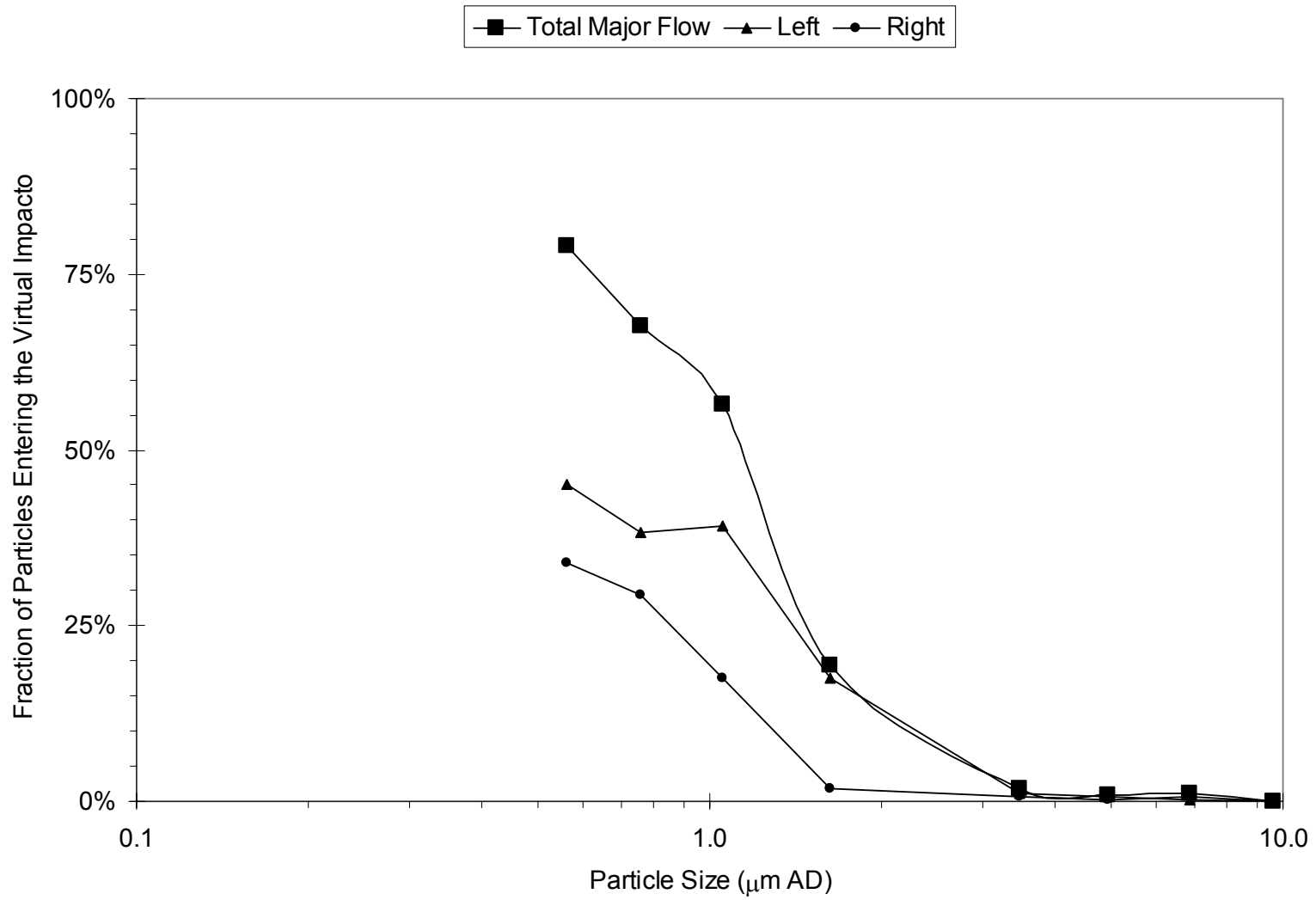


Figure 46. Collection efficiency in the left and right major flow of LSVI Unit 8 at a nozzle Reynolds number of 445 at 10% minor/total flow ratio.

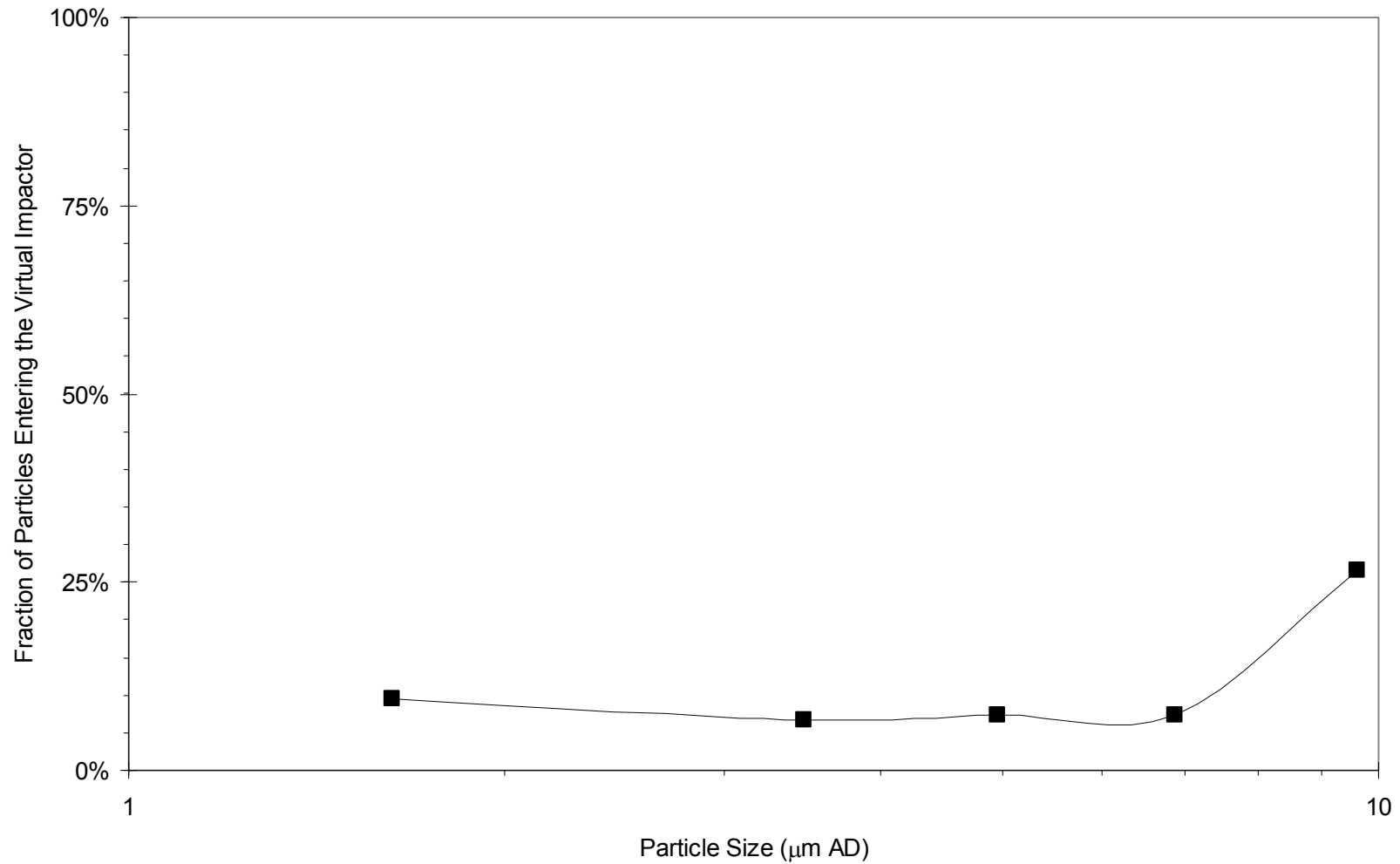


Figure 47. Wall losses in the accelerator and receiver nozzle throat of LSVI Unit 8 at a nozzle Reynolds number of 445 at 10% minor/total flow ratio.

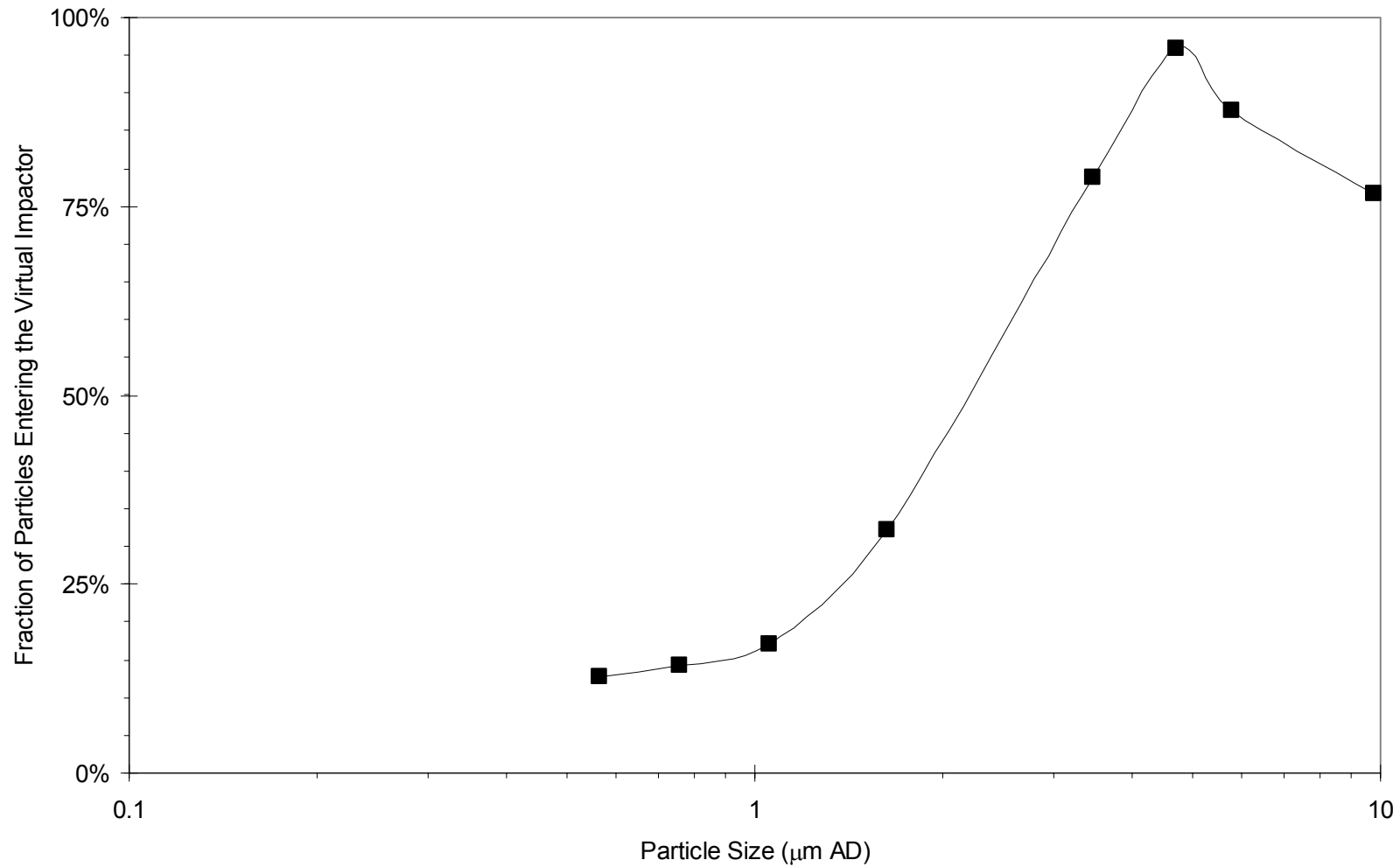


Figure 48. Collection efficiency in the minor flow of CSVI Unit 2 at a nozzle Reynolds number of 270 at 10% minor/total flow ratio.

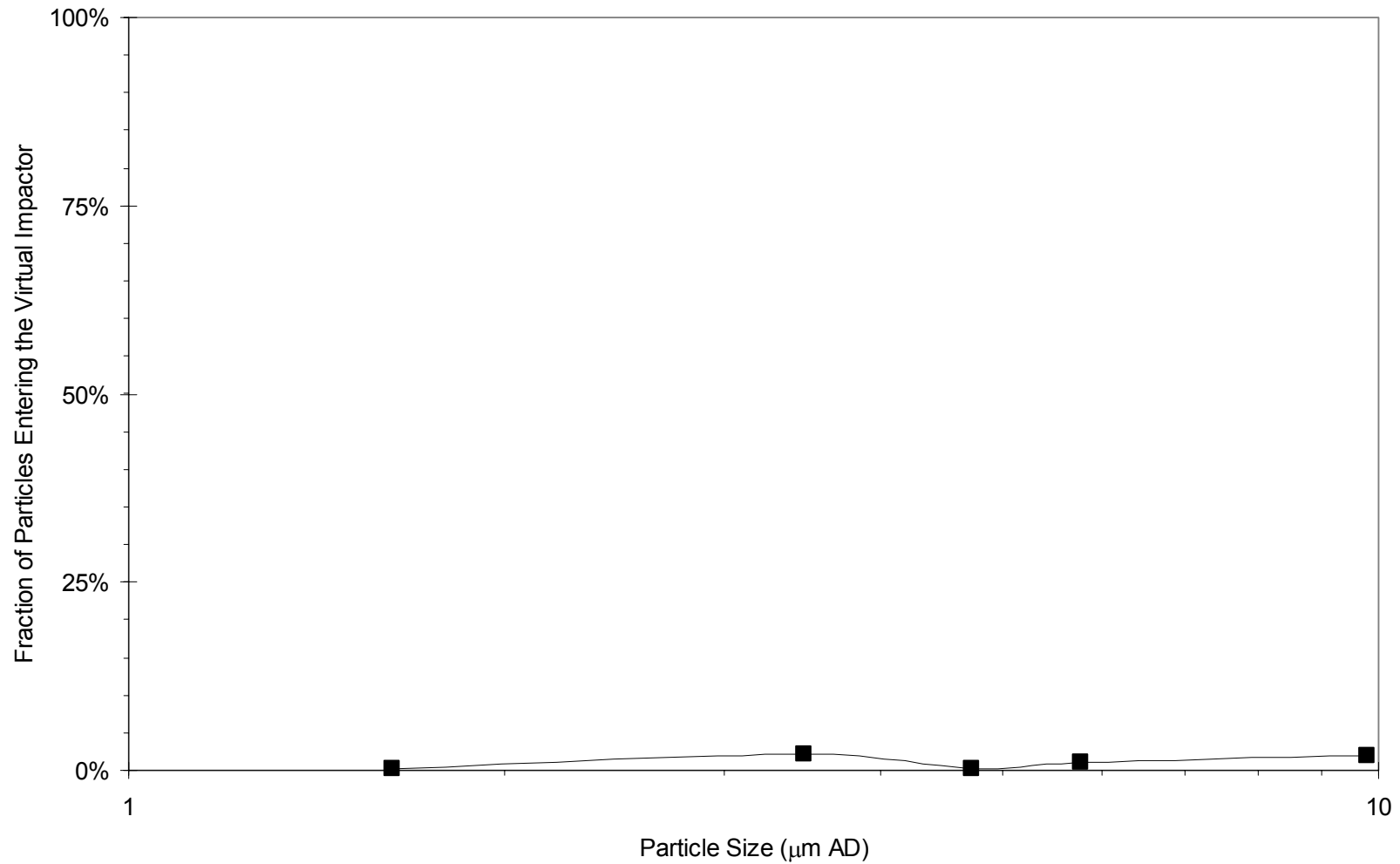


Figure 49. Wall losses in the accelerator and receiver nozzle throat of CSVI Unit 2 at a nozzle Reynolds number of 270 at 10% minor/total flow ratio.

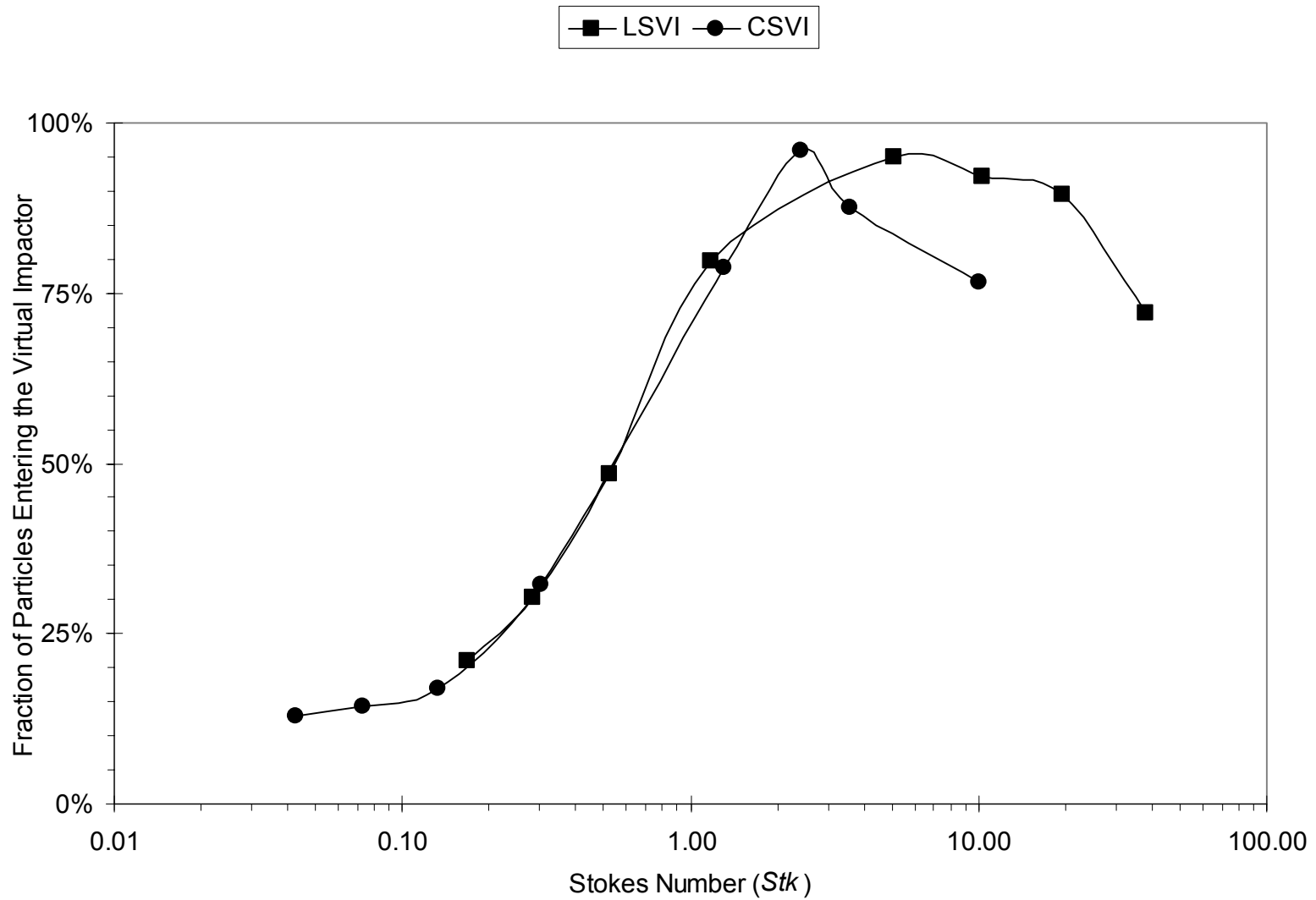


Figure 50. Collection efficiency in the minor flow of LSVI Unit 8 and CSVI Unit 2 at 10% minor/total flow ratio.

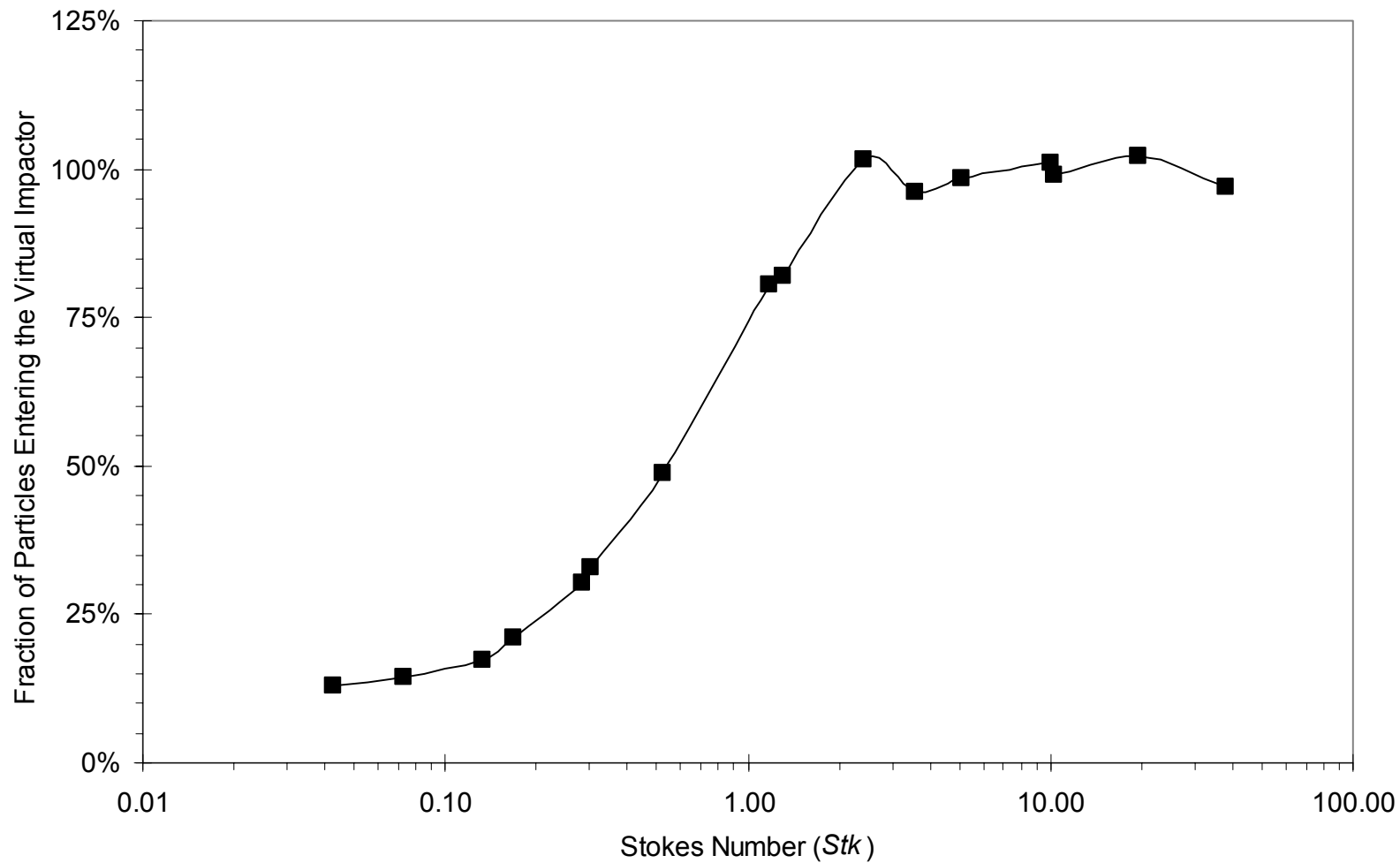


Figure 51. Wall-loss corrected collection efficiency in the minor flow of LSVI Unit 8 and CSVI Unit 2 at 10% minor/total flow ratio.

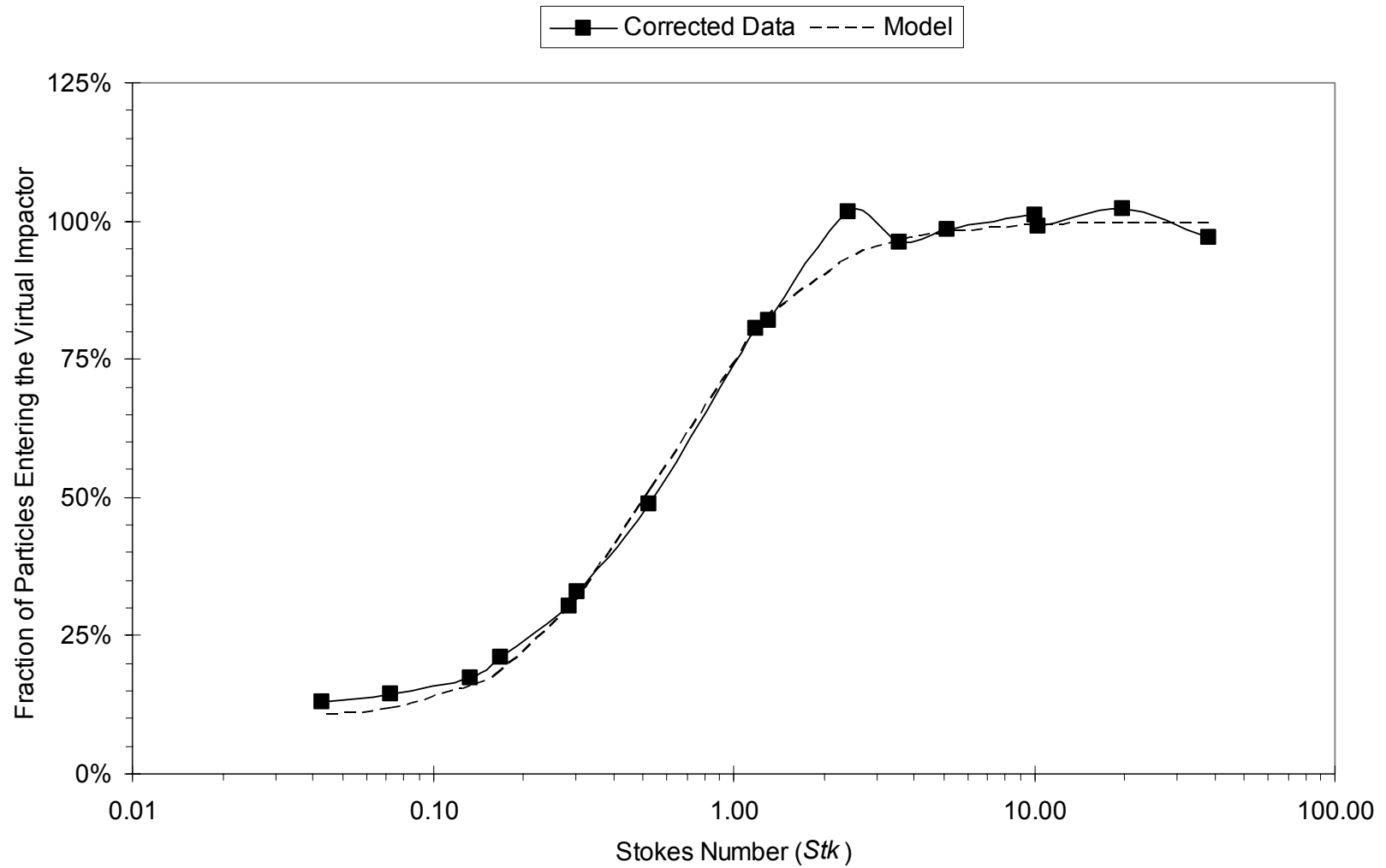


Figure 52. Model fit to wall-loss corrected collection efficiency data of LSVI Unit 8 and CSVI Unit 2 at 10% minor/total flow ratio.

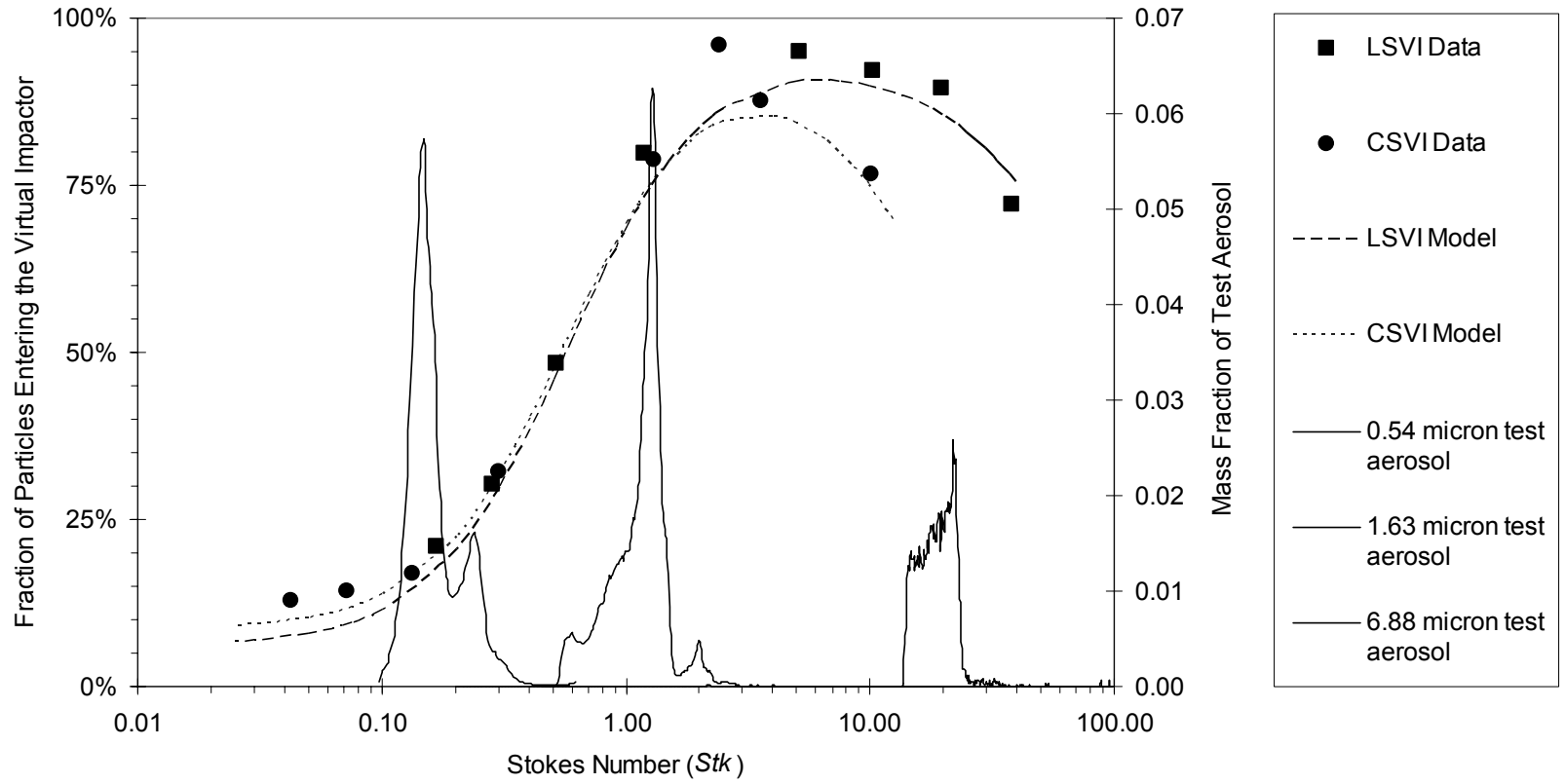


Figure 53. Comparison of collection efficiency curves of LSVI and CSVI units with variance in test aerosol particle size.

Table 7. Comparison of cutpoint Stokes numbers for virtual impactors at 10% minor/total flow ratio of present and previous studies.

Reference	Nozzle Type	Nozzle Width (mm)	L/W	Re	Pressure Drop (kPa)	$(Stk_{50})^{1/2}$	Stk_{50}
Hinds (1982)	Circular	*	*	*	*	0.49	0.24
"	Rectangular	*	*	*	*	0.77	0.59
Sioutas et al. (1994b)	Rectangular	0.35	43	2,370	12.20	0.55	0.30
"	Rectangular	0.23	65	1,110	8.50	0.50	0.25
"	Rectangular	0.23	65	1,780	18.10	0.48	0.23
Sioutas et al. (1994c)	Rectangular	0.33	170	4,460	30.00	0.45	0.20
Ding and Koutrakis (2000)	Rectangular	3.05	2.5	1,500	0.04	0.69	0.48
"	Rectangular	3.05	2.5	4,400	0.35	0.71	0.50
"	Rectangular	3.05	2.5	7,300	1.02	0.68	0.46
"	Rectangular	3.05	2.5	12,000	2.74	0.70	0.49
"	Rectangular	3.05	2.5	15,000	4.11	0.68	0.46
Current Study	LSVI	0.305	290	445	0.53	0.76	0.58
"	CSVI	0.508	940	270	0.06	0.76	0.58
Hari (2003)	Numerical	0.305	(2D Sim.)	445	*	0.93	0.86

(* not applicable or unreported)

APPENDIX B
SOUND MEDIA FILES

Sound Media File 1. Recording of sound at inlet of LSVI Unit 8 at total flow rate of 42 L/min.*

Sound Media File 2. Recording of sound at inlet of LSVI Unit 8 at total flow rate of 47 L/min.*

Sound Media File 3. Recording of sound at inlet of LSVI Unit 8 at total flow rate of 57 L/min.*

Sound Media File 4. Recording of sound at inlet of LSVI Unit 8 at total flow rate of 66 L/min.*

*to active sound file, right-click on the title, select "open link" (requires appropriate hardware and software for playing *WAV* files)

VITA

Name: John Steven Haglund

Date and Place of Birth: June 9, 1971
Minot, ND

Educational Background: Master of Science in Mechanical Engineering
(August 2000)
Texas A&M University
College Station, TX
Bachelor of Science in Mechanical Engineering
Mathematics Minor
(May 1995)
Montana State University
Bozeman, MT

Permanent Mailing Address: 1120 2nd St. S.E.
Minot ND, 58701